

Politecnico di Torino
Corso di Laurea Magistrale in

Ingegneria Energetica e Nucleare



Tesi di Laurea Magistrale

Innovative and Bio-Based Binders for Lithium Sulfur Batteries

Relatori

Massimo Santarelli
Carlotta Francia

Candidato

Matteo Saracino

Dicembre 2019

Indice

0 – Abstract	4
1 – An introduction to Li-S batteries	5
1.1 – An overview of present and future energy scenario	5
1.2 – Lithium Sulfur batteries: history, chemistry and challenges	8
1.2.1 – History of Li-S	8
1.2.1 – Chemistry of Lithium Sulfur batteries	10
1.2.2 - The Carbon/Sulfur composite cathode: macro, meso and micro pores.	11
1.2.3 – Lithium Anode	13
1.2.4 – Electrolyte	15
2 - Materials introduction and experimental section	20
2.1 - Cathode materials characterization: sulfur, carbons.....	20
2.1.1 – Elemental sulfur	20
2.1.2 – Conductive Carbons	22
2.2 - Binders Analysis.	23
2.2.1 - Polyvinylidene Fluoride.....	24
2.2.2 - Sodium Alginate	25
2.2.3 - Chitosan	26
2.2.4 - Polyacrylic acid (PAA).....	27
2.2.5 - CMC-SBR	28
2.2.6 – Polyelectrolyte Binders	29
2.3 – Experimental procedure: materials preparation and cell assembling.....	30
2.3.1 – C/S composite preparation.	30
2.3.2 – Development of Li-S cathode: ink realization and spreading, drying on Aluminum foil and electrodes cutting.	36
2.3.3 – Battery assembly.....	43
3 – Outcomes and discussion.....	47
3.1 – Galvanostatic Testing: software and instruments.	47
3.2 - A Study of cathodes with low mass content of biodegradable binders: challenges, results, comparison with traditional binders.	51
3.2.1 – AC and KJBC cathodes with low content of sulfur - Graphs	51

3.2.2– AC and KJBC cathodes with high content of sulfur - Graphs	59
3.3 - A Study of KJBC 70% S cathodes with higher mass content of biodegradable binders, innovative electroactive binders (PEBs), for long cycling: challenges, results, comparison with traditional PVdF.	68
4 -Conclusions	74
5 - Acknowledgments/ Ringraziamenti.....	75
Bibliography	76

0 – Abstract

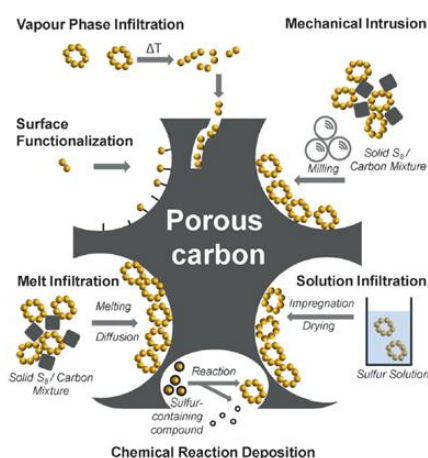


Fig.1ab – Various methods for carbon infiltration into the carbon matrix

With the increasing demand for efficient and economic energy storage, Li-S batteries have become attractive candidates for the next generation high-energy rechargeable Li batteries because of their high theoretical energy density and cost effectiveness. This two wheeling ideas of interesting energy density and overall reduced cost and weight of material with respect to the current market, are translated in this thesis work.

Indeed, starting from the very base common commercial, cheap and abundant material like carbons and sulfur, this experimental work undertakes several simple methods of cells production.

The Ball Milling technique [Fig 1ab], foresees a simple

mechanical grinding of the C/S composite making use of a mill and very hardness balls. The quickness of this method, united with a low cost and matched with a consistent mathematical model, could make this type of process suitable for an industrial scale up in the future.

The main final path that this thesis undertakes, is finally the use of proper electroactive binders to guarantee not only compactness and good contact between the electrode components, but also to interact with the electrochemistry of Li-S cells, in order to keep away the capacity fading that is typical of these type of batteries, and whom is the main reason that is limiting their introduction in the market.

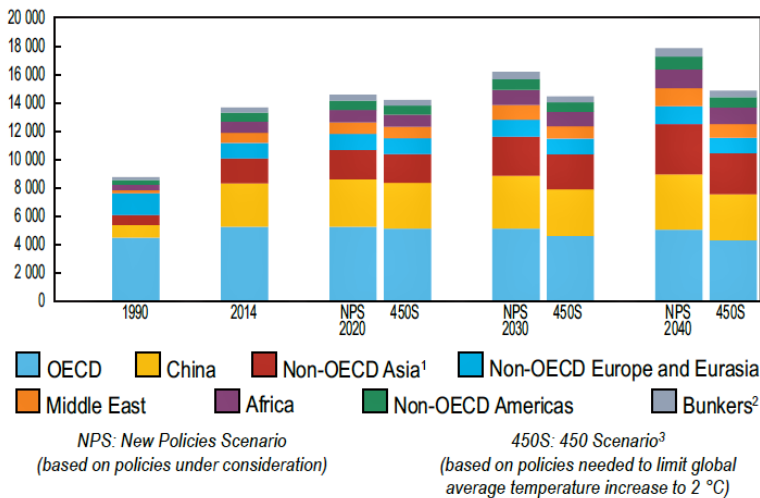
In order to achieve this goal, there are some interesting biodegradable polymeric binders that are eco-friendly because they can be naturally found in nature (for instance algae, wasted shells of shellfish...), possess long chains reach of electroactive functional groups that can actively influence the Li_xS_y polysulfide species formation during the complex Li-S redox reactions and they are cheaper compared to other syntenic binders.

These type of binders will be compared to the traditional polyvinyl fluoride, who is simple to implement but is syntenic, not as much economic, not eco-friendly, has no interaction with polysulfides species and finally makes necessary the use of a toxic solvent with an high boiling point (i.e. in an industrial perspective expensive to evaporate).

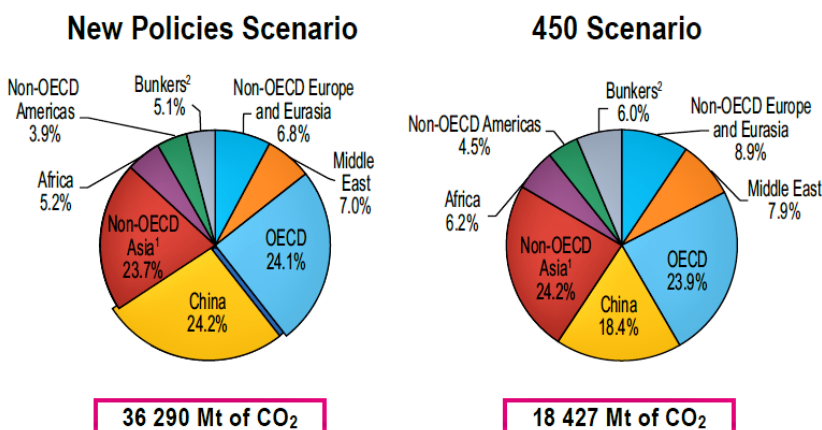
Beside them, also some new interesting long chain synthetic polymers will be exploited seeking for durable lithium sulfur battery performances, called Polyelectrolyte Binders (PEBs).

1 – An introduction to Li-S batteries

TPES outlook by region and scenario to 2040 (Mtoe)



CO₂ emissions by region and scenario in 2040



1. Non-OECD Asia excludes China.
 2. Includes international aviation and international marine bunkers.
 3. Based on a plausible post-2016 climate-policy framework to stabilise the long-term concentration global greenhouse gases at 450 ppm CO₂-equivalent. CO₂ emissions are from fossil fuel combustion or
 Source: IEA, World Energy Outlook 2016.

Fig.1 – Future scenario of energy demand and CO₂ emission - IEA Key World Energy Statistic 2017. Reproduced from ref. [2]

1.1 – An overview of present and future energy scenario

The economic and demographic growth that is occurring especially in the developing countries is making the world society more and more energetic. Currently this large energy demand is achieved primarily with traditional fossil sources. However, experts have predicted a probable depletion of oil stocks within the next 40 years, while gas and coal reserves will last at most 150 years [1]. As can be seen from the graph below [fig.1], even in the hypothesis in which countries adopt solutions to reduce the increase in CO₂ and thus mitigate the increase in the world average temperature (maximum 2 ° C in the next 40 years) , the demand for primary energy is anyway destined to grow more and more. As a result, to avoid further worsening of the climate and

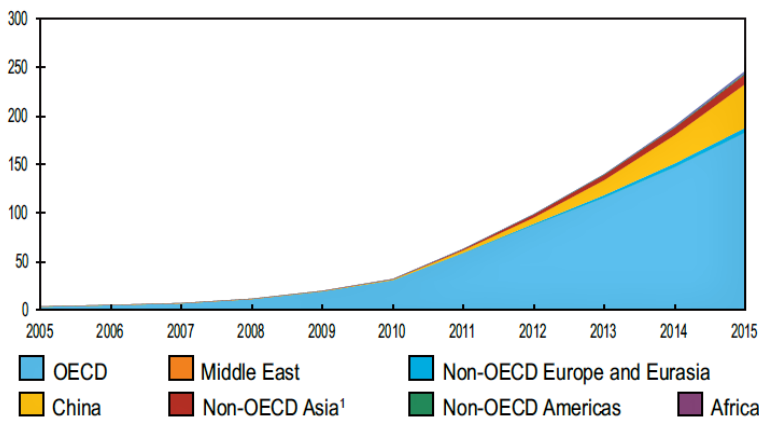
subsequent disasters, research has focused on renewable and clean forms of energy. Technologies such as solar photovoltaic and wind turbines [Fig.2] have already been on the market for several years but present a major problem: being intermittent, often the supply of energy does not coincide temporally with the demand of the user, or vice versa to a high demand Users often find the unavailability of power supply.

New storage technologies are therefore necessary to ensure greater flexibility in power generation, making energy supply more synchronous than the day / night load curve characteristic of power grids.

New energy policies for achieving these goals have therefore led the electrochemical batteries to be the focus of new studies and research.

In the last 25 years lithium ion batteries (LIBs) have been the protagonists of the market, as they are installed in 90% of existing portable electronic devices. The success behind the LIBs lies in their stability and durability; in fact they retain most of their initial capacity even after numerous cycles.

World solar PV electricity production from 2005 to 2015 by region (TWh)



World wind electricity production from 2005 to 2015 by region (TWh)

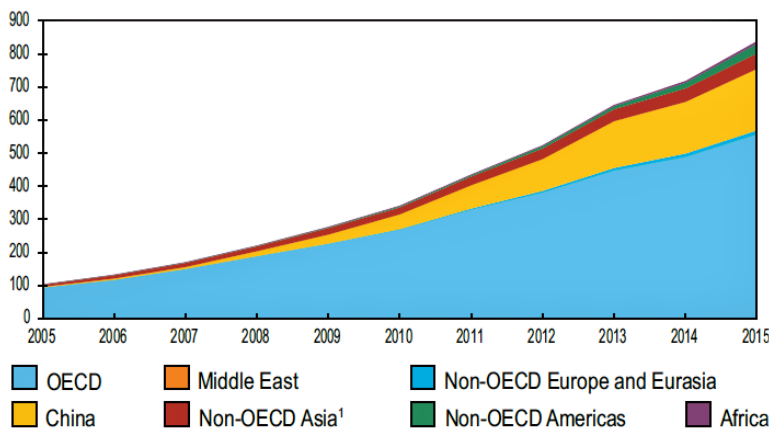


Fig.2 – Explosion of photovoltaic energy production from 2005 to 2015 - IEA Key World Energy Statistic 2017 pag.22-24. Reproduced from ref. [3]

Although research on LIBs continues to make further improvements, they still have a low gravimetric energy (100-150 Wh/kg). This still makes them unsuitable for higher power applications such as storage for power grids and electric vehicle batteries. These last ones require a gravimetric density of energy such to travel at least 500 km with a charge, and it is the objective that the scholars would like to reach. As can be seen from the pie chart [3], 2015 data, almost half of the oil demand comes from the road transport sector. Electric vehicles therefore appear to be the most viable alternative in order to reduce CO2 emissions from current internal combustion engines to almost zero. Lithium/Sulfur batteries, currently under development, appear to be an

excellent alternative to the LIBs. First of all, sulfur is a very abundant, economical and non-toxic element. Assembled with lithium to form a lithium cell (anode) - sulfur (at the cathode) could theoretically supply 1675 Wh / kg of capacity, a value significantly higher than the recent commercial lithium ion (LiCoO₂ / C, 387 Wh / kg), while a practical capacity value could be around 300-600 Wh / kg, a value two or three times higher than the LIBs, and a cost of about \$ 150 per tonne. In the face of these advantages, there are some problems of an electrochemical nature that most hinder this technology, in particular limiting its cycling and durability, these features still makes them unsuitable for higher power applications such as storage for power grids and electric vehicle batteries. These last ones require a gravimetric density of energy such to travel at least 500 km [4] with a charge, and it is the objective that the scholars would like to reach. As can be seen from the pie chart [Fig.3], 2015 data, almost half of the oil demand comes from the road transport sector. Electric vehicles therefore appear to be the most viable alternative in order to reduce CO2

emissions from current internal combustion engines to almost zero. Lithium batteries, currently under development, appear to be an excellent alternative to the LIBs.

First of all, sulfur is a very abundant, economical and non-toxic element. Assembled with lithium to form a lithium cell (anode) - sulfur (at the cathode) could theoretically supply 1675 Wh/kg of capacity, a value significantly higher than the recent commercial lithium ion (LiCoO₂/C, 387 Wh/kg), while a practical capacity value could be around 300-600 Wh/kg, a value two or three times higher than the LIBs, and a cost of about \$ 150 per tonne. In the face of these advantages, there are some problems of an electrochemical nature that most hinder this technology, in particular limiting its cycling and durability, fundamental characteristics for the introduction on the market. The low electrical conductivity of sulfur causes the cathode to require further additions of additives (usually more or less porous carbon structures), which increase the mass of non-active material thereby reducing the volumetric energy density. Moreover, during the oxide reduction reactions, the formation of highly soluble polysulphides (Li_xS_y) occurs, which in fact leads to a loss of active material (sulfur) by dissolution into an electrolyte. These problems will be addressed in more detail in the chapters to follow.

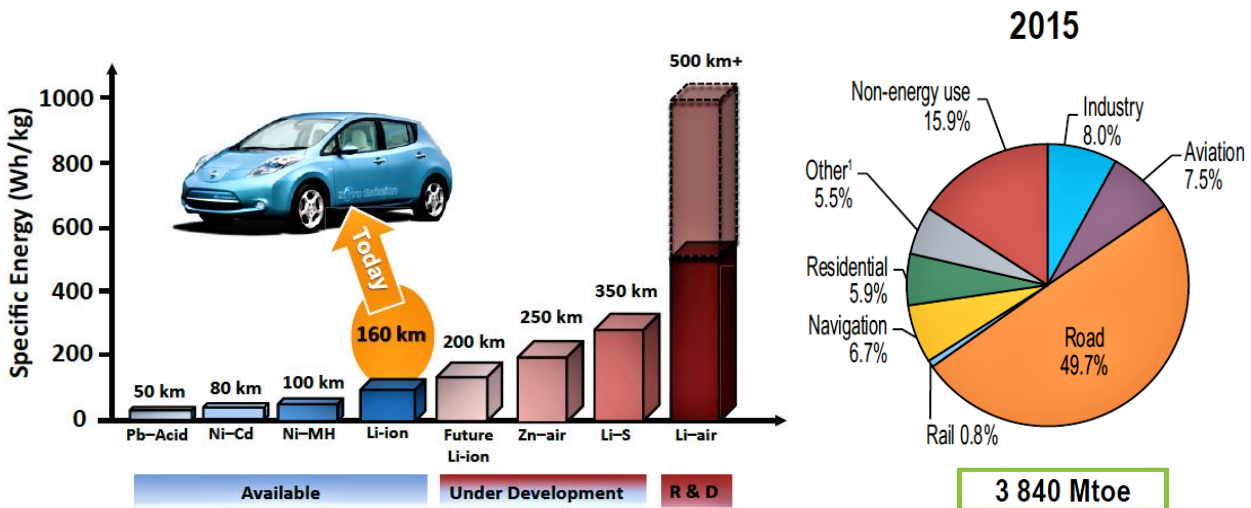


Fig.3 - DX – Oil demand by sector - 2015 - IEA Key World Energy Statistic 2017 pag.22-24

SX – maximum kilometers range of different battery technologies. Reproduced from ref(s). [3] [4]

1.2 – Lithium Sulfur batteries: history, chemistry and challenges

1.2.1 – History of Li-S

[5] - Since their discovery in the '60s, lithium-sulfur cells have been considered a promising technology, potentially able to dominate the market of batteries for powering electrical and electronic systems.

1962 - With the patented work of Herbert and Ulam [8], sulfur was proposed as a positive electrode and Li (or Li alloy) as a negative electrode in dry electric cells and storage batteries. The identified electrolyte was alkaline or alkaline-earth perchlorate, iodide, sulfocyanide, bromide, or chlorate dissolved in a primary, secondary or tertiary amine.

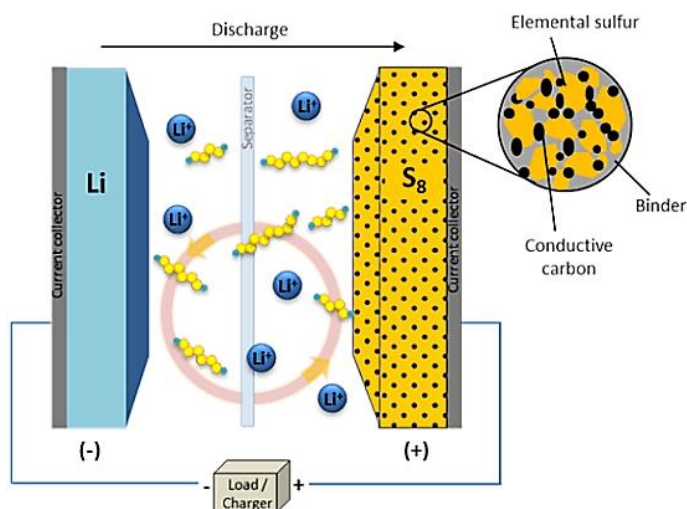


Fig.4 - Schematic structure of an Li-S battery

1966 - Four years later, Herbert filed another patent [9], which was a continuation in part of their previous patent, with the solution the electrolyte preferably constituted by a salt of lithium dissolved in a propyl, butyl or amylamine, preferably isopropylamine. In the same year, Rao patented high energy density metal-sulfur batteries [10]. The electrolyte consisted of cations of light metals or ions and ammonium anions of tetrafluoroborate, tetra-chloroaluminate, perchlorate or chloride salts which were dissolved in

organic solvents. The solvents were propylene carbonate, γ -butyrolactone, N,N-dimethylformamide or dimethylsulfoxide and the cells were pedestrian between the 2.52 and 1.16 V voltages with respect to Li.

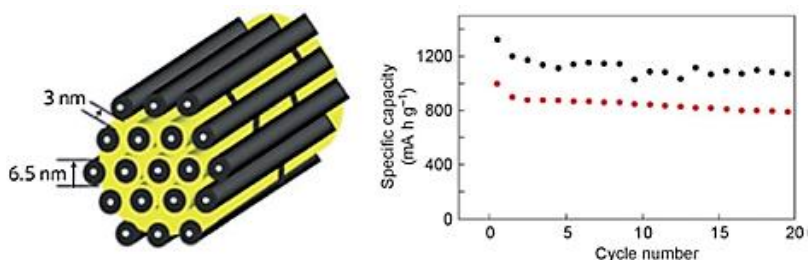


Fig.5 - Ya-Xia Yin, Sen Xin, Yu-Guo Guo, Li-Jun Wan - LithiumSulfur Batteries: Electrochemistry, Materials, and Prospect, Copyright 2009 - Nature Publishing Group – Reprinted from ref(s). [6][7]

1970 - Moss and Nole, represented a patent for the battery that used Li and sulfur electrodes with non-aqueous electrolyte [11]. Today there are over 700 different patent families such as those shown above. Since the 90s, the research

has been suspended with the advent of lithium-ion cells (LIBs), which are still the most widespread.

2000s - Following the rapid development of new emerging applications such as the appearance of new civilian transport vehicles, new intermittent renewable energy sources and the supply of energy for military use, the study of more electrochemical systems was once again necessary.

2009 - The Li-S cells gained even more attention when Nazar et al. have published experimental data of cells with effective capacity up to over 1300 mWh / g, using mesoporous carbon [Fig.5][6]. Following this pioneering work by Nazar, publications in the literature have increased considerably in number and diversification, counting more than 2500 publications containing the words "lithium sulfur batteries" and over 70,000 citations on the subject [Fig.6]. Most of these works have turned their attention to the development of a sulfur cathode such that, through more or less articulated carbon structures, it is possible to absorb / absorb the polysulfides and prevent them from dissolving, with a consequent increase in the percentage of unusable sulfur. Another

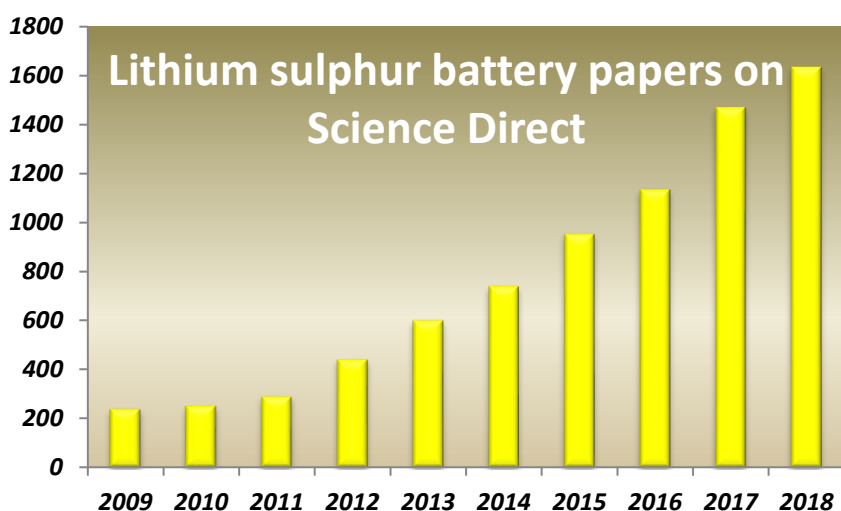


Fig.6 - Number of publications per year searching "Lithium Sulfur battery" on Science Direct

important objective of this period was the study of an electrolyte suitable for lithium sulfur cells.

Different solvent / salt mixes in liquid form were proposed, such as PEO (Poly (ethylene oxide) -based electrolytes) and dioxolane electrolytes, which is currently one of the most used solvents. For reasons of safety and durability linked to the problem of the progressive dissolution of polysulfides, a

solid electrolyte configurations were also proposed (Li₂S-P₂S₅, Li₂S-SiS₂, thio-LISILICON). Solutions with a high concentration of salts were also advanced to stem the problem of the dissolution of lithium salts.

1.2.1 – Chemistry of Lithium Sulfur batteries

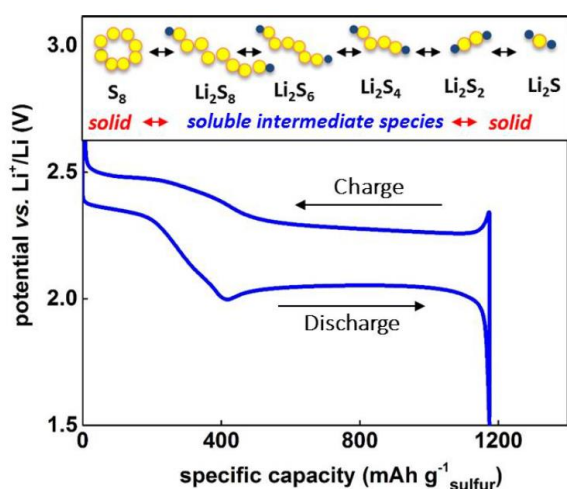


Fig.7 – Charge/discharge voltage vs. capacity, soluble/solid species formation during the process. Reproduced from ref. [12]

[13] - A conventional Li–S cell is composed of a sulfur cathode, a Li anode and a liquid electrolyte placed in between. At the open circuit voltage (OCV), due to the difference between the electrochemical potentials of the Li anode and the S cathode, the Li–S cell ensures a maximum voltage. Upon reduction (discharge), molecules of elemental sulfur (S_8) are reduced by accepting electrons which leads to the formation of high-order Li polysulfides Li_2S_x ($6 < x \leq 8$) at the upper plateau (2.3–2.4 V vs. Li). As the discharge continues, further polysulfide reduction takes place progressively stepping down voltage to

2.1 V (vs. Li) and lower order Li polysulfides chains Li_2S_x ($2 < x \leq 6$) are formed. There are two discharge plateaus at 2.3 and 2.1 V with ether-based liquid electrolytes, which represent the conversions of S_8 to Li_2S_4 and Li_2S_4 to Li_2S , respectively. At the end of the discharge, Li_2S is formed, which is both electronically insulating and insoluble in the electrolyte. Apart from Li_2S , the rest of sulfur reduction species are highly soluble in aprotic solvents.

The reduction process is accompanied by a decrease in cathode electrochemical potential until the battery reaches the terminal voltage (normally ≤ 1.5 V). The opposite reaction (oxidation, charging) arises when an external electric field with a certain potential difference is applied, leading to the decomposition of Li_2S to Li and S. During this process, the cathode electrochemical potential gradually increases till the battery voltage returns to OCV. The redox process displays two pairs of redox peaks, corresponds well with the CV of the Li–S battery. The overall redox couple described by the reaction $S_8 + 16Li \rightarrow 8Li_2S$ lies at an average voltage of approximately 2.2 V vs. Li. This potential is around 30% less than that of conventional cathode materials in LIBs. However, the lower potential is not detrimental and compensates by its high theoretical capacity, which makes sulfur the highest energy density solid cathode material.

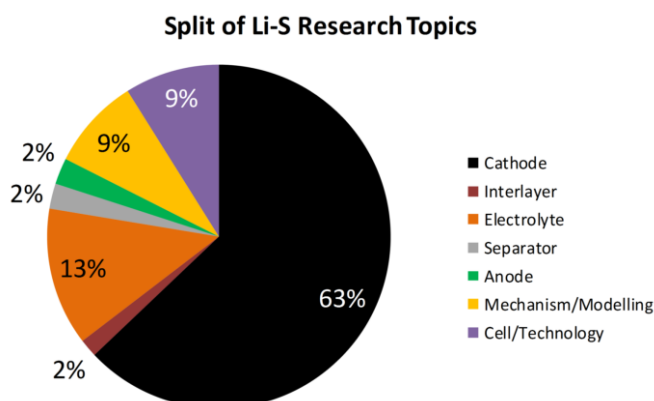


Fig.8 – Split of Li-S research topics. Reproduced from ref.[12]

1.2.2 - The Carbon/Sulfur composite cathode: macro, meso and micro pores.

The main efforts to improve the electrochemical performances of Li-S batteries have been on the development of carbon-based sulfur composite cathodes. Following the report of high-capacity Li-S cells in 2009 [6] with highly ordered mesoporous carbon and sulfur,

studies on sulfur-carbon composite cathodes have grown rapidly.

In fact, more than 30% of research topics are nowadays focused on cathode side [fig.8].

In order to effectively house sulfur, the host must contain the sulfur without significantly diminishing the overall practical properties of the cell, that is, the gravimetric/volumetric energy density. The optimal material to satisfy these conditions is lightweight, conductive, and can “wrap” the insulating sulfur, such as one made predominately of carbon. Carbon is highly effective as an electronic conduit to enable redox accessibility of the sulfur, but it can also act as a framework to encapsulate the redox products. A straightforward solution is to introduce pores in the carbon that sulfur can impregnate. Pore size is defined by the IUPAC as being either macro (>50 nm), meso (2 - 50 nm), or micro (<2 nm).

Macroporous carbons have been the least utilized for Li-S cells due to their open architecture, which is highly ineffectual at containing soluble polysulfides. However, if the macroporous carbon is coupled to a high viscosity electrolyte, the lithium polysulfides are limited in mobility and will predominately remain at the cathode.

Watanabe et al. [14] used an ordered inverse opal carbon to house sulfur and replaced the commonly used low viscosity organic electrolytes with a high viscosity glyme-Li salt. This electrolyte is similar to a room temperature ionic liquid in that it consists purely of [Li(glyme)]⁺ cations and TFSI⁻ anions. It afforded relatively stable cell cycling with a reversible capacity of over 700 mAh/g after 50 cycles and a coulombic efficiency of 97% [15].

Most of the recent reported research on porous carbon cathodes has focused on mesoporous carbons (MCs), following one of the first pioneering composite cathode developed by Nazar et al. [6].

Nazar and her group used an ordered mesoporous carbon synthesized by Ryoo and his co-workers [16], designated as CMK-3.

CMK-3 is formed by ordered carbon nanotubes of diameter of 6-7 nm, and pore size around 3.4 nm [Fig.5]. The composite CMK-3/S in a mass ratio of 70:30 S/C, plus an hydrophilic polymer coating, showed optimal performances yielding a reversible capacities up to 1320 mAh/g. In fact, tailing these positive outcome in literature, a mesoporous carbon has been used in this work as

well, named Ketjenblack® (EC-300J, AkzoNobel). Ketjenblack carbon has a very high specific area and a medium particle size of 30 nm. Its peculiarities are described further on in the material section.

Although the mesoporous carbon materials have been successful in preparing stable sulfur cathodes, the electrochemistry of S_8 ring molecule still exists in the systems, and the dissolution and shuttle of polysulfides cannot be eliminated. Looking at some past work in the literature, microporous carbon materials have been considered for an optimal confinement. For example, Aurbach et al. [17] discovered that by sulfur dispersion into microporous carbon fibers with an average pore diameter of about 1 nm, the electroactivity and cyclability of sulfur are greatly improved. However, it remains a challenge to completely solve the problems resulted from the electrochemistry of cyclo- S_8 .

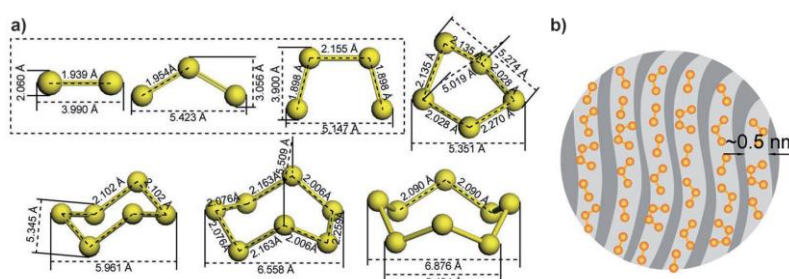


Fig.9 – From S_2 simple structure to “chair” configuration of S_8 ring. On the right the reduced dimension of sulfur molecules if the carbon channels are sufficiently small (~0.5 nm). Reproduced from ref. [18]

Guo et al. [18] have found that, even the carbon pore size reaches a critical value (for example, 0.5 nm) [Fig.9], sulfur could still be loaded into the carbon channel. Given that the pore size is less than the dimensions of cyclo- S_8 (ca. 0.7 nm), the ring-like configuration cannot be maintained, and sulfur can only be stored as chain-like

sulfur molecules in the microporous carbon coated carbon nanotube substrate. The confined S molecules show strong interaction with the carbon wall, eliminating the unfavorable transition between cyclo- S_8 and S_4 (during which soluble polysulfides form) and exhibiting a novel electrochemical behavior with a single output plateau at about 1.9 V.

Interestingly, the typical plateau at about 2.3 V (vs. Li_+/Li), which is ascribed to be the reduction from the common cyclo- S_8 molecule to the electrolyte-soluble polysulfides (Li_2S_n , $n=4-8$), is not observed in its voltage profile. The novel electrochemistry of the confined chain-like sulfur molecules essentially solves the critical problem of polysulfide dissolution in conventional Li-S batteries. As a result, the sulfur/(microporous carbon coated carbon nanotube) composite cathode exhibits optimal electrochemical properties in terms of specific capacity (1670 mAh/g upon the first discharge), cycling stability (1149 mAh/g after 200 cycles), and high-rate capability (800 mAh/g at 5C).

To reach a large specific capacity for the carbon/chain-like sulfur composite, a high sulfur loading rate should be guaranteed, which requires the carbon host to have a large micropore volume. However, the preparation of microporous carbon with sufficient pore volume for a chain-like sulfur content of more than 50 wt% is still challenging with current synthetic techniques.

1.2.3 – Lithium Anode

[19] - Comparing to the rapid escalation of studies regarding cathode materials, the lithium side has not been deeply treated in recent years studies.

Lithium Sulfur batteries usually contain pure metal lithium as anode, which essentially carries two main problems: lithium reacts with both electrolyte solution and polysulfides.

The performance of the negative electrode in Li/S batteries is in fact strongly related to the sulfur-based positive electrode and this interdependence is best illustrated through the so-called redox shuttle mechanism of soluble polysulfide intermediates. The traditional reaction pathway for the reduction of sulfur (S_8) which occurs at the positive electrode during discharge is:



The final reduction product (Li_2S) is insoluble in the electrolyte, however, driven by a concentration gradient, the longer chain polysulfide ions (Li_2S_8 , Li_2S_6 , and/or Li_2S_4) readily diffuse

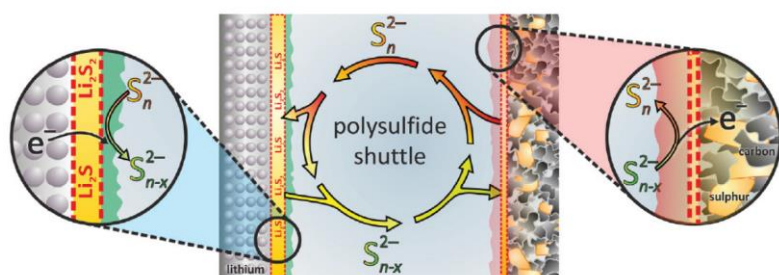
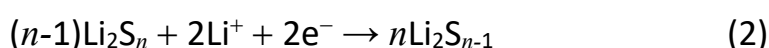
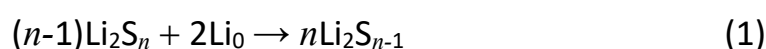


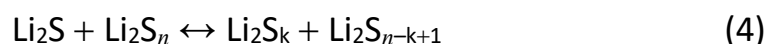
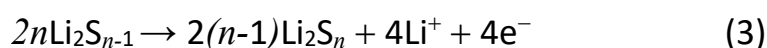
Fig.10 – A schematic view of PSs shuttle reaction mechanism. Reproduced from ref.[19]

from the positive to the negative electrode, where they may undergo both chemical and electrochemical reduction, to form either shorter polysulfides or precipitate as Li_2S . The whole shuttle mechanism is well illustrated in the schematic cell below [Fig.10].

In the former case, if the polysulfides are still soluble, they can diffuse back to the positive electrode. During charge, these short-chain polysulfides are then electrochemically reoxidized into long-chain polysulfides (Equation (3)), which diffuse again to the negative electrode in a possibly endless process, creating an internal shuttle phenomenon. This redox shuttle has direct consequences, such as a low CE (overcharge) and a severe propensity of Li–S cells to self-discharge (Equation (1)).

However, the underlying cause of the shuttle is the instability of the negative electrode/electrolyte interface evidenced in both (Equation (1)) and (Equation (2)): metallic Li is not passivated by a solid electrolyte interphase (SEI) as detailed hereafter.





In order to effectively mitigate these problems, i.e. ensuring a durable protection of the Li electrode, several strategies are reported in literature.

One effective approach to mitigate these problems is to isolate the highly active Li anode from electrolyte solution and soluble polysulfides through introducing a thin and stable passivation layer on Li anode. Apart from the protection of Li anode, the passivation layer should be permeable for Li^+ , allowing fast transfer of Li^+ under electrical field. The passivation layer thereby functions as the solid electrolyte interphase (SEI) layer between Li anode and electrolyte solution. The protection layer can be realized on Li anode ex situ before assembling the batteries, or in situ during the operation of the batteries, through modifying the Li anode or introducing suitable additives in electrolytes.

1.2.3.1- Lithium Anode protection strategies

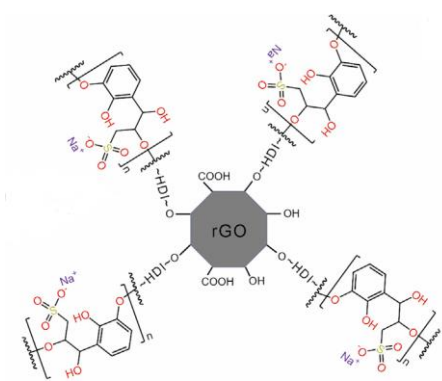


Fig.11 – Structure of graphene oxide (rGO) /lignosulfonate (SL) composite. Reproduced from ref.[20]

Solid polymer electrolytes with good Li^+ conductivity have been employed as a protection layer of Li anode. The protection layer covered on Li anode is synthesized by a cross-linking reaction of the curable monomer (poly(ethylene glycol) dimethacrylate) in the presence of liquid electrolyte (a mixture of tetra(ethylene glycol) dimethyl ether (TEGDME) and LiClO_4) and a photoinitiator (methyl benzoylformate). Compared with pure Li anode, the protected Li anode shows much improved charge–discharge characteristics. After 50 cycles, the protected Li anode shows a smoother and denser

surface morphology. However, owing to the sluggish Li^+ transport through polymer electrolyte, the introduction of polymer electrolyte on Li anode might compromise with the low discharge capacity at room temperature [7]

Tianyu et al. [20], introduced a “charge-repulsion” approach using a negatively charged multi-function graphene composite separator to effectively suppress the shuttling of the negatively charged PS ions.

A low-cost by-product of the chemical industry, lignosulfonate (SL), with abundant negatively charged sulfonic and dendritic groups, is used for the first time in Li-S batteries to suppress the PS

shuttling effect. By combining SL with reduced graphene oxide (rGO) through covalent bonds [Fig.11], they have created a rGO@SL composite with rich negative charges to enable a robust separator that can effectively retard PS shuttling while simultaneously ensuring excellent Li-ion transport characteristics. It can thus enable a highly robust Li-S cathode with extraordinary cycling stability, with <0.026%/cycle capacity decay for 1,000 cycles at 1.5 mg_S/cm² mass loading and <0.074%/ cycle decay over 670 cycles at 3.8 mg_S/cm² mass loading , both among the most robust cycling performances at comparable mass loadings reported to date.

With a strong charge environment effect to suppress the PS shuttling process while ensuring uniform Li-ion transport, the unique the design of rGO@SL/PP composite separator has enabled highly robust Li-S batteries with stable cycling performance over 1,000 cycles at a high current density of 5 mA/cm² (2 C) [Fig.12].

Lastly, it is important to note that the negatively charged separator can be easily integrated with other optimized electrode architecture by simply replacing the traditional separators with the newly designed separators without modifying the complicated electrode structure, and thus may be readily implemented with most advanced developments in the field to produce a rapid impact on practical technologies.

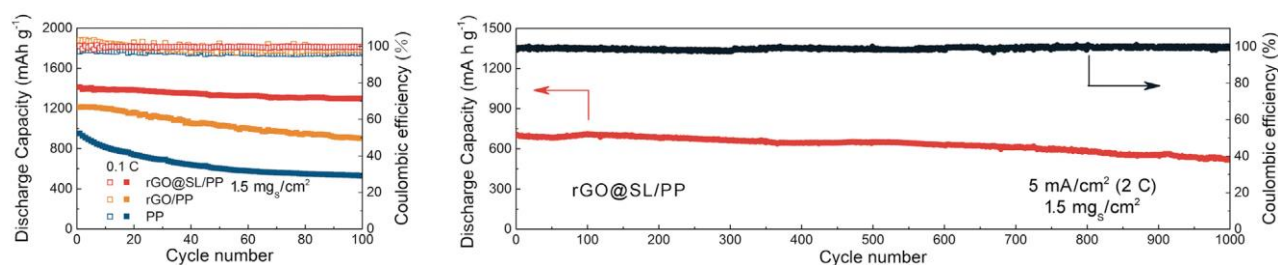


Fig.12 – Remarkable performance of Li-S cell thanks to the rGO/SL based barrier, on the left with 0.1 C of current, on the right at 2C. Reproduced from ref.[20]

1.2.4 – Electrolyte

The electrolyte is physically the very core of every existing battery concept, but at the same time is conceptually in the center of the studies of researchers and developers. The reason of this high amount of efforts is due to the growing awareness that many limitations to interesting parameters such as efficiency, life-length, and safety come from this specific component. Is indeed the second most studied component right after the cathode [Fig.8].

A critical point for any battery technology is the complex, multifaceted role to be filled by the electrolyte. In a generic way it can rather easily be summarized in some basic and general properties needed to be fulfilled to allow for a functional and practical battery:

- *ionically conductive,*
- *electronically insulating,*
- *thermally stable,*

- *chemically stable,*
- *electrochemically (meta-)stable,*
- *compatible with and wetting the electrodes and the separator,*
- *non-toxic/green*
- *low cost*

The exact demands on each property and approximate target values will of course differ by the battery technology, but also with the device operation conditions, the user demands, the installation requirements, and the market targeted.

Nevertheless, for the LIB technology there is more or less a standard electrolyte. On the contrary, due to the different and more complex chemistry, we cannot say the same about Li-S batteries. Yet, some of the parameters as well as assembling paths are really similar, because of the wide overlap of materials used.

A suitable electrolyte for lithium sulfur batteries is always selected taking into account the its chemical interaction with the polysulfides (PS). So, a good electrolyte for LiS should include the following attributes:

- *stability vs. Li metal anodes,*
- *stability vs. elemental sulfur and polysulfides (PSs) — both anions and radicals*
- *known and controlled solubility of PSs.*

The most often mentioned feature of Li-S batteries, mainly related to the last requirement above, is the PS redox shuttle mechanism. As described above in the dedicated anode paragraph, the

shuttle mechanism consists, in brief, of a chain of parasitic reaction that are detrimental for the metal anode: the result is a SEI formation on metal surface which has low Li^+ conductivity, leading to an inevitable loss of performance during cycling.

Moreover, the irreversible dissolution of active material in EL solvents lower the power density.

Unfortunately, this phenomena happens because of the high solubility of intermediate polysulfides in most of aprotic solvents used in liquid electrolytes.

Several strategies can be applied to limit the described drawbacks, the main three present in the literature are:

- *use of a solid state electrolyte, which indeed doesn't dissolve the PSs but usually has lower Li^+ conductivity compared to the liquid state ELs, thus leading to a low power flexibility (limited maximum*

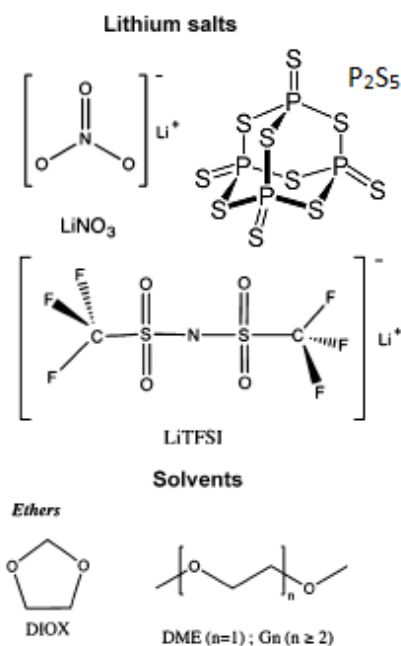


Fig.13 - Most used solvent, salts and additives in Li-S – Partially reprinted from ref. [24]

current). This interesting field has been deeply explored in recent years

- Polysulfides previously dissolved as conductive salts. Through this method, the quantity of active material that can be further dissolved is limited, but of course still anode protection is needed.
- specific salts addition that enhances the durability of Li anode by a stable as well as Li⁺ conductive SEI passivating layer. Lithium nitrate LiNO₃ and phosphorus pentasulfide P₂S₅ are widely used for this purpose.
-

1.2.4.1 – Standard solvents and salts for Li-S liquid electrolytes

The choice of electrolyte is a parameter of high importance and should be strongly taken into consideration. In particular, solvents need to be carefully selected in order to be chemically compatible with soluble, but also very reactive polysulfide species, especially S₃⁻. For example, Li₂S₂ soluble species (especially radical ones) are strongly reactive with carbonate-based electrolytes. As demonstrated by Yim *at al.* [21], polysulfides reacts with nucleophilic addition or substitution with carbonates species, leading to a sudden degradation of active material. Anyhow, there are some works in literature that successfully make use of carbon based electrolytes: Barchasz *at al.* [22] demonstrated the possibility of using alternative ether-based solvent with an high Donor number (i.e. high solvation ability); a conditioning parameter which influences PSs precipitation at the end of discharge phase.

The intrinsic nature of solvents, as well as their chemical and physical properties (especially viscosity), are fundamental to predict how the interaction with PSs will result in terms of solubility, mobility and reactivity into the electrolyte.

Majority of today's electrolytes are based on binary mixtures of different ethers, mostly 1,3-dioxolane (DIOX) and 1,2-dimethoxyethane (DME), usually in equal volumetric proportions.

[Fig.13] A whole family of high molecular weight ethers, such as diethylene glycol dimethylether

(diglyme, DEGDME), tetraethylene glycol dimethylether (tetraglyme, TEGDME), polyethylene glycol dimethylether (PEGDME), and 1,3-dioxolane (DOL or DIOX) has also been extensively studied [23]

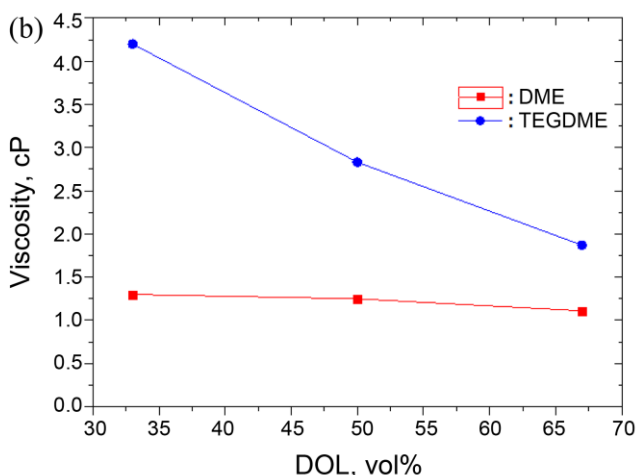


Fig.14 - Searching the optimal volume ratio of DME:DOL – TGEDME:DOL to have the lowest viscosity –Reprinted from ref.[26]

Gao *at al.* [25] did in 2011 an in-depth study about ether based electrolytes. Among different type of carbon based ELs, they found out that the most promising are a mix of DME:DOL (1,2-dimethoxyethane: 1,3-dioxolane) in 1:1 volume ratio and TEGDME.

DME is highly polar and has a large donor number (DN) of 18.6, enabling to solvate PSs and is most often used together with DOL, with an even larger DN of 24, which also acts to stabilize the Li metal anode surface by means of creating a solid electrolyte interphase (SEI).

(Li-S Batteries - The Challenges, Chemistry, Materials and Future Perspectives - Ch.4 - Lithium-Sulfur Battery Electrolytes - Ch - 4.2. Liquid Electrolytes - 4.2.1.1. Basic electrolyte formulations) TEGDME and DOL/DME electrolytes, with $\text{Li}^+\text{CF}_3\text{SO}_3^-$ salt dissolved, show the two classic distinct voltage plateaus at around 2.4 and 2.1 V, respectively, which was consistent with previous results in literature.

The first discharge plateau was 50 mV higher in TEGDME than in DOL/DME, but the second discharge plateau was 75-100 mV lower in TEGDME.

The differences could be due to the significant difference in viscosity between the solvents, which is one of the key parameter for a proper EL selection, thus having an influence to the local concentration (and possibly equilibria) of the elemental sulfur and polysulfides.

Looking at the graph above from Kim and Jeong report in 2011 [26] is possible to see that a mixture of DME:DOL has lower viscosity of about 1.20 – 1.25 cP (centipoise) ,almost constant as a function of volume fraction of DOL.

Indeed, the archetypical Li-S electrolyte, if any such really exists, is 1 M LiTFSI in 1:1 (v/v) DME:DOL. Furthermore, a quantity of 0.1-0.2 M of LiNO_3 is usually added for lithium anode protection. The effect of lithium nitrate is described briefly in the next subchapter [27].

In conclusion, due to the good properties described above, the “standard” EL composition has been used in for the experiments of this thesis.

1.2.4.2 – The use of LiNO_3 and P_2S_5 for an optimal protective SEI

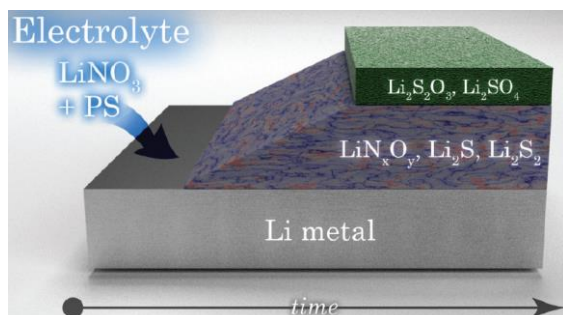


Fig.15 – The effect of Lithium nitrate on SEI formation on anode side. Reprinted from ref.[28]

The most popular approaches conducted in terms of electrolyte improvement are related with the use of additives. The commonly known one is lithium nitrate (LiNO_3), used to stabilize the metallic lithium surface as initially studied by Aurbach *et al.* [29] and followed by extensive reports of Zhang [30]: the passivation film formed with LiNO_3 is known to effectively suppress the redox shuttle of the dissolved lithium polysulfides on Li anode. On the cathode, LiNO_3 undergoes a

large and irreversible reduction starting at 1.6V in the first discharge, and the irreversible reduction disappears in the subsequent cycles. Moreover, the insoluble reduction products of LiNO_3 on th[] cathode negatively affect the redox reversibility of sulfur cathode. These results indicate that both the Li anode and sulfur cathode consume LiNO_3 , and that the best benefit of LiNO_3 to Li/S battery occurs at the potentials higher than 1.6V.

As a matter of fact, the potential range of charge/discharge cycles of all the galvanostatic tests has been set between 2.4 and 1.6 Volts.

The use of phosphorus pentasulfide (P_2S_5) as electrolyte additive has been also tested and proved as an efficient boost for Li-S batteries performance. Lin *et al* [31] found out that P_2S_5 has a double beneficial function:

- 1) P_2S_5 promotes the dissolution of Li_2S and mitigates the loss of capacity caused by the precipitation of Li_2S . The overall reaction transform the low soluble Li_2S and Li_2S_2 into highly soluble complexes (Li_2S_2 , Li_2S_4 , Li_2S_6 , Li_2S_8).

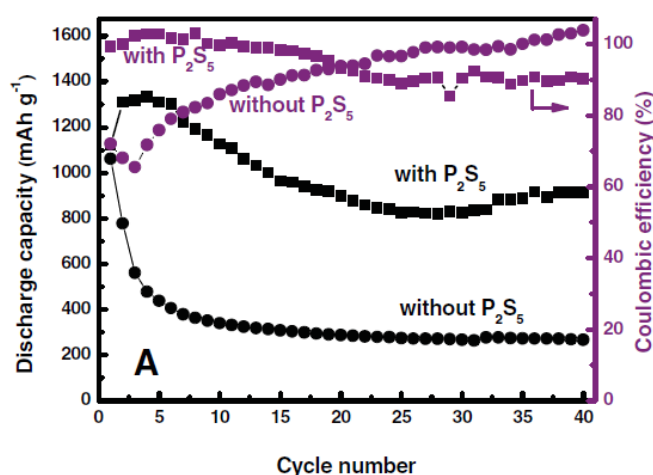


Fig. 16 - The beneficial effect of introducing P_2S_5 into the electrolyte. Reproduced from ref.[31]

- 2) P_2S_5 passivates the surface of lithium metal and therefore eliminates the polysulfide shuttle phenomenon. The major component of the passivation layer is Li_3PS_4 . The PL functions as the SEI with a dense structure that is able to conduct Li^+ while preventing access of the PSs to the surface of the metallic lithium. The protection of the lithium surface blocks the PSs shuttle and thus results in a high columbic efficiency for battery cycling.

The capacity retention of cycling Li-S battery was greatly improved when P_2S_5 was used as an electrolyte additive [Fig.16].

1.2.4.3 – Solid state Electrolytes (SSEs)

Alternatively to liquid electrolytes, solid-state lithium ion conductors, also named as solid electrolytes, have attracted great attention in recent years as promising alternatives to conventional liquid aprotic electrolytes.

Indeed, the use of solid electrolytes in Li-S batteries is able to address several key challenges caused by liquid electrolytes.

Solid state electrolytes (SSEs), present some intrinsic advantages with respect to conventional aprotic electrolytes [32] :

- SSEs are much safer than volatile and flammable liquid electrolytes in current Li-S batteries
- SSEs can inherently avoid the shuttle effect since soluble polysulfides cannot permeate into the solid electrolytes, in which direct electrochemical conversion between sulfur and Li_2S occurs instead of the formation of polysulfides

- SSEs exhibit high Li-ion transference numbers at room temperature, which is crucial to the uniform deposition of Li and the suppression of lithium dendrite formation.
- Furthermore some SSEs, such as $\text{Li}_2\text{S}-\text{P}_2\text{S}_5$ (Li_3PS_4), garnet-type $\text{Li}_7\text{La}_3\text{Zr}_2\text{O}_{12}$, and solid polymer electrolytes are compatible with Li metal anodes, and if combined show desirable stability at high voltages and can significantly boost energy density as well as overall cell performance.

For example, Agostini *at al.* [33] employed a glass type P_2S_5 - Li_2S solid state electrolyte. P_2S_5 - Li_2S presents a typical linear increasing of ion conductivity as a function of temperature, in line with other similar ceramic structures of P_2S_5 - Li_2S [34].

Moreover, the authors studied the ionic conductivity variation as function of pressure: by applying a sufficient pressure, the ceramic layer undergoes an increase on conductivity, may be due to the transition from cluster-like ordered structure to an amorphous structure that has higher conductivity. The main obstacle, was the poor contact between the SE and the cathode solid material, which leads to an increase of internal resistance. The assembled cell showed a very stable but low capacity, around 400 mAh/g.

2 - Materials introduction and experimental section

The goal of this work is to highlight the importance of the binders in preparation of cathodes in lithium sulfur cells. In particular not so much attention has been paid regarding sulfur load which is on the contrary a very important parameter especially when we want to compare Li-S cells with the mature technologies like Li-ion cells. However, this is not the objective of the thesis.

2.1 - Cathode materials characterization: sulfur, carbons.

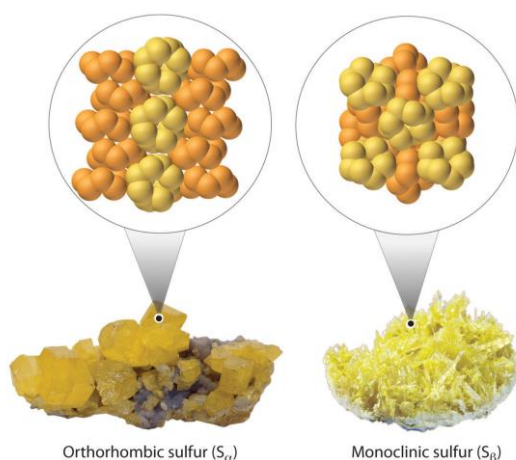


Fig.17 - Main allotropic forms of sulfur S_α and S_β – reproduced from ref.[35]

2.1.1 – Elemental sulfur

Elemental sulfur as an active material can be used as-received for the electrode preparation.

A conductive carbon additive is always needed in order to provide an electronic percolation of the whole electrode, given the insulation nature of sulfur.

Polymeric binder instead is used for bonding all the electrode components together, and provides sufficient adhesion to the current collector.

Sulfur is typically found as a light-yellow, opaque, and brittle solid in large amounts of small orthorhombic crystals.

Because it is 0.0384% of the Earth's crust, sulfur is the seventeenth most abundant element following strontium. Most sulfur is recovered directly as the element from underground deposits by injecting super-heated water and piping out molten sulfur (sulfur melts at 112 °C).

Known from ancient times (mentioned in the Hebrew scriptures as “brimstone”) sulfur was classified as an element in 1777 by Lavoisier. Pure sulfur is tasteless and odorless with a light yellow color. Samples of sulfur often encountered in the lab have a noticeable odor, because of very small quantities of H₂S gas are formed on the surface. Sulfur is the tenth most abundant element in the known universe [35].

2.1.1.1 – Physical properties and allotropic forms

Sulfur has an atomic weight of 32.066 grams per mole and is part of group 16, the oxygen family. It is a nonmetal and has a specific heat of 0.706 J g C . The electron affinity is 200 kJ mol and the electronegativity is 2.58. Not only does sulfur have twice the density of water, it is also insoluble in water. On the other hand, sulfur is highly soluble in carbon disulfide and slightly soluble in many common solvents. Sulfur can also vary in color and blackens upon boiling due to carbonaceous impurities. Even as little as 0.05% of carbonaceous matter darkens sulfur significantly.

Compared to other elements, sulfur has the most allotropes.

While the S₈ ring is the most common allotrope, there are over 30 different form.

At ambient temperature, the most common allotropic forms of Sulfur are S_α and S_β [Fig.17], both made up of S₈ molecules. At higher temperatures, Sulfur undergoes other structural transitions [35].

At any rate, for Li-S batteries is important to know how the sulfur behaves at different temperatures, in order to study even more better strategy of sulfur infiltration into carbon matrix:

- Monoclinic sulfur becomes liquid sulfur at 119 °C. Liquid sulfur is straw-colored liquid made up of molecules and other cyclic molecules containing a range of six to twenty atoms.
- At 160 °C, this becomes a dark, viscous liquid called Liquid sulfur. The molecules are still made up of eight Sulfur atoms but the molecule opens up and transforms from a circle into a long spiral-chain molecule.
- At 180 °C, the chain length and viscosity reach their maximum. Chains break and viscosity decreases at temperatures that exceed 180 °C.
- Sulfur vapor is produced when liquid boils at 445 °C. In the vapor that is produced, molecules dominate but as the vapor continues to heat up, the molecules break up into smaller groups of Sulfur. To produce plastic sulfur, S₈ is poured into cold water. Plastic sulfur

is rubberlike and is made up of long, spiral-chain molecules. If plastic sulfur sits for long, it will revert to rhombic sulfur.

2.1.2 – Conductive Carbons

One of the prime goal during the production of Li-S cells is to ensure an optimal hosting of the sulfur molecules. However, at the same time, both ionic and electronic conductivity should be guaranteed. To do so, a mix of Ketjenblack® (EC-300J, AkzoNobel) and Timcal®C45 high conductive carbon has been used. The KetjenblackC EC-300J is an high porosity carbon with a pore volume of 310-345 ml/g and an internal surface area of approximately 800 m²/g and a particle size about 30 nm. As it's possible to see in the picture [Fig.19] using KJB EC300J, and even more with the EC600J, you can ensure a really low resistivity with less than half of competitor's carbon loading .

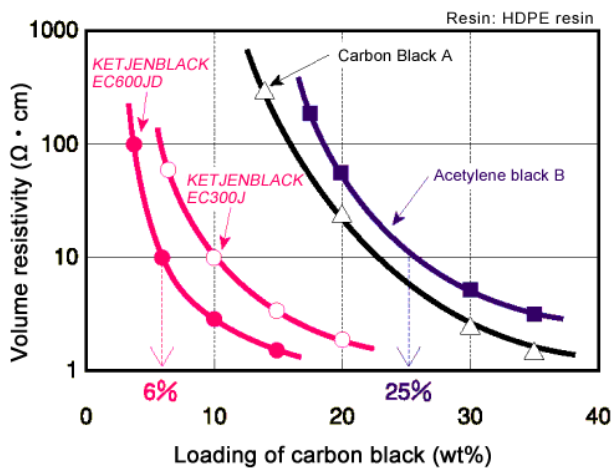


Fig.18 – Comparison of Volume resistivity, Ketjen black Vs. Carbon Black e Acetylene Black

As further additive, carbon black TIMCAL® SUPER C45 has been introduced as high electronic conductive carbon. The standard composition chosen for the cathode construction was usually a mass ratio of 70% of active material (Sulfur) and 30% of hosting material (KJB plus C45). Furthermore, a Further 7% to 10% of binder was added over the previous carbon sulfur mix.

The optimization of Sulfur infusion into the carbon structure was not count as main scope of the thesis, so, for a good mixing of the S/C powder a vibratory ball mill has been chosen. The whole procedure will be described further

on.

Another undertaken path has been the use of activated carbon for sulfur hosting instead of , via activated carbon structure (AC). Activated Carbon is well known for its high specific surface area due to its meso and micro porosities. In this material, the BET surface area is not linked to the grain size (Picactif®, 8000-15000 nm), but rather linked to the meso and micro porosities. Thanks to the superior porosity, an high number of internal channels are present, leading to a specific surface area up to 1900 m²/g. A comparison between AC and KJ carbons has been made in literature in the past by Barchansz *at al.* [36] .

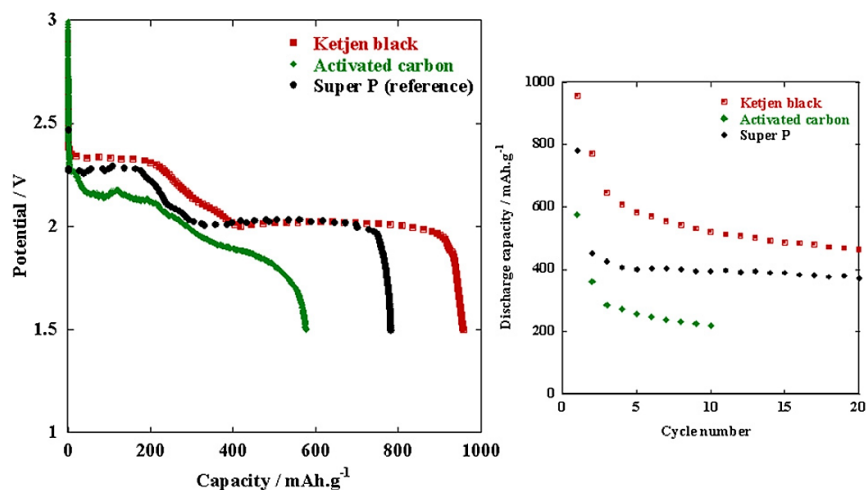


Fig.19 – Comparison of three different carbon as material for composite cathodes in Li-S, both in terms of potential curve and cycling behaviour. Reprinted from ref. [36]

A test of 20 cycles was performed by the author, using a composition of 80/10/10 % of carbon/Sulfur/binder (standard PVdF) for both the two type of carbon materials. Analysing the results, KJ cathode shows an improved initial capacity as well as a slower capacity fading during cycle, turning out as best among the two.

Thanks to the decrease of the

particles size, and the presence of micro porosities, the KB-based electrode surface area is assumed to be higher, even after sulfur dissolution, than that obtained for the AC-based one. As a result, the amount of passivation products that can be deposited on the electrode at the end of discharge could be increased, and the full electrode passivation can be delayed. On the contrary, the AC shows larger particle size along with meso and micro porosities. Surprisingly, despite the AC high specific surface value, the complete electrode passivation may not be delayed. Thus, it can be assumed that these micro and meso porosities may not be involved in the precipitation process due to their weak accessibility. The pores size may not be large enough to allow the polysulfides to quickly diffuse, and to homogeneously precipitate in the porous volume.

The change in carbon black material does not have a significant role on the cycle life. As the fading may be linked to the electrode pulverization, the carbon particle size and its specific surface area do not have a relevant impact on the resulting electrode morphology after one cycle. No matter which carbon additive is involved in the electrode composition, the morphology changes would be the same during cycling (sulfur dissolution and lithium polysulfide precipitation), and the electrode pulverization would occur anyway. As a matter of fact, and despite the interesting features of KB, the corresponding cell shows only 500 mAh g₋₁ after 20 cycles. As a conclusion, the KB carbon proves to be the most powerful material to improve the Li/S cell capacity. However, the resulting capacity still remains relatively low as compared to other reported developments, and this approach does not allow to significantly improve the electrochemical performances. To this purpose, a novel electrode architecture was developed based on the use of porous current collectors as positive electrode.

2.2 - Binders Analysis.

The first and main role of a binder in whatever Lithium cell cathode or anode, is to create a strong and durable connection between particles of active material and matrix structure. The most

common binders are indeed formed by polymers, whose long chain branches form a grid of connections inside the electrode.

The ramification guarantees also mechanical strength to the electrode which in many cases, like in Li-S batteries, have to undergo a significant volume expansion during discharge.

2.2.1 - Polyvinylidene Fluoride

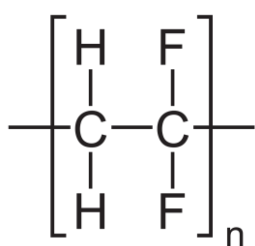


Fig.20 – PVdF monomer

Being the core of the thesis, binders will be studied starting from the most standard one, which is **PVdF** - Poly (Vinylidene diFluoride). PVdF [Fig.20] is well known to be chemically stable in organic solvents usually exploited in Li-ion cell. However, it has poor conductivity both from ionic and electronic point of view. Another negative side of PVdF is that, as solid

powder, it needs to be dissolved in **NMP** (N-methyl-2-pyrrolidone), which is a toxic solvent [58] really difficult to evaporate (boiling temperature of 203°C at atmospheric temperature) from prepared cathode ink. We indeed experienced very long time of evaporation of NMP from slurries. In addition, it is reported that NMP can dissolve sulfur to some extent and destroy the structure of active materials, thereby affecting the cycling performance of Li-S batteries [37].

Another negative characteristic has been demonstrated by Lacey et al: PVdF can block pores of highly porous carbon black of almost any size. This drawback occurs because of bad swellability of PVdF in widely used (DME:DOL)-based electrolytes, access of the electrolyte to the carbon

surface area and pore volume is so restricted, with potentially severe detrimental effects on the available capacity of the cell [38].

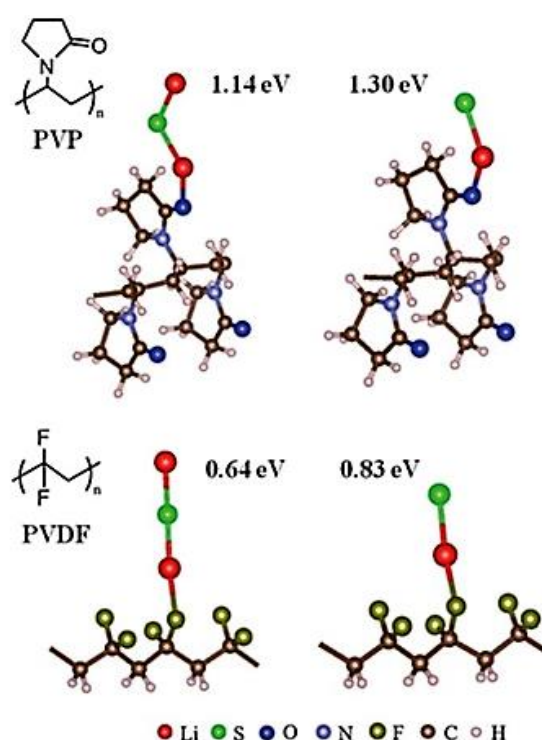


Fig.21 – Active (PVP) vs. Inactive (PVdF) binder, intermolecular force intensity with LiS and Li₂S. Reproduced from ref.[39].

The last issue, specifically important for this work, is the fact that PVdF cannot interact in a significant way with insoluble polysulfide.

Having not any functional group, the Van der Waals forces between fluorine atoms and Li₂S is not sufficiently strong to ensure a good trapping mechanism of polysulfides. In fact, the symmetric structure of fluorine atoms in PVdF chains make the polymer ineffective under coulombic forces point of view.

Other binders such as PVP [Fig.21], can increase the capacity retention of Li-S cells by forming a stronger bonds with lithium polysulfides, thanks to more complex functional group

2.2.2 - Sodium Alginate

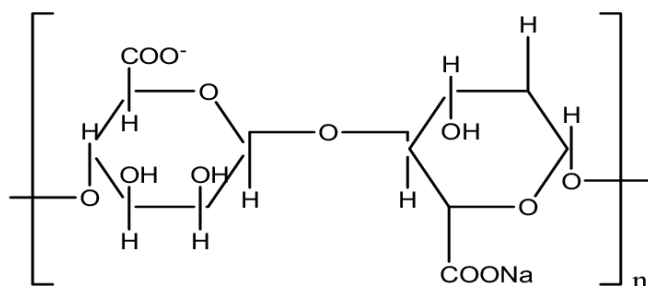


Fig.22 – Sodium alginate monomer.

Sodium alginate ($\text{NaC}_6\text{H}_7\text{O}_6$) is a linear polysaccharide derivative of alginic acid comprised of 1,4- β -D-mannuronic (M) and α -L-guluronic (G) acids [Fig.22]. Sodium alginate is a cell wall component of marine brown algae, and contains approximately 30 to 60% alginic acid. The conversion of alginic acid to sodium alginate allows its solubility in water, which assists its extraction. Bacterial alginates are

synthesized by only two bacterial genera, *Pseudomonas* and *Azotobacter*, and is used for protection from the environment and the synthesis of biofilms in order to adhere to surfaces. This method of synthesis allows the bacteria to produce alginates with a well-defined monomer composition, which may allow the production of “tailor-made” bacterial alginates.

The biggest advantage of alginates is its liquid–gel behaviour in aqueous solutions. When monovalent ions (eg, sodium in sodium alginate) are exchanged for divalent ions (especially calcium), the reaction proceeds almost immediately, changing from a low viscosity solution to a gel structure. The gelled mass is a copolymer composed of two kinds of monomer units.

Alginic acid is used as a hydrocolloid in various applications such as food manufacturing, pharmaceuticals and in

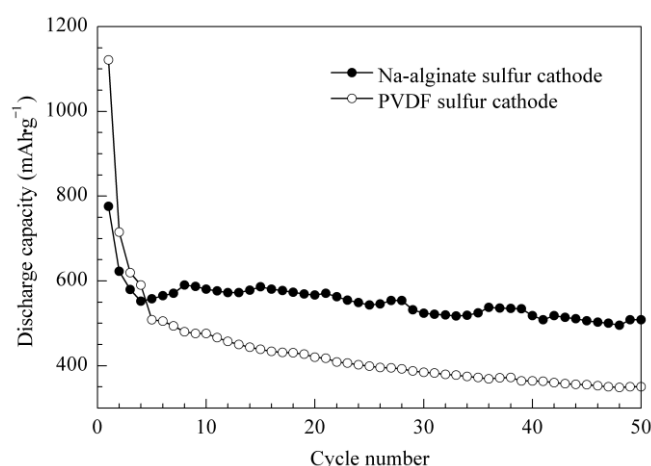


Fig.23 – Cyclability of Na-alginate Vs. Traditional PVdF – Reprinted from ref. [41]

textiles and cosmetics, particularly as an emulsifier, and is also used in dentistry to make molds. More recently, alginate have been studied extensively due to its tissue compatibility and use in tissue engineering, including the regeneration of skin tissue, cartilage, bone, pancreas, liver, muscles and nerves, in addition to being used in the encapsulation of cells for the controlled release of drugs [40].

Sodium alginate has been recently tested as binder in Li-S by Bao *at al.* [41], with good results of both from increasing capacity and capacity retention after several cycles [Fig.23].

The authors prepared cathodes using Na-alginate dissolved in water and PVdF dissolved in NMP for comparison. The alginate-based cathode showed a remarkably more porous structure with respect to PVdF, thanks to the good swellability. In this way, the electrolyte can reach more active material thus increasing the mass specific capacity. Furthermore, the

carboxyl functional group of the alginate can play an active role in retaining the polysulfides, hence limiting the loss of useful sulfur after long cycli

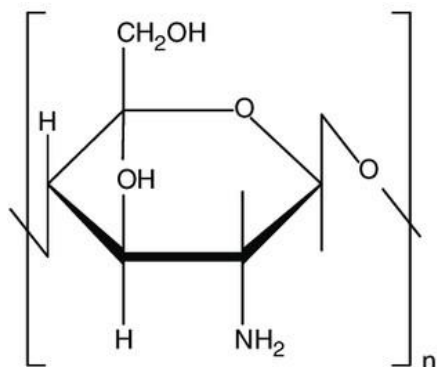


Fig.24 – Chitosan Monomer

2.2.3 - Chitosan

Chitin polysaccharide is a β -(1–4)-2-acetamido-2-deoxy-D-glucose (N-acetylglucosamine) with a structure similar to cellulose fibers. The difference between chitin and cellulose is due to the hydroxyl groups, which are replaced by acetamido groups in chitin. The main natural source of chitin is the shells of crustaceans (crab, shrimp and lobster), and is mainly obtained from the waste of fishing

industry. It is also be found in insects, molluscs and fungi. The major application of chitin is the production of chitosan [Fig.24], the deacetylation product of chitin, which has several applications. During the alkaline deacetylation (NaOH) of chitin, the acetyl bonds are broken to form glucosamine, which contains a free amino group. Chitosan cannot be considered to be a uniform polymer, but a partially acetylated polymer or a copolymer. Only polymers with a degree of deacetylation above 50% are considered to be chitosan. The properties and applications of chitosan depend heavily on the degree of deacetylation and the size of the polymer chain. Chitosan is soluble in dilute organic and inorganic acids, where it forms a viscous solution. These solutions are used to produce fibers, films and coatings. Due to these properties, chitosan can be used in several forms including gel particles, nanoparticles, membranes, fibers, nanofibers, sponges and in solution. Chitin and chitosan are biocompatible, biodegradable and non-toxic polymers, with biomedical applications in tissue engineering, wound healing, as excipients for drug delivery and also in gene delivery [40].

In 2015, Chen *at al.* [42] studied chitosan as functional additive for Li-S batteries. They demonstrated that Chitosan can effectively confine polysulfides: by adding chitosan in an Li_2S_6 -containing electrolyte, the initially intense brown color solution became shallow almost

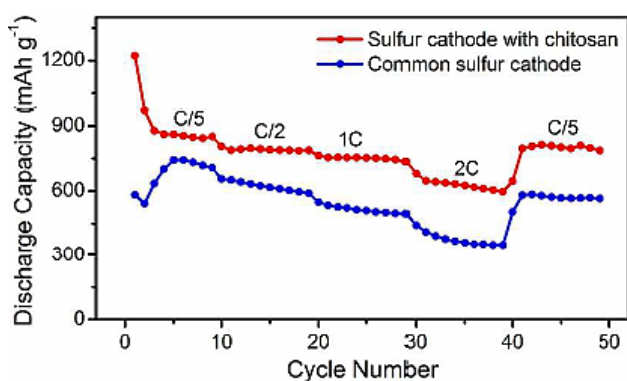


Fig.25 – Discharge capacity over cycling of C/S cathode with chitosan Vs. Traditional cathode. Reprinted from ref. [42]

immediatly, sign that chitosan absorbed polysulfides in the solution. Starting from this simple observation, the behaviour of chitosan in Li-S cathode can be further explained.

It is known that polysulfide easily dissolves into the ether-based solvents during discharge and charge due to the low viscosity of and salvation by the ether-based electrolyte. The hydroxyl groups or amine groups of the chitosan increased the surface hydrophilicity of the cathode with chitosan, which will be beneficial in

suppressing the shuttle effect by adsorption of polysulfide. On the discharge/charge of the battery, the migrating of polysulfide will be suppressed and immobilized by the hydroxyl groups or amine groups of the chitosan. The interaction of polysulfide and chitosan should have a clear effect on the electrochemical performance of the batteries, as verified by the added chitosan into the cathode that showed improved stability and capacity retention [Fig.25].

2.2.4 - Polyacrylic acid (PAA)

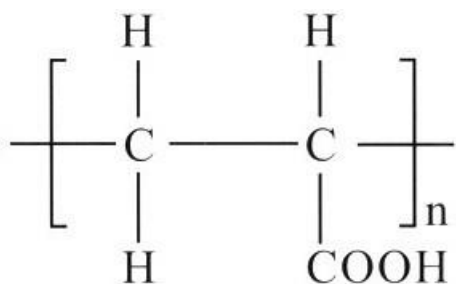


Fig.26 – PAA monomer

PAA is a polymer constituted by chains of acrylic acid monomers [Fig.26]. PAA is a polyelectrolyte, which means that is soluble in aqueous media (neutral pH), due to the ionization of the pendent carboxyl side chains. Thanks to its hydrophilicity, PAA in form of dried solid particles can quickly swell and absorb many times its weight of water, urine or other aqueous solutions.

Hence, PAA is widely used in diapers, adhesives, detergents and many other household and personal care products.

Polyacrylic acid is mainly synthesized by radical polymerization. The reaction can take many hours but can be dramatically accelerated by increasing the temperature and pressure. Molecular weight is a fundamental parameter especially as dispersant application, thus is crucial to control molecular weight distribution during the reaction.

In 2012, Zhang *at al.* [43] investigated the properties of PAA as a Binder for cathodes in Li-S

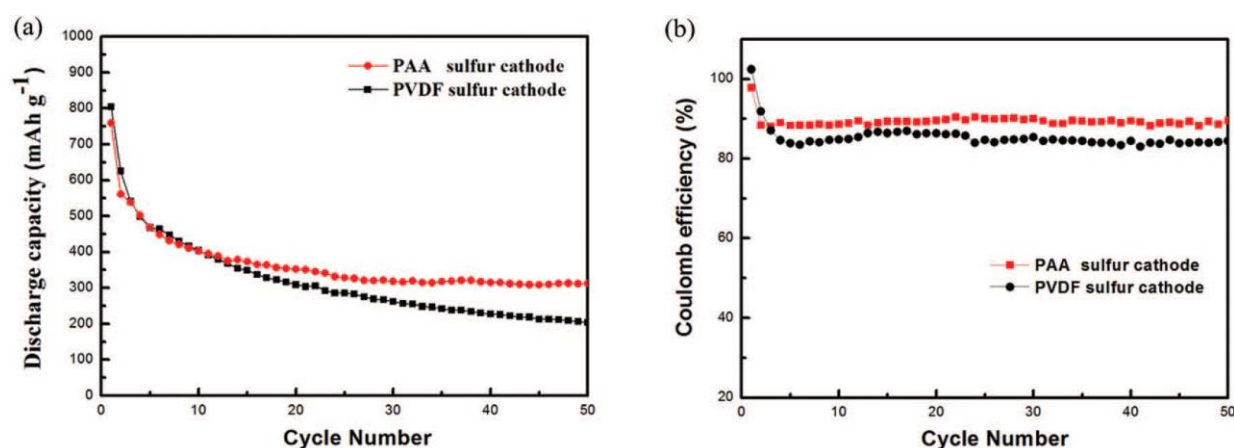


Fig.27 – Enhanced cyclability of a PAA containing cathode with respect to PVdF cathode. Reproduced from ref. [43]

batteries, as an alternative to PVdF both for performance improvement as well as avoiding the use of toxic NMP.

They found out that the cathode containing PAA showed a significant increase of conductivity due to a more porous internal structure with respect to the traditional PVdF, compared at the same C/S : binder mass ratio. That imply an improvement of initial capacity and capacity retention [Fig.27].

Other application of PAA in this field has been undertaken via the use of polymer as additive separator layer to avoid polysulfides shuttle effect on anode [44]

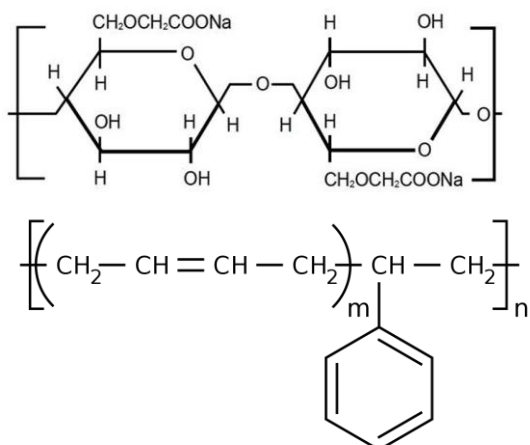


Fig.28 – Monomers of CMC (top), and SBR (bottom)

2.2.5 - CMC-SBR

CMC-SBR is a binder composed by two different components. CMC (carboxyl methyl Cellulose Sodium), is a sodium salt derived from polymer carboxymethyl cellulose. CMC polymer (also named cellulose gum) is obtained by substitution of some hydrogen with carboxymethyl groups in the hydroxyl group of the glucose monomers [Fig.28]. The degree of substitution, i.e. how many hydroxyl group are

replaced along the chain, is an important parameter which strongly influences the properties of CMC. For example water solubility is related to carboxymethyl groups presence.

CMC, which has two functional groups, carboxylate anion and hydroxyl, is well-known as an effective dispersion and thickener agent for aqueous suspension.

The addition of SBR (styrene butene rubber) [Fig.28], which is an elastomeric polymer, confers a

good flexibility, a stronger binding force and an higher heat resistance to the cathode.

Zhang *at al.* [45], successfully demonstrated how the use of CMC-SBR mix used as binder can effectively improve the performance of Sulfur cathode. Compared with conventional poly(vinylidene fluoride) (PVDF) binder, the SBR_CMC binder significantly improves cycling performance of the sulfur cathode. Studies on the electrode slurries show that the SBR_CMC mixture is

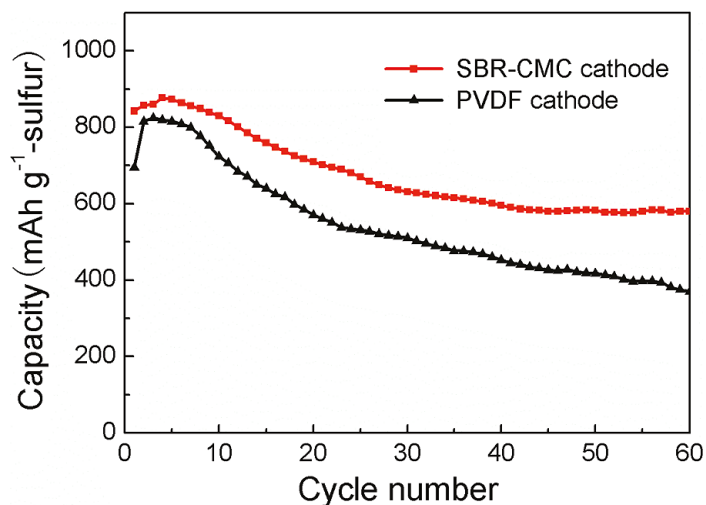


Fig.29 – Performance of CMC-SBR cathode Vs. PVdF. Reproduced from ref.[45]

not only a high adhesion agent but also a strong dispersion medium, which favors the uniform distribution between insulating sulfur and conductive carbon black (CB) and ensures a good electrical contact, leading to a high sulfur utilization. Furthermore, their experiments show that the improvement in cyclability [Fig.29] is ascribed to structural stability of the sulfur cathode promoted by the SBR_CMC binder during charge/discharge cycles due to the combined effects of homogeneous distribution of the S and carbon particles in the composite cathode, the low electrolyte uptake, and the suppressed agglomeration of Li₂S.

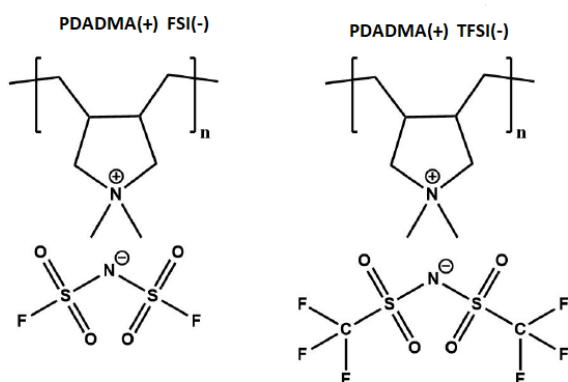


Fig.30 – Molecular architecture of the two monomer salts of the involved PEBs. Reprinted using ref. [46]

2.2.6 – Polyelectrolyte Binders

Promising electrochemical and dynamical properties, as well as high thermal stability, have been the driving forces behind application of ionic liquids (ILs) and polymerized ionic liquids (PILs) as electrolytes for high-temperature lithium-ion batteries (HT-LIBs) [46]. In this work instead, the use of PILs as polymeric binders (polyelectrolyte binders, in short **PEBs**) in lithium sulfur cells has been explored.

The experimented PEB of the thesis was essentially the salt Poly(diallyldimethylammonium) - bis(trifluoromethane)sulfonimide, in short called **PDADMA-TFSI**.

Three different molecular weight of **PDADMA-TFSI** were used: 500 kg/mol, 1000 kg/mol, and finally 380 kg/mol which has also a different anionic group, bis(fluorosulfonyl)imide **FSI** instead of **TFSI**. Both 500k and 1000k have an higher molecular weight with respect to the usual commercialized version, which is usually in range 200000-350000 g/mol [47].

As underlined by Li *at al.* [48], PEBs play a double active role concerning both the facilitated transport of lithium ions throughout the electrode, which is key to attaining fast S/Li₂S interconversion kinetics at high current densities, and restricted active material diffusion, which is critical in minimizing capacity fade at high sulfur loading.

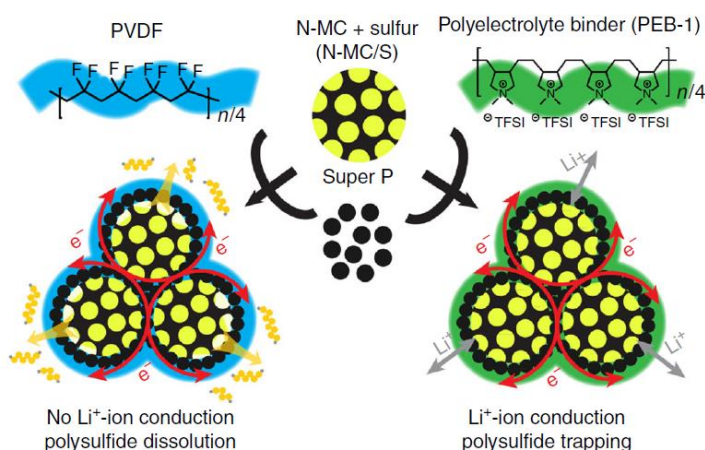


Fig.31 – The polysulfide trapping ability of PDADMA⁺/TFSI⁻, with respect to PVdF. Partially reprinted from ref. [48]

The PEBs in exam are designed to achieve a good ion transportation as well as reduced cell impedance by allowing Li-ion hopping along a plurality of weakly associated, and thus mobile, bis(trifluoromethanesulfonyl)imide (TFSI⁻) counter ions associated with the cationic polymer backbone.

An improved polysulfide retention is due to the hydrophobic and covalent character of higher order and electrolyte-soluble lithium polysulfides that leads to preferential and strong electrostatic interactions with the cationic polymer backbone (diallyldimethylammonium monomers), which could be leveraged to prevent their diffusion from the cathode on cycling. In fact, a significant

capacity retention (over 70% after more than 200 cycles at C/5 current rate), can be observed in cycling performance graph.

Finally, the areal sulfur load seems not to influence the capacity retention of the cell, so that potentially PEBs could lead to an easier scale up for industrial production of high performance Li-S batteries.

A likely explanation is that a significant fraction of the polysulfide trapping occurs at the interface of the electrolyte and the porous carbon host for sulfur-active materials.

Given that PEBs could be easily scaled to meet the demands for high-volume production, it may be a good choice for advanced Li-S battery manufacturing, as might other cationic polyelectrolytes with mobile anions (e.g., PF_6^- , TfO^- , FSI^-).

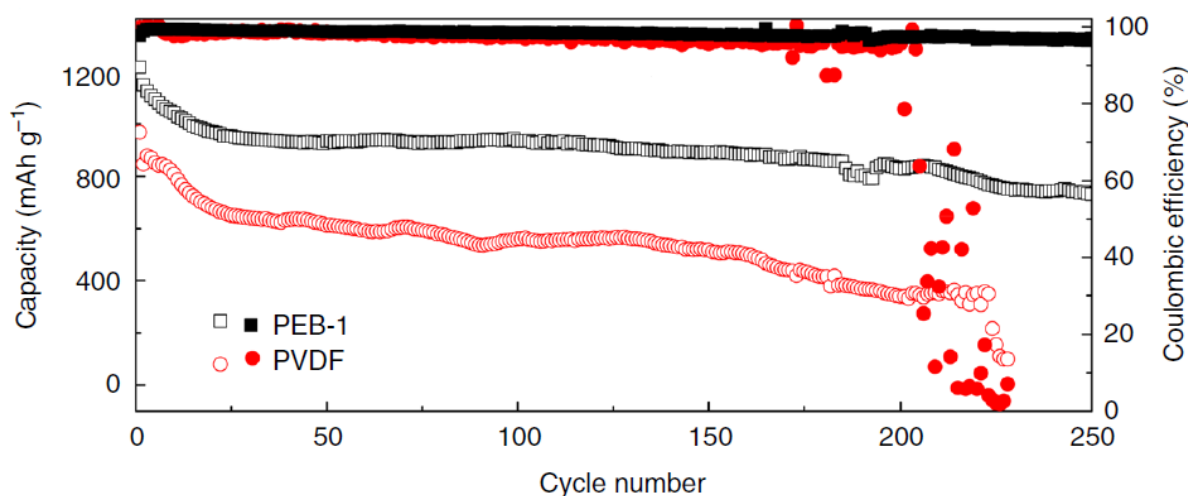


Fig.32 - The Greater stability of PEB after long cycling, compared to common PVdF cathode. Reproduced from ref. [48]

2.3 – Experimental procedure: materials preparation and cell assembling.

In this chapter will be described in detail how the cathodes have been prepared: from elemental solid sulfur and carbon, to final cell assembling in glovebox.

On the top a schematic view of the cathode construction process, ending with the final battery assembling in inert ambient (glovebox).

2.3.1 – C/S composite preparation.



Fig.34 – As received raw materials Aldrich 99% sulfur and Akzo Nobel Ketjenblack EC-300 J carbon

The process of creating every lithium sulfur cells starts from the cathode's raw materials: solid sulfur and solid carbon.

Two type of composite powder KJBC-S and AC-S have been prepared, and for each composite two different mass ratio have been chosen:

- KJBC-S (C/S **50:50** w/w)
- KJBC-S (C/S **30:70** w/w)
- AC-S (C/S **50:50** w/w)
- AC-S (C/S **30:70** w/w)

A really important clarification must be made: in case of 50% of sulfur only, the quantity of active material per unit surface is really low. Therefore, that part of the study is mainly made to show how a low quantity of sulfur leads to an higher stability of the cells over cycling with respect to an high sulfur load.

One gram per each composition has been prepared tailing the mass ratios reported above with the followings steps:

- The two as received material have been weighted in a small plastic square dishes [\[Fig.34\]](#)
- Subsequently, sulfur and carbon has been mixed in a mortar, in order to preventively crush the bigger aggregations of sulfur and make the powder suitable for the next step.
- The last step foresees an high energy mixing via vibrating ball-milling, in order to have a final homogeneous composite material



2.3.1.1 – Weighing and crushing the C/S powder

Using a KERN® balance (ABT 220-4M, max weight 220 g, sensibility 0.1 mg [\[49\]](#)), the two elemental components KJBC and sulfur have been weighted following the up described proportions. One gram of each the four composition has been produced, as it was sufficient to make an acceptable number of positive electrodes (average weight of prepared materials on cathode was around 5-6 mg). The steps of the procedure were:

$$(1) SE_{n,GM} = \frac{m_{GM}}{4} v_{rel,n}^2 (1 - COR^2)$$

$$(2) SE_{n,GV} = \frac{m_{GM}}{2} v_{rel,n}^2 (1 - COR^2)$$

$$(3) \overline{SE}_n = \frac{\sum_{i=1}^z SE_{n,i}}{z}$$

$$(4) P_{m,n} = CF \cdot \overline{SE}_n$$

$$(5) E_{m,n} = \frac{P_{m,n}}{m} t$$

- After taring the balance, the material has been placed into the above mentioned plastic plates for the weight reading. Especially carbon, which is composed by quite light and volatile particles, require an absolute stable air around the balance.

- Subsequently, the sulfur and carbon composite has been crushed and mix in an agate stone mortar

[Fig.35]. Besides making the composite powder homogeneous, this manual-mixing phase is also useful to crush sulfur bigger agglomerations.

- The resulting raw material has been stored in 8x8 cm square dishes and covered with aluminum foil. Now the C/S compound is ready to be treated in the vibrating ball mill.

2.3.1.2 – Ball-milling – Some theoretical notions

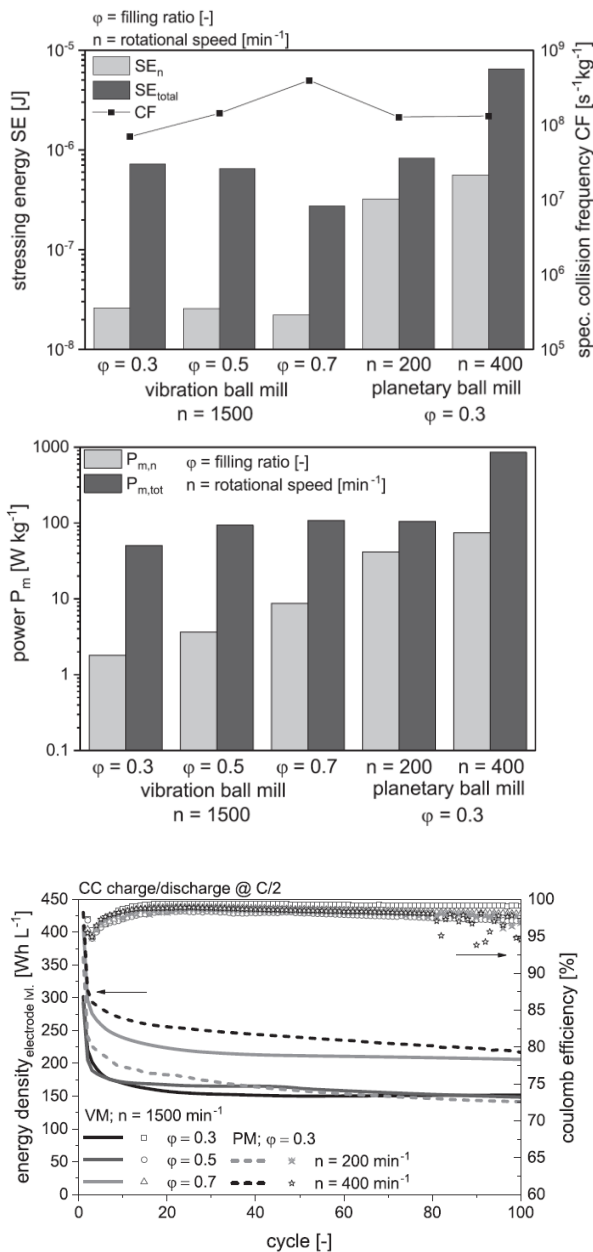


Fig. 37 – Stress energy, Power given to the mass in normal direction, and finally cells performances with VM treated cathode at different value of filling ratio ϕ
 Reprinted from Ref. [52]

A good indication of how the parameters should be in a material processing can be found in Titscher *at al.* work [52].

Titscher and his group studied the physics of ball milling by making use of a numerical method (DEM, Discrete Element Method). The purpose of the work was in fact to study how the ball milling technique influences the characteristics of the treated C/S mixture; in terms of particle size, energy transferred to the mass, and finally the effective energy per kg gained by the final product, (i.e. the positive electrode).

Differently on what has been done for this thesis, the chosen composition of study in [52] was a mass ratio of 35:65 (C/S).

In the study has been employed two kind of mill, the planetary mill and the vibration ball mill. For the second one, which is also the case of our study, the key parameters were: filling ratio of the grinding media ϕ (ratio between the volume of grinding media and the volume available in the vessel), frequency kept at 25 Hz, and working time fixed at 300 minutes for VM and 60 minutes for PM.

The choice of the time has been determined after FEM calculation of stress energy and mean stress energy ($SE_n, \overline{SE_n}$). The stress energy is proportional to the collision masses, the relative velocity between corpses, and coefficient of restitution COR (equation (1) and (2)).

COR is a dimensionless parameter take into account plastic or elastic properties of the media, and it depends on rolling and static friction coefficients μ_r , μ_s .

The values of **COR**, μ_r , μ_s must be experimentally measured and successively adjusted. COR has an interval of existence [0;1], COR=0 corresponds to a perfect elastic corpse, while COR=1 is the ideal case of totally plastic corpse.

The mean stress energy is the sum of the stress energy within a certain interval divided by the total number of collisions (equation (3)) in a certain interval.

The last two equations (4)(5) describes the given power $P_{m,n}$ and energy absorbed per unit mass by the C/S composite $E_{m,n}$.

The specific energy absorbed can be a really important parameter, if too high, the ball milling process could lead to an irreversible damage of the porous structure. A practical example of negative effect of too intensive treatment will be showed below.

Based on the selected process parameters of the milling process, different energy distributions of impacts in normal and tangential direction are expected. The regime of motion of the grinding media changes in dependence of the parameters chosen for the filling ratio, rotating speed, size of grinding media, and vessel volume, allowing to alter the number of normal collisions and frictional stress events.

Looking at the graph [Fig.37], we can see that for the higher value of φ the Li-S battery shows better performances both in terms of energy density and coulomb efficiency over hundreds of cycles.

This behavior can be explained by some physical considerations.

With an increase of the grinding media filling ratio the mean stress energy decreases for the individual media contacts within the vibration ball mill. Furthermore, based on the calculated total mean stress energy and the stress energy in normal direction, the main part of the stress energy takes effect in tangential direction. This leads to a high impact of friction energies and the fact that the highest stress energies can be achieved at a low filling ratio (vibration ball mill). A filling ratio of 0.7 leads to lower SE but promotes higher collision frequency simultaneously.

2.3.1.2 – Ball-milling – A practical approach

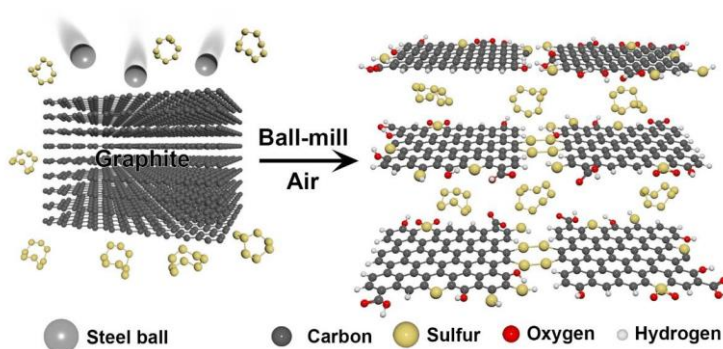


Fig.38 - Example of ball-milling effect on a Graphite – Sulfur mix – sulfur atoms are embedded into the graphite structure via intensive energy treatment– Figure Reproduced from [50]

For lithium-sulfur batteries it is very important to incorporate sulfur into the pores of the carbon material, as well as to distribute sulfur homogeneously within the electrically conductive carbon material. [Fig.38].

A mathematical study for the specific case of my experiments

has not been made. Indeed, the parameters **COR**, μ_r , μ_s require the proper instrument and laboratory experiments to be evaluated.

Furthermore, in order to know the real combination of normal and tangential forces, a dedicated simulation using DEM must be performed, and it would require itself a stand-alone essay. Basing on materials that were available at the laboratory, some initial parameters can be extrapolated. It must be again specified that the frequency and time were arbitrarily chosen by the literature. The same initial value of frequency of [52] has been used, equal to 25 Hz. The total time of processing has been set at 2 hours.

The available container in charge of hosting the grinding media were two Retsch® stainless steel vessels [Fig.40] with an available internal space of 10 ml. The internal jar's walls are made of a very hard layer of zirconium oxide, which delivers a negligible amount of contaminants even during intensive use. The same material forms the two grinding media, two \varnothing 12 mm balls. Knowing the diameter of the balls and the volume available inside the jars, is possible to calculate parameter ϕ :

$$\phi = \frac{2V_{GM}}{V_{vess}} = \frac{\frac{8}{3}\pi\left(\frac{D}{2}\right)^3}{V_{vess}} = 0,181$$

Due to the low filling ratio we can expect intensive mean stress energy and low collision frequency.

The total power given to the composite can be divided in two terms, the power due to the impact on normal direction (equation (4)), and a second terms which represents the power dissipated coming from tangential forces (friction):

$$P_{tot} = P_{m,n} + P_{tan} \quad eq. (6)$$

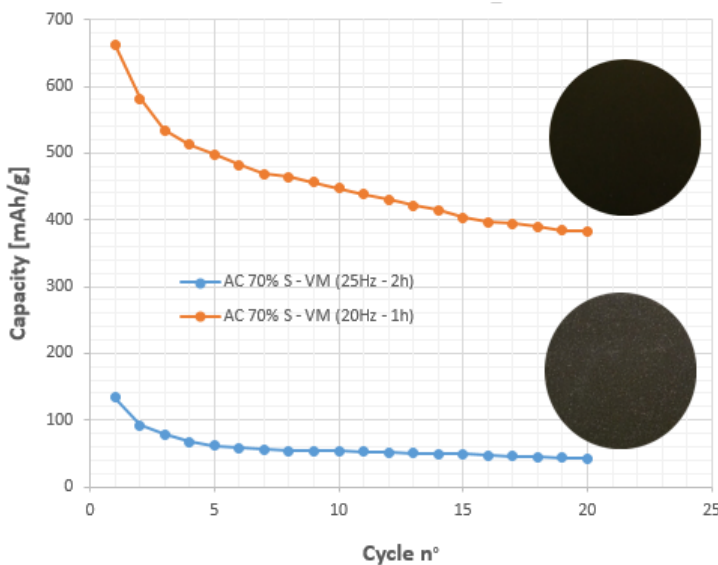


Fig.39 – A comparison between batteries performance in terms of cyclability. Activated carbon composite with 70% of sulfur using Vibrating Mill at 25Hz for two hours, and 20Hz for 1 hour. There are several glowing particles in the second cathode, which are the results of an intense action of friction forces

Or, in alternative can be also calculated knowing the torque M and the rotational speed n , both initial parameters set on VM display :

$$P_{tot} = 2\pi Mn \quad eq. (7)$$

Looking at the graph of the total power [Fig.37,(b)], it's clear that the more the filling ratio decrease, the more the power due to tangential forces (friction) is dominant.

Furthermore, in our case $\sim 1/5$ of the volume is occupied by the balls, that are quite free to move developing higher relative velocities and so higher

normal stress energies according to eq. (1).

In fact, the values of time and frequency initially set lead to an irreversible damage to the porous structure of activated carbon [Fig.39]. After the spreading of cathode ink, the resulted dried C/S composite (70:30 S/C), ready to be inserted in the cells, shows several glowing particles: because of the high intensity of the frictional forces between the grinding balls and the C/S composite, the AC turns to a sort of graphite form, very dense and hard. As a consequence, the binder cannot properly be in contact with particles because the internal channels were partially destroyed (AC has bigger particles but is reach in channels, i.e. high internal surface). Furthermore, during cell assembly in the glove box the material shows a poor suction ability with respect to the electrolyte, again for the same reasons explained above.

Therefore, in order to reduce the power and the total energy given to the mass (eq. from 4 to 7) , the values of frequency and time has been revised to 20 Hz and 1 hour of work.

The improvement in terms of performance can be seen in graph [Fig.39].



Fig.40 - In order from left to right: the 400 MM mixer mill, and the two milling cups. On the bottom a closer view of the user display

2.3.1.3 - Ball-milling - The steps of the process

After the treatment in the mortar, the C/S composite the two stainless steel/zirconia vessels were filled with 0.5 gram of material each and two zirconia balls. The two vessels have been accommodated a **Retsch® MM 400** vibration mill [51][Fig.40].

The MM 400 is a mixer mill

with several possibilities of regulation. The user can set the shaking frequency in a range from 3 to 30 Hertz, and working time from 10 seconds up to 99 minutes.

It's even possible to store up to 9 programs, with different time and frequency values.

Structurally is composed by two clamping devices in which two milling cups (vessels) can be hosted at the same time.

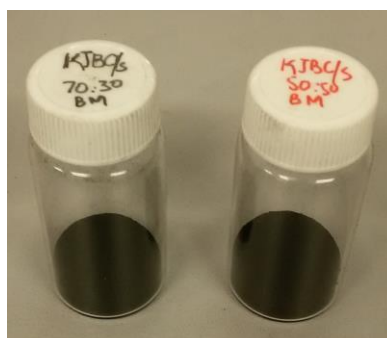


Fig.41 – the ball milled powder of 70:30 and 50:50 KJBC

The working principle of the mixer mill is simple: when the user starts the machine, the two cup holders oscillate with a certain amplitude (related to the length of the rotating arms), and with the predefined frequency.

The clamping devices possess a centering position with the function of maintain the jars in position. The intensity of clamping can be regulated using a black hand-wheel. At last, a

rotating pin can lock/unlock the hand-wheel, which could eventually unscrew during the operation due to vibrations.

More details on the right use of MM 400 can be found in the manual [53].

By making a double grinding in parallel, an equilibrium of inertial forces can be ensured, having the same corpses on right and left holder.

Moreover, more material at the same time can be processed, promoting the time optimization and laboratory organization.

Using the digital display [Fig.40], we set the key parameters of time and frequency at 20 Hz and 30 minutes. The treatment of one hour has been completed in two steps of half hour with a break in between.

The material tends to stick on zirconia walls after some time of treatment, especially in case of composites with 70% of Sulfur. In order to ensure an homogeneous mix, the powder need to be removed from the walls using a lab spoon or spatula.

The same time and frequency as well as method of 30 minutes load/break/30 minutes load has been applied to the four compositions (see chapter 2.3.1).

The after-milling composite was always reduced by several time in volume with respect to the initial condition. Both the as received carbon, especially the KJBC, were quite light, volatile and massive.

In this way it was possible to store the total of 1 gr. of C/S powder in small glass jar [Fig.41]

2.3.2 – Development of Li-S cathode: ink realization and spreading, drying on Aluminum foil and electrodes cutting.

From now on, the work is divided in two different part:

- 1) For each of the composition showed in subchapter 2.3.1 a quantity of 7% in weight of each binder has been added in ink preparation procedure. In this first part we wanted to analyze not only the effect of the binder on performances, but also compare the behavior of activated carbon and Ketjen black carbon.

For each of the four C/S composite, five binder (CMC:SBR, chitosan, alginate, PAA and PVdF) have been tested for a total of 20 combinations.

Due to the high amount of combinations, only 20 cycles have been performed for each cell.

- 2) A long Cycling test (100 cycles) in which chitosan and alginate cathode(renewable binders) have been compared to PVdF and the three PEBs cathode described before (all synthetic), in a 10% ratio in mass using a 70% sulfur C/S KJBC composite.

2.3.2.1 – Ink preparation: insertion of the binders

As the C/S composite is now well mixed and Sulfur is embedded into the carbon structure, the composite is ready to be mixed with conductive carbon and the binder.

Firstly a 2.5 ml Eppendorf® tube with round shaped bottom has been placed in a 10 ml glass beaker. Inside the tube two small Ø 3 mm stainless steel balls have been introduced. The function of the balls will be explained further on.

Secondly, all these objects have been weighted on the KERN® balance (ABT 220-4M), which has been set on tare mode.

Now, a mix of C/S, conductive carbon and binder has been created for all the 20 combinations, as follow:

- 100 mg of C/S powder has been withdrawn from the glass jar [Fig.41]
- An additional quantity of 10 mg of electro-conductive carbon super C45 Timcal® (see subchapter 2.1.2) has been added to the powder in order to improve the conductivity of electrons, for a total mass of 110 mg of **KJBC/S/C45**, or **AC/S/C45**.
- The calculation of 7% in weight of the binder quantity is based on those 110 mg; the following proportion has been used:

$$110 [mg]: 93 = X [mg] : 7$$

$$X = 8.28 [mg]$$

Given the mass corresponding to 7%, each binder was available in a different form:

Sodium Alginate: available in 5% w/w solute/solvent. A “gelatin” like semi-solid solution, very dense and viscous, with a turbid yellow appearance [Fig.42]. In order to extract from the solution the right quantity of alginate the following calculation has been made:

$$m_{binder,sol\%} = m_{binder,7\%} * \frac{\%solution(solvent + solute)}{\%solvent}$$

$$m_{alginate,5\%} = 8.28 [mg] * \frac{105}{5} = 173.9 [mg]$$

Poly-acrylic acid (PAA): available in 5% w/w solute/solvent. A “gelatin” like semi-solid transparent solution, very dense and viscous [Fig.42]. In order to extract from the solution the right quantity of PAA the following calculation has been made:

$$m_{PAA,5\%} = 8.28 [mg] * \frac{105}{5} = 173.9 [mg]$$

Chitosan: available in 3.75% w/w solute/solvent. A “gelatin” like semi-solid solution, very dense and viscous, with a turbid yellow appearance [Fig.42]. In order to extract from the solution the right quantity of alginate the following calculation has been made:

$$m_{chitosan,3.75\%} = 8.28 [mg] * \frac{103.75}{3.75} = 229 [mg]$$

Polyvinylidene Fluoride (PVdF): directly available in solid form, as a white and very volatile powder.

CMC:SBR: the only case in which the binder is constituted by a combination of two species. The combination has been empirically chosen as 1:1 w/w mass ratio, so a total of 4.14 mg SBR + 4.14 mg CMC. SBR was available in form of very light and volatile solid, difficult to manage because very sensible to electrostatic fields.

CMC instead was at disposal as highly concentrated emulsion, with a pale brown appearance.

[Fig.42]

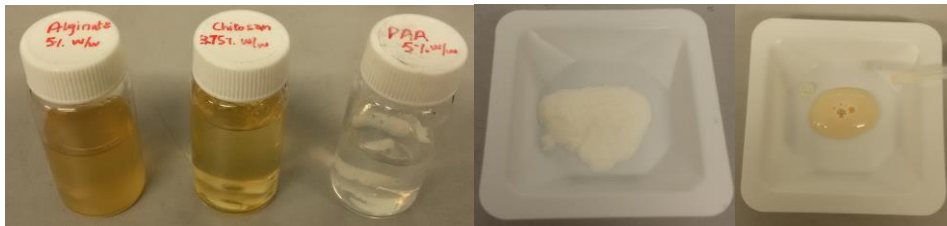


Fig.42 – In order: sodium alginate, chitosan and PAA solution. On the right solid CMC and the brown emulsion of SBR.

- For the long cycling part of the study, the calculation of binders’ mass is similar:

$$110 [mg]: 90 = X [mg] : 10$$

$$X = 12.22 [mg]$$

Sodium Alginate: available in 5% w/w solute/solvent. A “gelatin” like semi-solid solution, very dense and viscous, with a turbid yellow appearance [Fig.42]. In order to extract from the solution the right quantity of alginate the following calculation has been made:

$$m_{binder,sol\%} = m_{binder,7\%} * \frac{\%solution(solvent + solute)}{\%solvent}$$

$$m_{alginate,5\%} = 12.22 [mg] * \frac{105}{5} = 256.67 [mg]$$

Chitosan: available in 3.75% w/w solute/solvent. A “gelatin” like semi-solid solution, very dense and viscous, with a turbid yellow appearance [Fig.42]. In order to extract from the solution the right quantity of alginate the following calculation has been made:

$$m_{chitosan,3.75\%} = 12.22 [mg] * \frac{103.75}{3.75} = 338.09[mg]$$

PEBs: directly available in solid form. They required a dried room to be weighted.

- The various binders required to be dissolved in a solvent to form the ink together with the mixture KJBC/S/C45. All the binders are soluble in water with the exception of PVdF and PEBs. PVdF as well as PEBs must be dissolved in NMP, a toxic solvent described previously. To do so, some initial quantity of solvent has been added into Eppendorf® tube to start the partial dissolution of the binder.
- As reported in literature, to help the dissolution of chitosan, a drop of formic acid has been added to the water solvent (volume varying from 500 to 800 µl) [53.b].

2.3.2.2 – Ink preparation: exploiting the MM 400 mixer for an homogenous ink



Fig.43 – The ink ready to be mixed inside the Eppendorf Tube

Now, the material is ready to be mixed properly with the solvent to make an homogeneous ink. This goal has been achieved by exploiting again the Mixer mill MM 400.

Firstly, a piece of tape has been wrapped around the top of the tube’s plug, in order to avoid the leaking of the mixture [Fig.43]. Successively, the tube has been placed into one 25 ml milling cup similar to the one used before.

Once closed, the milling cup has been placed into the mixer mill holder. A mixing program at 20Hz and 20 minutes of time has been set, making a break in between at 10 minutes to qualitatively check the viscosity.

In absence of a viscometer, the viscosity was verified empirically by opening the tube and checking the mobility of the balls inside the ink.

The up described metal balls inside the tube serves the scope of stirring the ink during mixer mill shaking.

An important note must be reported : very often some polymers, especially chitosan and alginate, needed some additional time to swell.

For that reason very often the mixture has been left to rest more in between and also after the mixing.

In some cases, instead of solution form [Fig.42], alginate has been directly dissolved in solid form [Fig.44], because the “jelly”-like behavior of the solution make it very sticky and difficult to weight in small quantities. If on one hand solid alginate was easier to manage,



Fig.44 – Solid sodium alginate

on the other hand required longer period to swell properly.

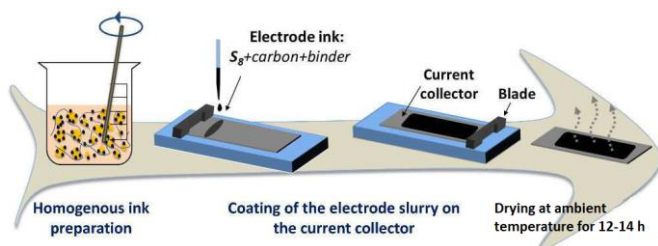


Fig.45 – A schematic view of the ink preparation pathway divided in four step. Picture mostly imported from Walus’ thesis, ref. [23], Ch. 2.2

2.3.2.3 – Ink spreading and drying onto Aluminum foil

Once the ink, often named at this phase “slurry”, can be considered sufficiently fluid, but not too liquid, the work can proceed with the spreading on the aluminum foil, in order to form a thin layer which will act as a cathode. The aluminum

foil will act as a base structure of our composite cathode, but at the same time being a conductive metal will work as current collector.

The chosen Al foil it was also covered with a thin layer of carbon on one side, in order to improve the adhesion forces between the current collector and the cathode material (C/S, once dried) .

The cathode realization pathway is illustrated at [Fig.45], in details the steps undertaken in the lab were:

- Firstly, the aluminum foil has been lied down on a glass sheet. In order to obtain a perfectly smooth surface as well as create a perfect adhesion, some drop of pure ethanol has been put between the Al-lamina and glass surface. The adhesion forces of ethanol molecules will also help to keep the lamina fixed in

position on the next step. A further piece of tape has been used for this purpose.

- Now that the foil is ready, a **BYK-Gardner® 2101 Automatic Film Applicator** [54] has been exploited to create a smooth film from material ink. The Gardner 2101 is formed by a large base [Fig.46,(a)] in which the glass and with the aluminum foil will be located. On the top of the base there is a traverse of carriage able to move back and forth with a predefined velocity from 50 to 500 [mm/s] [Fig.46,(b)]. For further details see the manual at Ref.[56].

Using the command display [Fig.46,(c)], is possible to regulate the speed of the bar, with an increment of 10 mm/s.

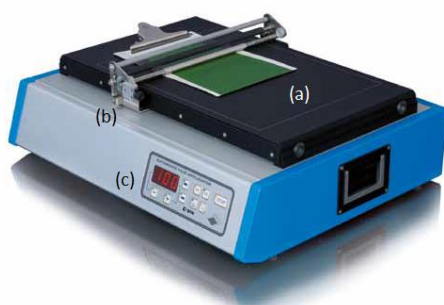


Fig.46 – BYK-Gardner® 2101 Automatic Film Applicator. (a) the base, (b) traverse of carriage, (c) command display. From Ref. [54]

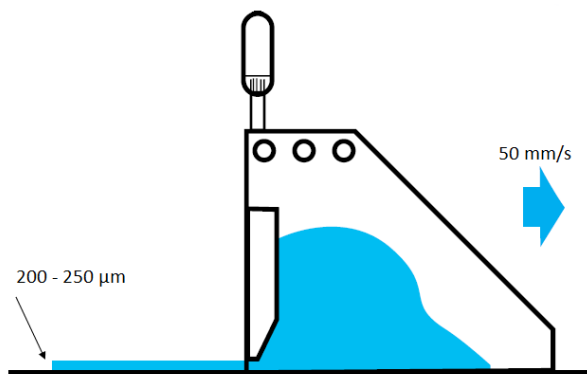
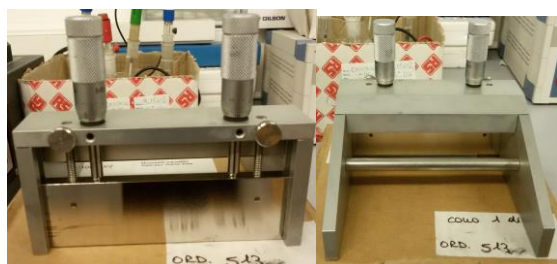


Fig.47 – The doctor blade front and back, and it’s working

- Once the foil is ready on the film applicator, it's time to extract and distribute the slurry in a single row on the short side of the rectangular Al-foil. For this scope, a pipette has been used [Fig.45, step 2].
- At this point, a **Doctor Blade** [55][Fig.47] has been used to smear uniformly the ink. The thickness of the spread material can be chosen by rotating the two micrometer's knob [Fig.47].

In our specific case has been chosen a variable thickness between 200 and 250 micrometer [μm], essentially depending on the behavior of the slurry in terms of viscosity. The more is viscous, the more will require a lower thickness.

Once the Doctor Blade is positioned back to the fresh ink row and leaning to the traverse, the procedure of spreading can start by pushing the forward button. When the ink is totally distributed, the doctor blade can be removed and the traverse of carriage will return by pushing the backwards button (see the manual [56] for all the display functions; slide 26). A schematic view of ink spreading at [Fig.45], step 2 and 3.

- Finally, the distributed slurry can be put under the laboratory hood, at ambient temperature and pressure for drying for 12 – 14 h. This phase is particularly important for the binders dissolved with NMP, because it is both toxic and difficult to evaporate. Below are reported some example of different binders after the evaporation [Fig.48].



Fig.48 – The dry C/S/B preparation. In this example the case of the cathodes for long cycling with 10% of Binder.

2.3.2.4 – Cutting of the electrodes and drying after vacuum.

After 12-14 h of drying, now it's time to check if the slurry is sufficiently dry, without any visible presence of solvent. Usually the NMP requires a lot of time to completely evaporate (low vapor pressure at ambient temperature (25°C)[57]) even if is subject to continuous ventilation in a laboratory hood. On the other hand it has also a good interaction with many organic molecules and structures being an aprotic solvent with high polarity [59], even if they are weakly polar or non-polar (PVdF and Carbon Black for example).

For this reason the slurries treated with NMP results qualitatively more homogeneous and with less imperfections than water ones.

Water for its part requires lower time to evaporate and it is obviously non-toxic.



Fig.49 – Hohsen® 16 mm puncher [60]

Anyhow, now the electrodes can be cut from the dried inks, to do so, an Hohsen® Ø 16 mm cells puncher

[60][Fig.49] has been

used. For reason of availability for the long cycling part of the study a Ø 15 mm cells puncher has been used instead. Depending on the effectiveness of the slurry spreading, a different number of electrodes are available for cutting [Fig.50].

Now that the cathodes are ready, has been located in handmade aluminum bags [Fig.50], with the exact composition and date of fabrication reported in a label. In Order to eliminates further residual of solvent present in the electrodes, a Büchi® B-585 glass oven dryer [61] has been exploited. The cathodes undergoes a temperature of 50°C under vacuum for 5 hour. The Büchi® has different possibilities of settings in terms of



Fig.51 - Büchi® B-585 glass oven dryer [61]

temperature and time of operation [62]. It's possible to set and save different programs with predefined values, or even set several temperature values in different time intervals. At the end of the final drying the positive electrodes are ready to be inserted in the glovebox,



Fig.50 – On left An example of a good spreading of cathode ink, with 13 cathodes cutted (50:50 KJBC/S-PVdF). On the right the Al-bags that hosts the cathodes.

where they will be weighted and will be the main study component during the coin cell assembly.

2.3.3 – Battery assembly

2.3.3.1 – Inside the Glovebox



Fig.52 – The mBraun® glovebox [63].

After the drying of the last traces of solvent, the Al-bags have been entered into the glove box. The Glove box (mBraun® [63]) is an inert chamber filled with an inert gas (Argon in our case), pressurized by a compressor. The chamber is sealed with the exception of two intermediate chamber for communication (small and big). Thanks to these two openings is possible to take out or take in materials and tools, being careful about refilling the volume with Argon before every direct communication with the space work. In the upper part at the same side a command display is present. It is possible to set the chamber in different operating modes (work and rest), and switch off/on the lights inside. Furthermore, the

instant values of water and oxygen concentration are measured by some distributed probes and are continuously displayed on the control screen.

Generally they are both under 1 ppm, excluding anomalies such operator's error. In case of hazard, a red flashing message will appear on the control display.

In Li-S assembly, is fundamental to have an inert ambient due to the high reactivity of metallic Lithium with oxygen but especially with vapor.

The gum gloves, from which the instrument's name comes from, will allow the operator to manage materials and instruments inside the box maintaining at the same time the internal ambient unchanged in terms of physical properties and chemical composition.

2.3.3.2 – Coin Cells assembly

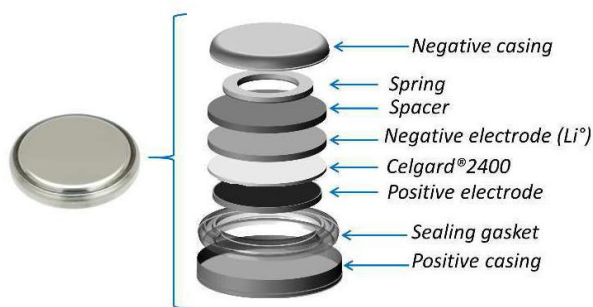


Fig.53 – All the components of a Li-S coin cell. Picture mostly imported from Walus' thesis, ref. [23]

The coin cell system, is the most used in the lab due to its simplicity and reduced dimension. Through this system is possible to test small samples of material. Moreover, is easy to allocate many small cell in multi-channel board for testing at the same time. A further advantage, is the simplicity of sealing: at the ending phase when all the components are in the right place, the cell can be closed in a single strike using a specific puncher designed for the CCs (coin cells).

The making of a cell begins in the glove-box by cutting the anode i.e. the metallic lithium from a row foil.

Pure Li was available as a tape-like form (width of some centimeters) rounded to form a compact coil.



Fig.53 – A simple punch, often used in other fields like leather precessing

A simple \varnothing 16 mm round shaped punch has been used as cutting tool [Fig.53].

Metallic lithium is really soft and it can be easily cut without any hummer

Now that the lithium is ready, the work can proceed with next components.

Some precautions must be taken we manage pure lithium: an excessive amount of Li traces after the contact with the gloves could cause damages to the cathodes, because of local short circuit (direct reactions between lithium and sulfur during cycling. For this reason it is advisable to manage pure lithium through the use of a little clamp,

possibly in plastic such that will not damage the lithium surface, very soft and easy to pierce.

The next step foresees one of the most important operation of the entire work: the weight of the cathode.

The positive electrode with the desired binder composition must be taken out from the aluminum bags carefully. Then, it can be weighted into a balance KERN-ABT 220 4M [49] located into the glove box. It was not an easy task with respect to the atmospheric ambient, the pressurized inside make the balance more unstable, requiring more time to find the equilibrium around a precise value.

The weight of the cathodes usually oscillates around 13-15 milligrams. The weight will be useful to calculate the amount of sulfur, and so the right current to impose for testing.

In the next step, the components of a coin cell [Fig.53] are one by one pick up and disposed on a clean piece of paper in the glove-box's plane. Since in our case the sealing gasket was directly stuck on the negative casing, the order of negative and positive external casing has been reversed with respect to Walus' procedure [Fig.53][23].

Therefore, the positive casing has been leaned upside down, and the cathode located inside it making use of plastic nippers, with the active material, the C/S/binder up.

From a practical point of view, the roles of male (now positive) and female (now negative) caps have been reversed.

In order to have a sufficient pressure and contact between the various components, two stainless steel separators for **CR20** [66] coin cells has been placed on male cap.

Afterwards, it's time to insert the electrolyte into the cell.

The composition of the electrolyte was the classic **1 M LiTFSI in 1:1 (v/v) DME:DOL + 0,25 M of LiNO₃** [68], with the latter lithium nitrate present for Lithium anode protection, as explained in previous chapters.

The volume of electrolyte must be proportional to the mass of sulfur effectively present, so it's necessary to interrupt briefly the work and go outside the glovebox, and calculate the mass of S. First of all, the mass of the current collector must be subtracted from the total mass. To know the exact weight of the Al Foil, about ten \varnothing 16mm , \varnothing 15mm diameter disk has been weighted, extrapolating a the mass as an average of the measured values of both the dimensions. As a results, the average masses were respectively 10.7 mg for 16mm and 9 mg for 15mm:

$$\bar{m}_{Al} = \frac{\sum_{i=1}^n m_{Al,i}}{n} [mg]$$

Now that the Mass of Aluminum is known, it's possible to calculate the mass of the ink:

$$m_{ink} = m_{tot} - \bar{m}_{Al} [mg]$$

For every sample prepared, 10 mg of high conductivity (C45) carbon where added over the 100 mg of KJBC/S , AC/S. Furthermore, on those 110 mg of total material two different percentages of binder **B%** has been foreseen, 7% and 10% depending on the study.

So the percentage of composite C/S, can be calculated as follow:

$$m_{C/S,\%} = (1 - B_{\%}) \left(\frac{m_{C/S}}{m_{C/S} + m_{C45}} \% \right) [-]$$

Finally, to obtain the mass of Sulfur:

$$M_S = m_{ink} \cdot m_{\%,C/S} \cdot S_{\%} [mg]$$

With **S%** that can assume the value 0.7 or 0.5, being 50% and 70% in mass of Sulfur the two ratios chosen for the study.

Once the amount of Sulfur is known, the proportional volume of electrolyte has been withdrawn using a Socorex® 10-100 [μl] micropipette [Fig.54]. The standard value used for all the experiments is 10 [μl]/mg(s) , even though is known that in order to be competitive with the LIBs in terms of energy density, the value should be 3-5 [μl]/mg(s) [64].



Fig.54 - Socorex® micropipettes in three different scales (1-10,10-100, 100-1000) [μl]

As Ning et al. reported in [64], the quantity of the electrolyte also depends on the porosity of the cathode material, i.e. the effective quantity of electrolyte depends on how much “empty” volume must be filled.

Since the objective of the thesis is centered on the effects of the binder, a conservative way to act is to keep the amount of EL at a high value, sacrificing the effective energy density (i.e. the energy calculated on the total weight of the battery), but at the same time being sure that the electrolyte will reach every part of the internal channels into the porosity structure. The microscope analysis (SEM) was not available, so it was also impossible to discover the exact value of porosity after the ball milling treatment.

Given the right amount of electrolyte, the volume has been distributed for 2/3 of its value on the cathode, and for 1/3 on the separator. A \varnothing 20mm **Celgard®EH2010 (trilayer PP/PE/PP)** [65] separator has been punched from an as received sheet, for this purpose.

The separator has been leaned on the male caps’ borders and successively wet with the electrolyte. The diameter of 20 mm was a reasonable choice to wrap completely lithium, avoiding any contact with the positive electrode which could cause a short circuit.

In the next phase, \varnothing 16 mm lithium has been carefully placed into the center of the separator using a proper plastic nipper. It’s the most delicate step of the procedure, since if the lithium disc is not perfectly in the center, it could be really difficult to press correctly all the materials together.

Now, a further spacer has been put over the negative electrode, and finally manual pressure has been applied on the top of it: in that way, lithium, separator and cathodes can be sufficiently in contact. Before coupling the female cap with the male one containing all the pressed components previously described, a metal spring has been located over the last spacer. After the final cell crimping, the spring will generate a force to keep all the battery constituent in position.

To do the final closing, a glovebox (Ar-filled) compatible **KCG® Digital Pressure Controlled Electric Crimper E160** [67] for CR20XX Coin Cells has been used directly into the glovebox.

3 – Outcomes and discussion

In this chapter are finally collected all the data about the various trails made on cathodes. The graphs has been divided by both the kind of carbon structure (AC or KJBC) and the percentage in mass of sulfur present.

A particular attention has been paid regarding the last study, in which the cells must endure for hundred cycles. In that part the so called “innovative binders” also defined as “electroactive” (due to their attitude of an electrostatic interaction with PSs), are tested and compare with Alginate and Chitosan the innovative binders who demonstrated to be sufficiently stable during time and relatively easy to threat.

3.1 – Galvanostatic Testing: software and instruments.

All the cells have been tested using the software **Arbin® MITS Pro (version 4.32)** [69].

Knowing the right amount of sulfur, every cell has been tested imposing a steady current of C/5. C/5 means a current that will make the cell discharge in 5 hours, in the ideal case of specific capacity of 1672 [mAhg⁻¹]. Of course, as can be seen in different studies in literature, the capacity will be lower. Because of several reasons analyzed through the literature in previous chapters, the active material cannot be exploited completely. Part of it will be lost due to dissolution of PSs, another part maybe can be reached because of inhomogeneity, and not perfect conductivity, of the porous structure that hosts it.

Anyway, the ideal case value has been taken to calculate the current as follow, given the M_s mass calculated in chapter 2.3.3.2 :



Fig.56 – 8 Channel board for cell testing [70]

$$I_{\frac{C}{5}} = \frac{1672 \left[\frac{\text{mAh}}{\text{g}} \right] * 10^{-3} \left[\frac{\text{g}}{\text{mg}} \right] * M_s [\text{g}]}{5 [\text{h}]} \quad [\text{A}]$$

The same formula has been used in the long cycling part of the study to calculate the C/10 current of the first cycle, putting 10h instead of 5h. A lower current serves to “stabilize” the cell at the first cycle for a long cycling test.

Given the calculated current, the coin cell has been inserted in a **8-Channel testing board** [Fig.56][70]. The Board is directly connected to an **Arbin® Tester**, which can impose

different degree of current up to 10 A and 10-20V.

For such a small application, all the current for the tested cells fell down in the range of 10⁻⁴ – 10⁻³ Ampere.

In [Fig.57], under **Step Label** column of the testing program, the three steps of every cycle are shows:


- **Rest:** the cell is set at resting mode for 3 minutes, during this time the OCV (Open Circuit Voltage) is measured after 30 seconds.
- **Discharge:** the current previously calculated is imposed with a negative sign. The voltage limit is set as 1.8 V, i.e. the cell will be discharged until the 1.8 potential is reached. Every minute the actual voltage value is saved, but also other DV_time can be selected basing on necessities.

	Step Label	Number Of Limits	Control Type	Control Value	Extra Control Value 1	Extra Control Value 2	Current Range
1	Step_A	2	Rest				
	Log Limit	Step Limit	Goto Step	Type1	Sign1	Value1	Type2
1	<input checked="" type="checkbox"/>	<input checked="" type="checkbox"/>	Next Step	PV_CHAN_Step_Time	>=	00:03:00	
2	<input checked="" type="checkbox"/>	<input type="checkbox"/>		DV_Time	>=	00:00:30	
2	Chg_2	2	Current(A)	-0.000298			Low
	Log Limit	Step Limit	Goto Step	Type1	Sign1	Value1	Type2
1	<input checked="" type="checkbox"/>	<input checked="" type="checkbox"/>	Next Step	PV_CHAN_Voltage	<=	1.8	
2	<input checked="" type="checkbox"/>	<input type="checkbox"/>		DV_Time	>=	00:01:00	
3	Dischg_2	2	Current(A)	0.000298			Low
	Log Limit	Step Limit	Goto Step	Type1	Sign1	Value1	Type2
1	<input checked="" type="checkbox"/>	<input checked="" type="checkbox"/>	Next Step	PV_CHAN_Voltage	>=	2.6	
2	<input checked="" type="checkbox"/>	<input type="checkbox"/>		DV_Time	>=	00:01:00	
4	Step_G	2	Set Variable(s)	Reset	Increment	Decrement	
	Log Limit	Step Limit	Goto Step	Type1	Sign1	Value1	Type2
1	<input type="checkbox"/>	<input checked="" type="checkbox"/>	Chg_2	PV_CHAN_Cycle_Index	<=	10	
2	<input checked="" type="checkbox"/>	<input checked="" type="checkbox"/>	End Test	PV_CHAN_Cycle_Index	>=	10	

Fig.57 – The program interface, with several possibilities of limits and values.

- **Charge:** the current previously calculated is imposed with a positive sign. The voltage limit is set as 2.6 V, i.e. the cell will be charged until the 2.6 potential is reached. Every minute the actual voltage value is saved.
- **Set Variable(s) – Number of cycles:** in the last phase the number of cycles is set to a fixed value, in our case 20 or 100 cycles. The program will return every time on the selected “Go To Step” phase, in our case the discharge (Chg in the figure), until the imposed number of cycles are completed.

The program described above can be stored in a chosen folder and then charged on the desired channel using the “Monitor & Control” window [Fig.58] by right-clicking on the channel row and using the option “Assing program”.

In the monitor and control window several instant parameters are showed in “real-time”, such as voltage, current, charge and discharge capacity. Once the program is assigned, the test can begin by selecting “Start Channel” .

Afterwards, a window will appear where it’s possible to give a name to the test and write some additional information in a text box. For instance, to simplify the successive data elaboration and interpretations, the following data of the cathode were listed:

Channel Name: MS_ACTCS_20HZ_ALG_NHT_CG1

Cathode Weight: WT 14.9 [mg]

Sulfur Weight: WT S 0,00177555 [g]

Test Date: 17/01/2018

Once the channel is operating, into the “**Status**” column, different messages can appear [Fig.59], depending on the current status of the operating cell.

In standard galvanostatic testing conditions, apart of “**Charge**” and “**Discharge**” indications, other important messages are “**Rest**” that means the cell is in resting phase, i.e. no current is flowing but the measure of the voltage is in progress. Other normal messages are “**Finished**” that indicates that the test is done, and “**Idle**” when the channel is empty with no cells inserted.

(0)/0/0	Test Name	Schedule Name	Status	Step Index	Cycle Index	Step Time (s)	Test Time (s)	Voltage	Current	Charge Capacity	Discharge Capacity	Charge Energy	Discharge Energy
001		test.sdu	Idle	1: Step_A, Rest	1	00:00:00	00:00:00	0.0000 (uV)	0.0000 (uA)	0.0000 (mAh)	0.0000 (mAh)	0.0000 (mWh)	0.0000 (mWh)
002		test.sdu	Idle	1: Step_A, Rest	1	00:00:00	00:00:00	0.0000 (uV)	0.0000 (uA)	0.0000 (mAh)	0.0000 (mAh)	0.0000 (mWh)	0.0000 (mWh)
003		test.sdu	Idle	1: Step_A, Rest	1	00:00:00	00:00:00	0.0000 (uV)	0.0000 (uA)	0.0000 (mAh)	0.0000 (mAh)	0.0000 (mWh)	0.0000 (mWh)
004		test.sdu	Idle	1: Step_A, Rest	1	00:00:00	00:00:00	0.0000 (uV)	0.0000 (uA)	0.0000 (mAh)	0.0000 (mAh)	0.0000 (mWh)	0.0000 (mWh)
005		test.sdu	Idle	1: Step_A, Rest	1	00:00:00	00:00:00	0.0000 (uV)	0.0000 (uA)	0.0000 (mAh)	0.0000 (mAh)	0.0000 (mWh)	0.0000 (mWh)
006		test.sdu	Idle	1: Step_A, Rest	1	00:00:00	00:00:00	0.0000 (uV)	0.0000 (uA)	0.0000 (mAh)	0.0000 (mAh)	0.0000 (mWh)	0.0000 (mWh)
007		test.sdu	Idle	1: Step_A, Rest	1	00:00:00	00:00:00	0.0000 (uV)	0.0000 (uA)	0.0000 (mAh)	0.0000 (mAh)	0.0000 (mWh)	0.0000 (mWh)
008		test.sdu	Idle	1: Step_A, Rest	1	00:00:00	00:00:00	0.0000 (uV)	0.0000 (uA)	0.0000 (mAh)	0.0000 (mAh)	0.0000 (mWh)	0.0000 (mWh)

Status	Indication
Idle	Channel is not being used.
Rest	The charge/discharge circuits are disconnected from the test sample, but the Voltage measurement circuit is still connected.
Charge	Present measured channel current is positive.
Discharge	Present measured channel current is negative.
Pulse	Channel is generating current or Voltage pulses
Internal Resistance	Channel is executing internal resistance diagnostic.
AC Impedance	Channel is executing AC impedance diagnostic.
Unsafe	Value of any parameters exceeds the safety limit set in schedule Global page.
External Charge	MITS Pro disables the current and Voltage control of the main channel and records the current that flows through the External Charge adaptor.
Wait	MITS Pro is waiting for some condition on one or more channels to be realized before proceeding with the schedule sequence. (used with SAFOR systems)
Finished	The test has proceeded to completion and terminated according to scheduled limit conditions.
Transition	The microcontroller has delayed data acquisition while it is processing operations associated with step changes.
AddIn	MITS Pro maintains a waiting condition on a channel while attempting to attain AddIn Values .

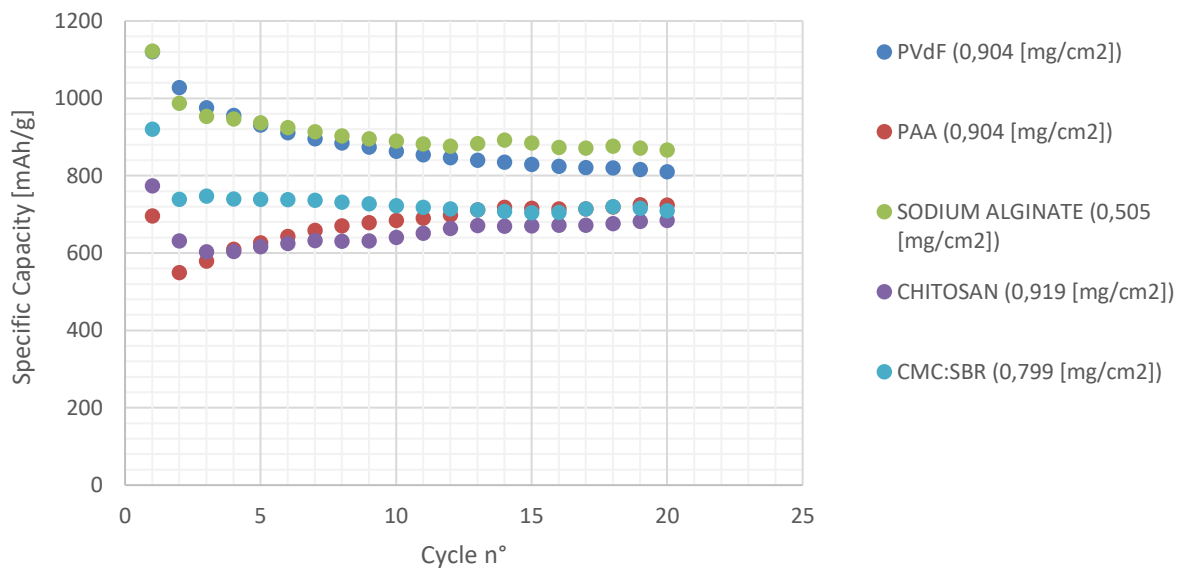
Fig.58 - the view of the Monitor & Control window, with all the real time measured values and messages.

In Fig.59 below are reported all the possible indication about the instant cell conditions.

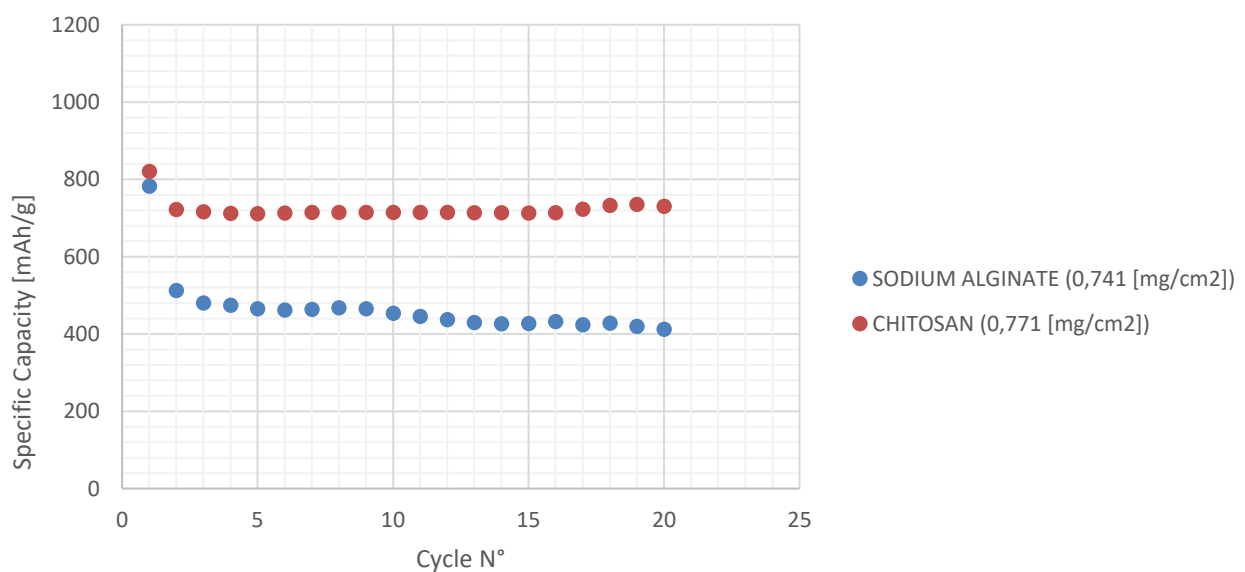
3.2 - A Study of cathodes with low mass content of biodegradable binders: challenges, results, comparison with traditional binders.

3.2.1 – AC and KJBC cathodes with low content of sulfur - Graphs

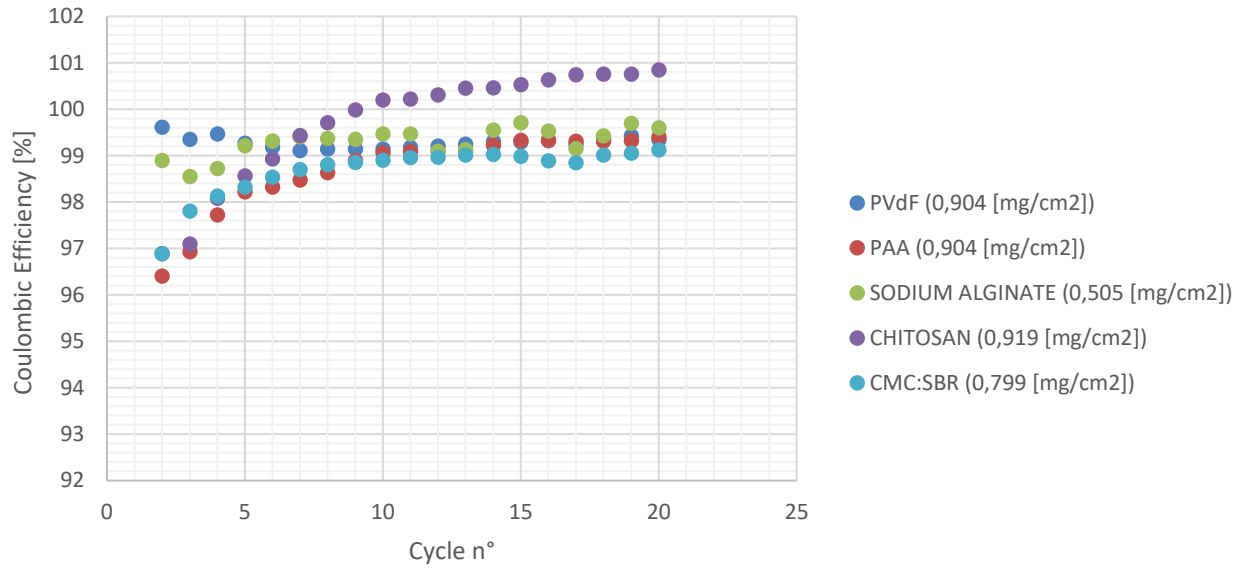
Graph.A1 - KJBC cathodes with 50% of Sulfur - Specific Capacity Vs. N° Of Cycles



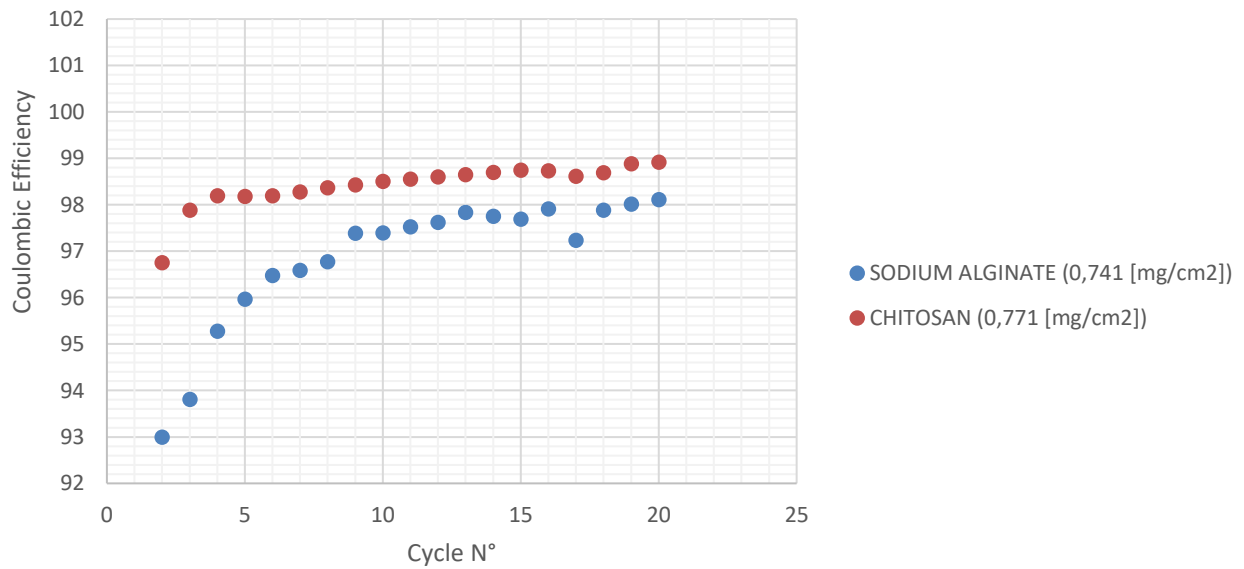
Graph.A2 - Activated Carbon with 50% of Sulfur - Specific Capacity Vs. N° Of Cycles



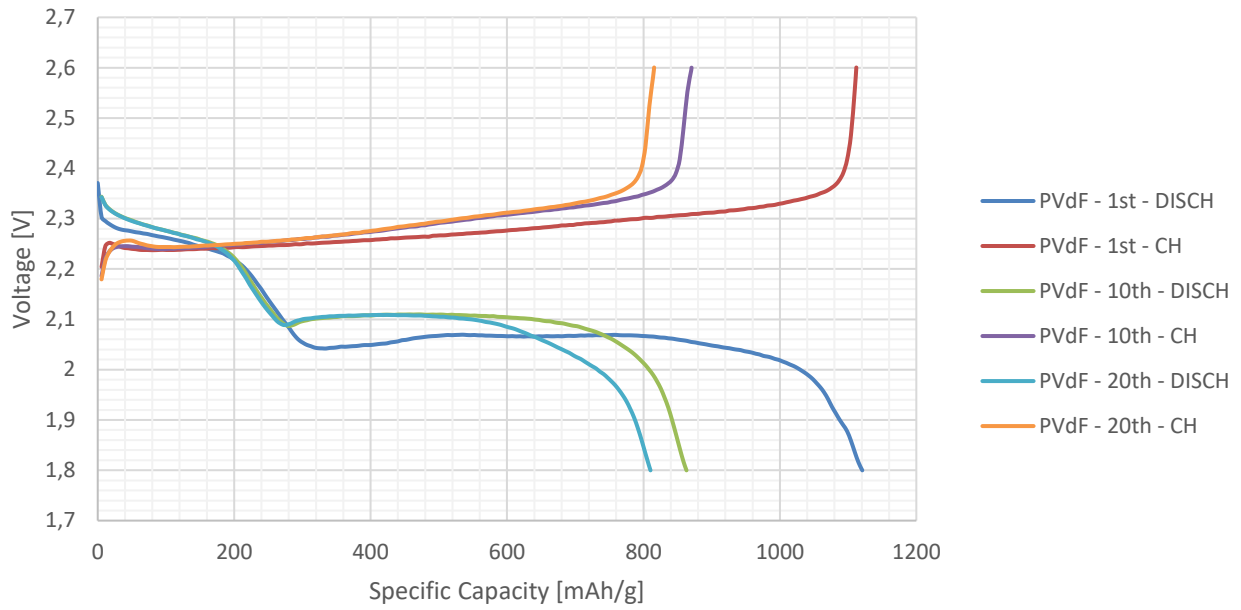
Graph.A3 - KJBC cathodes with 50% of Sulfur - Coulombic Efficiency [%] Vs. N° Of Cycles



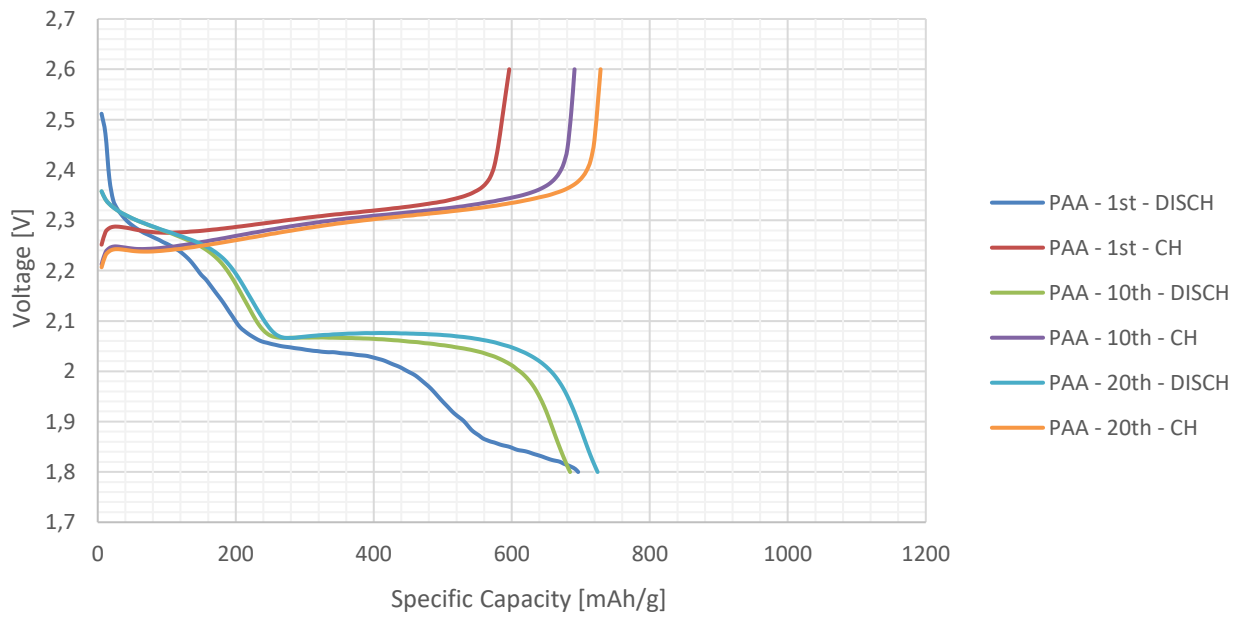
Graph.A4 - Activated Carbon with 50% of Sulfur - Coulombic Efficiency [%] Vs. N° Of Cycles



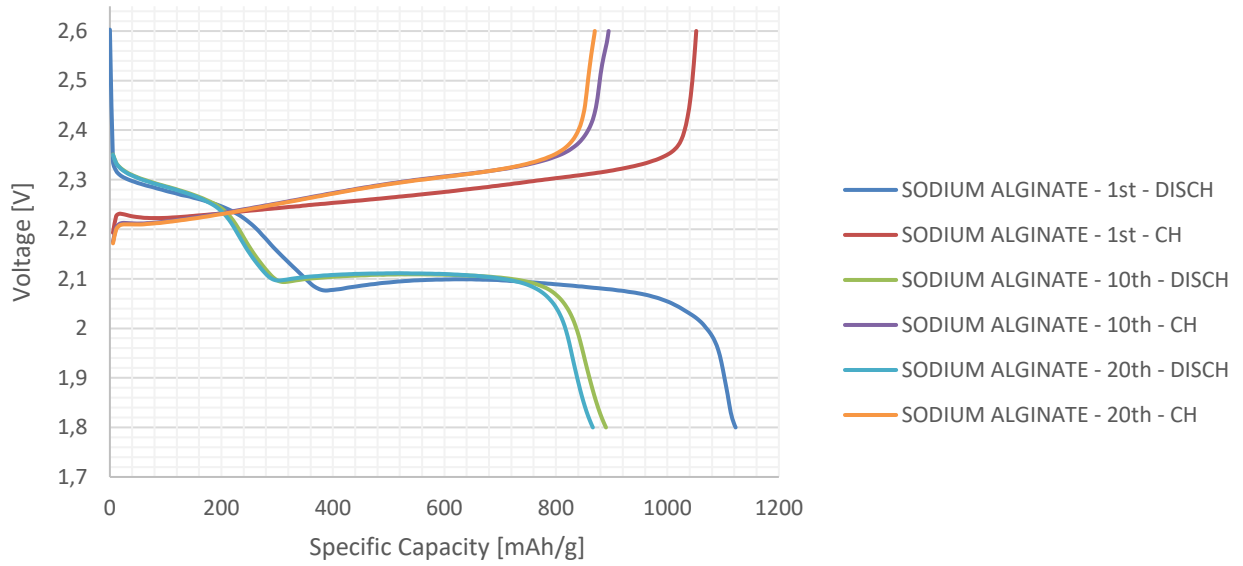
Graph.A5 - KJBC 50% Sulfur- **PVdF** binder - Voltage Vs. Capacity



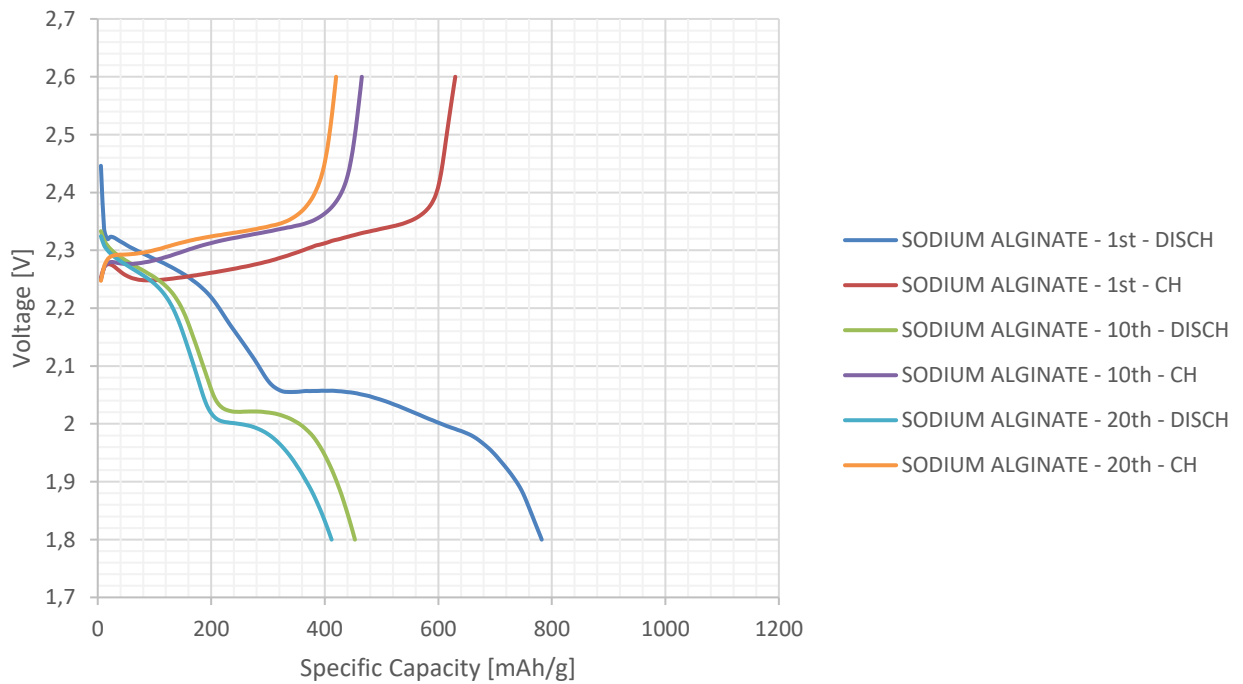
Graph.A6 - KJBC 50% Sulfur - **PAA** binder - Voltage Vs. Capacity



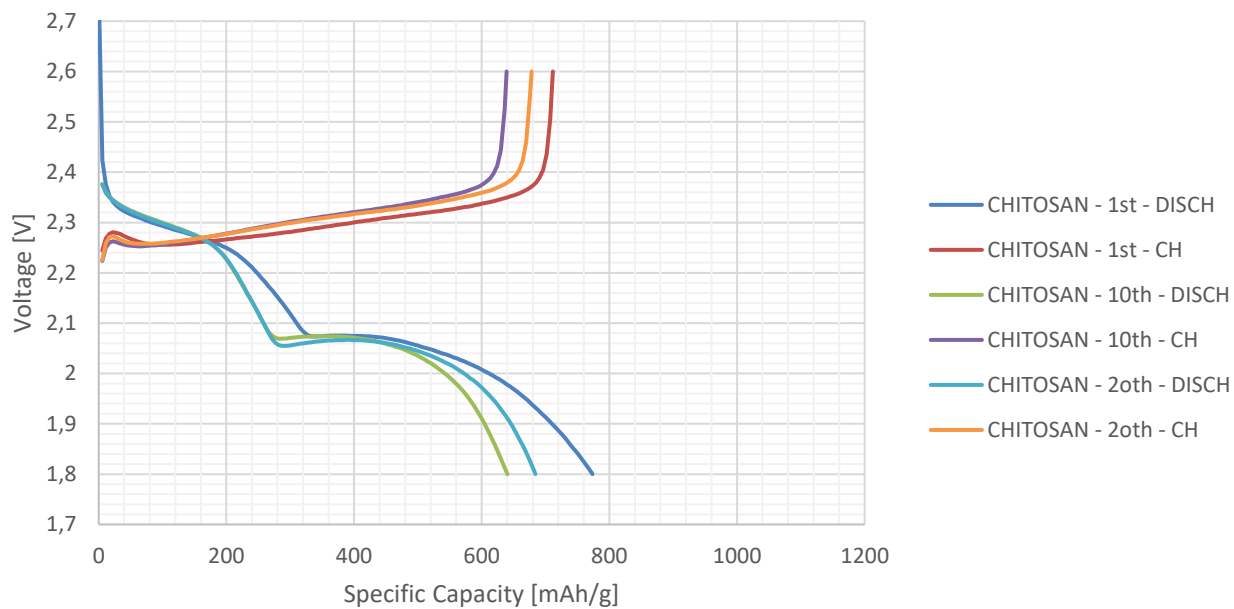
Graph.A7 - KJBC 50% Sulfur - **Sodium Alginate** binder - Voltage Vs. Capacity



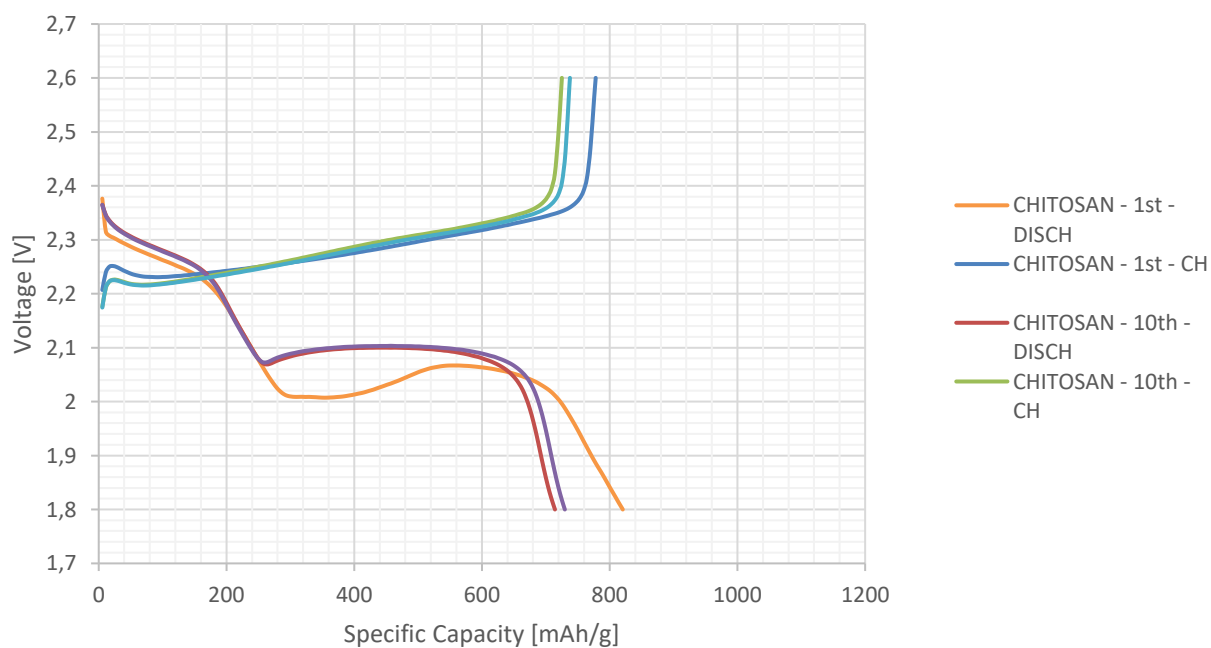
Graph.A8 - AC 50% Sulfur - **Sodium Alginate** binder - Voltage Vs. Capacity



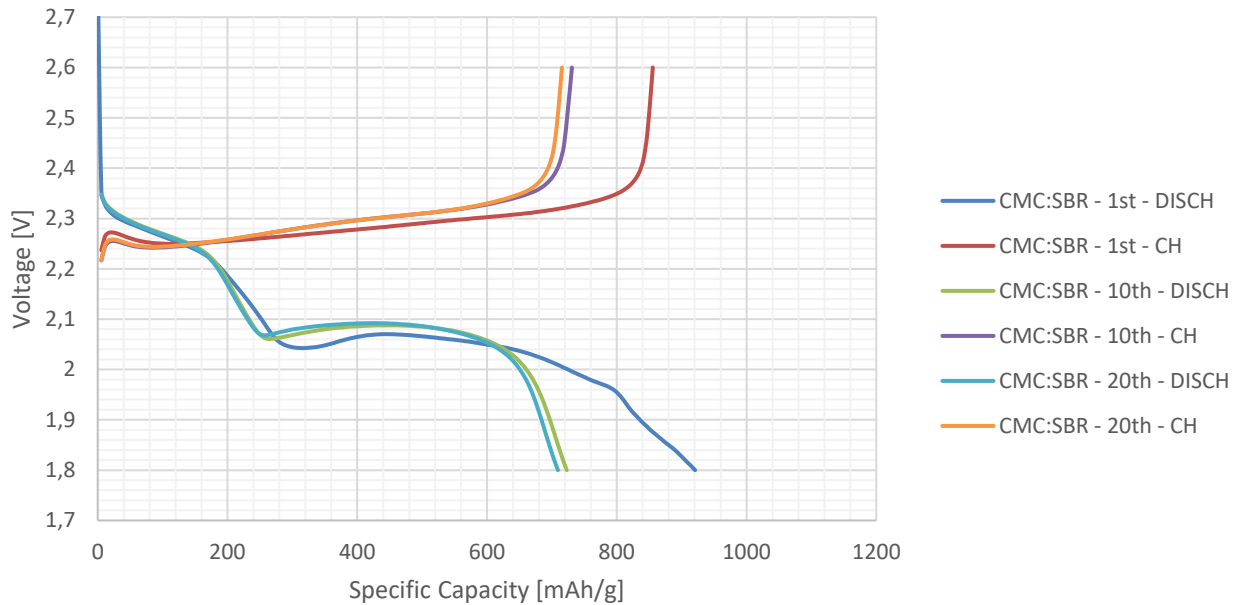
Graph.A9 - KJBC 50% Sulfur - **Chitosan** binder - Voltage Vs. Capacity



Graph.A10 - Activated Carbon 50% Sulfur - **Chitosan** binder - Voltage Vs. Capacity



Graph.A11 - KJBC 50% Sufur- **CMC:SBR** binder - Voltage Vs. Capacity



3.2.1.1 – AC and KJBC cathodes with low content of sulfur - Critical Analysis of Results – Stability and consistent voltage-capacity curves.

- Overall Observations on specific capacity and coulombic efficiency:** A first important general observation about the above reported results, is that a low content of Sulfur guarantee, in the first place, a really stable value of capacity during cycling for both activated carbon and KJBC [[Graph.A1](#), [Graph.A2](#)].
 The active material in low concentration is more difficult to be dissolved into electrolyte during soluble polysulfides species formation. With exception like KJBC-Chitosan [[Graph.A9](#)] and AC-Sodium Alginate [[Graph.A10](#)], almost all the voltage curves presents a long and flat second plateau, that is the one of the soluble PSs formations. That means that the functional group of the binder is probably helping the retention of PSs described in the previous chapters.
- Sodium Alginate [[ch.2.2.2](#)]:** the biodegradable binder shows a very high capacity in case of KJBC, especially at the beginning, of 1122 [mAh/g] and 867 [mAh/g] in the end [[Graph.A1](#)].

The coulombic efficiency fluctuated around 98-99% for all the 20 cycles [[Graph.A3](#)], meaning that there is a good sulfur utilization between charge and discharge.

In chapter 2.2.2 is mentioned how the good swelling ability of Alginate can favor the increasing of the cathode porosity, increasing in this way the void available for S_8 molecules.

In the case of activated carbon the capacity suddenly goes from 782 to 515 [mAh/g] from first to second cycle, but it is very stable decreasing until reach 412 [mAh/g] at the last one. A worst behavior in terms of coulombic efficiency can be observed for AC-Alginate at the beginning (from 1st to 5th cycle) [[Graph.A4](#)], meaning that there is a scarce sulfur utilization during discharge. This phenomena could be due to the fact that in AC combined with Alginate, the structure make the sulfur less available in early cycles.

- **Chitosan [[ch.2.2.3](#)]**: chitosan gives the best results in terms of capacity in the activated carbon case [[Graph.A2](#)], with respect to alginate [[Graph.A1](#)] resulting in an initial capacity of 778 [mAh/g] and final of 737 [mAh/g]. In this case chitosan presents also a very good coulombic efficiency [[Graph.A4](#)], a sign of the active roles that hydroxyl and amine groups play in retaining the PSs.
Concerning the voltage profiles, the first plateau is relatively steep in both the carbons, but the second plateau of soluble PSs formation is flat and extended in an almost equal way in 10th and 20th cycles, again a matter connected to the active role of functional groups in retaining the PSs. The third descending part is relative to the formation of Li_2S which, being an insulator, increase the internal resistance the more it's concentration in the carbon structure is higher. This part is usually steep, meaning a sudden drop of voltage. But not here, where seems that in some manner chitosan it's partially compensating the increasing of the internal resistance.
- **CMC:SBR [[ch.2.2.5](#)]**: because of time and availability of channels, it has been tested only for KJBC carbon. Here there is the combined effect of SBR (good for its elastic properties) , and CMC (functional for PSs). The capacity is even higher than Chitosan with an initial value of 920 and final of 715 [mAh/g]. The good elasticity given by the SBR accommodates the expansion due to the Li_2S formation, preserving the integrity and contacts between the phases, while CMC carboxyl groups help holding in positions soluble PSs species. More or less from the 6th-7th cycle, the coulombic efficiency is practically constant at a 99% [[Graph.A3](#)], meaning an optimal sulfur utilization among charge and discharge. Excluding the 1st cycle, the 10th and 20th cycles shows an almost equal curve, with an evident flat and long 2nd plateau [[Graph.A11](#)]

PAA [[ch.2.2.4](#)]: even though the literature reports the property of PAA of making the structure of the cathode more porous and conductive, here the usual phenomena of an

initial high capacity that decrease cycle of cycle has been reversed. The reason of this phenomena will be described further in the next comment section.

Therefore, an inferior number of internal channel containing the S_8 ring can be reached. For some reason, the capacity starts increasing cycle by cycle, starting from 596 to 729 [mAh/g] [[Graph.A1](#)]

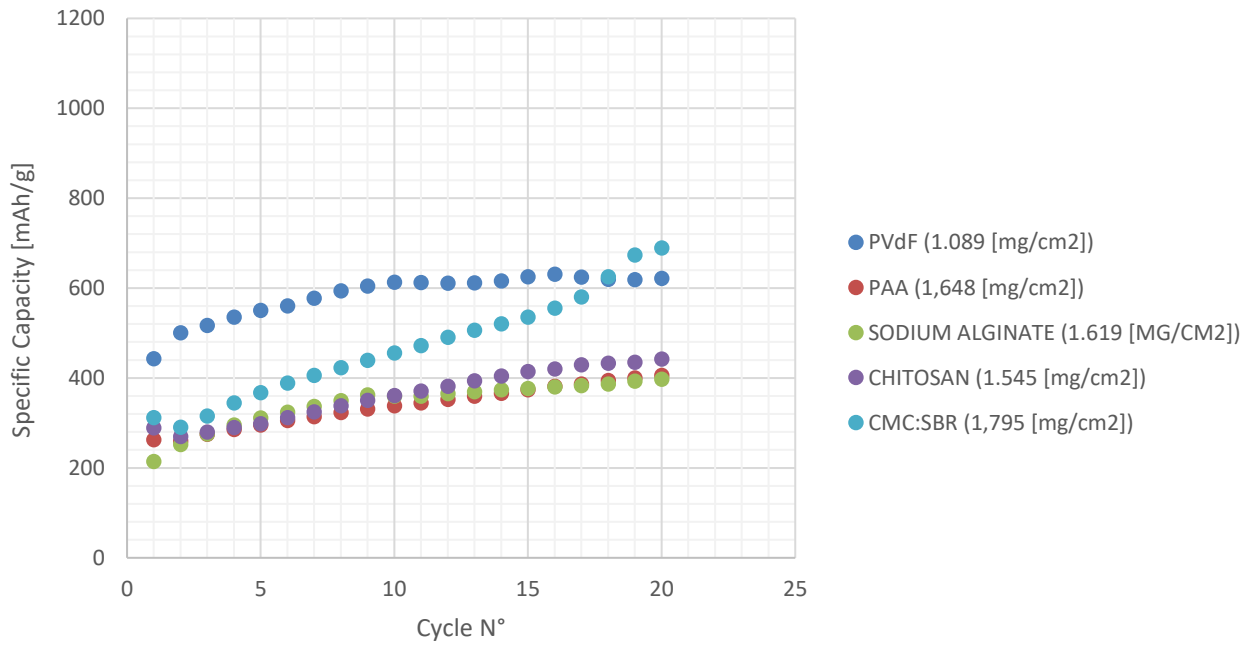
The Coulombic efficiency starts with the lowest value among KJBC 50% cathodes, but in the end it's inline with the other, with a value of 99% [[Graph.A3](#)].

The first discharge voltage curve ha a strange behavior in the last part, with a third plateau usually not present in Li-S batteries. With the increasing of capacity in 10th and 20th cycle, the voltage profile assumes the standard shape with a smooth and flat second plateau [[Graph.A6](#)].

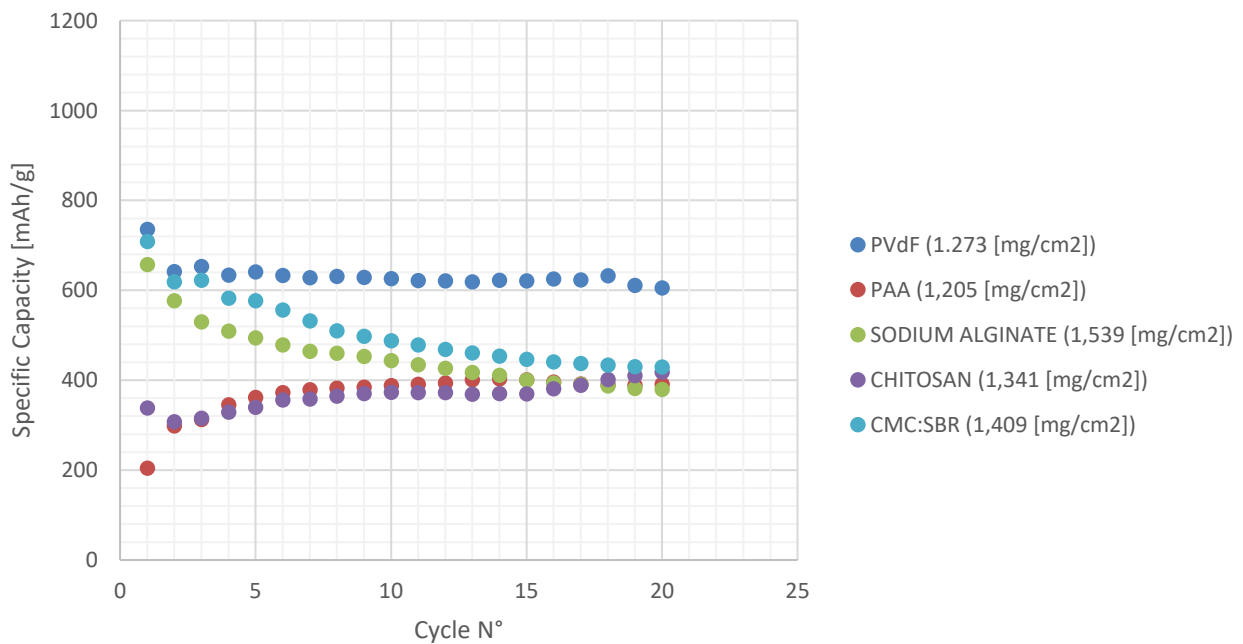
- **PVdF [[ch.2.2.1](#)]**: the use of NMP, being very interactive with AC and KJBC carbons, make the slurries very homogeneous and so the sulfur distribution regular. However, having no interaction with PSs, the capacity faded from 1050 to 800 [mAh/g]. The initial high capacity is indeed due to an initial high content of sulfur available [[Graph.A1](#)].
However, the non-biodegradable binder shows a very good performances, with good shaped voltage Vs. C_s curves [] This fact further underline the simplicity on manage the PVdF+NMP/AC or KJBC in cathode preparation, with respect to the bad interaction of the two hydrophobic carbons with water solvent [[Graph.A5](#)]

3.2.2– AC and KJBC cathodes with high content of sulfur - Graphs

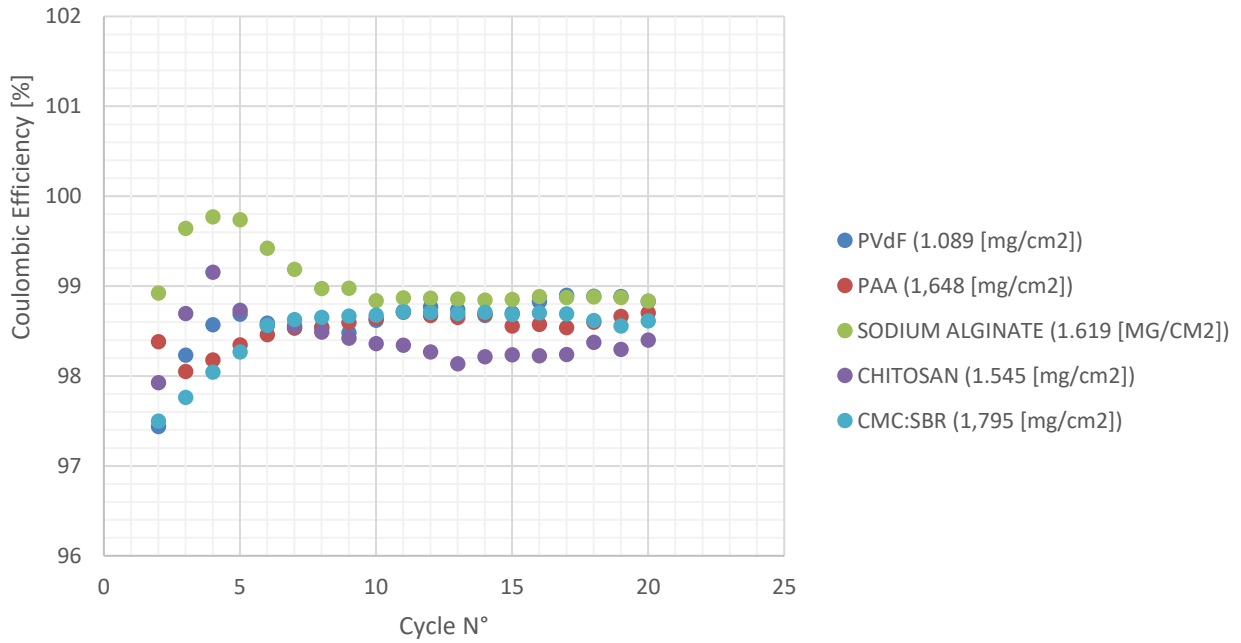
Graph.B1 - KJBC cathodes with 70% of Sulfur - Specific Capacity Vs. N° of cycles



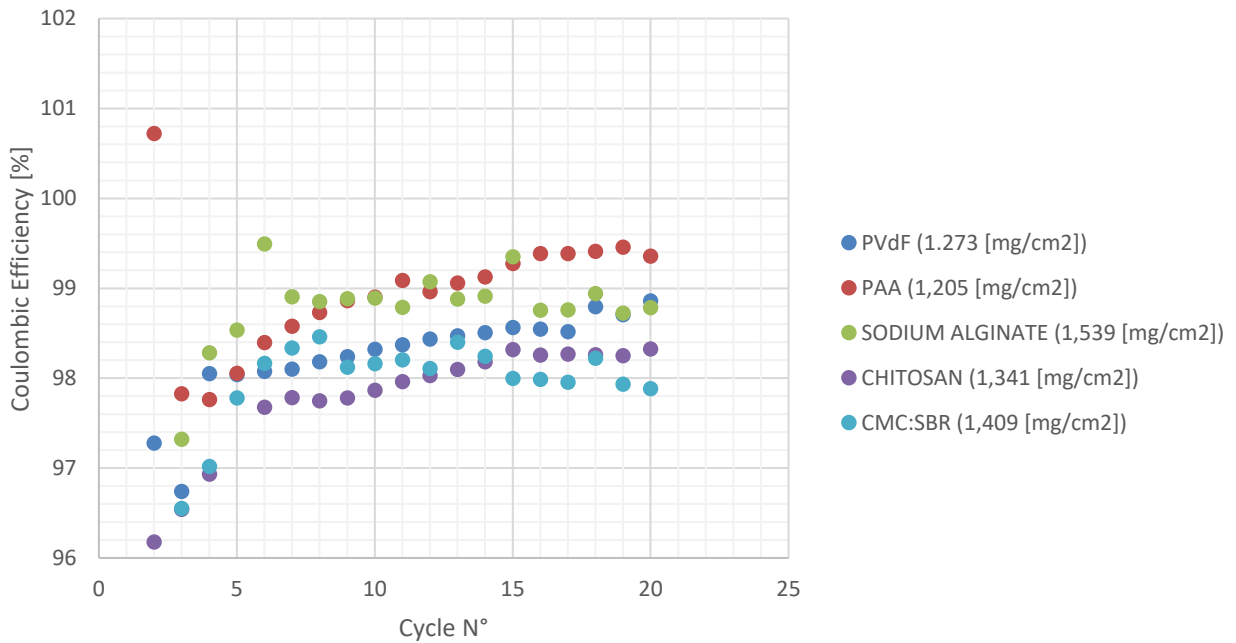
Graph.B2 - Activated Carbon with 70% of Sulfur - Specific Capacity Vs. N° of cycles



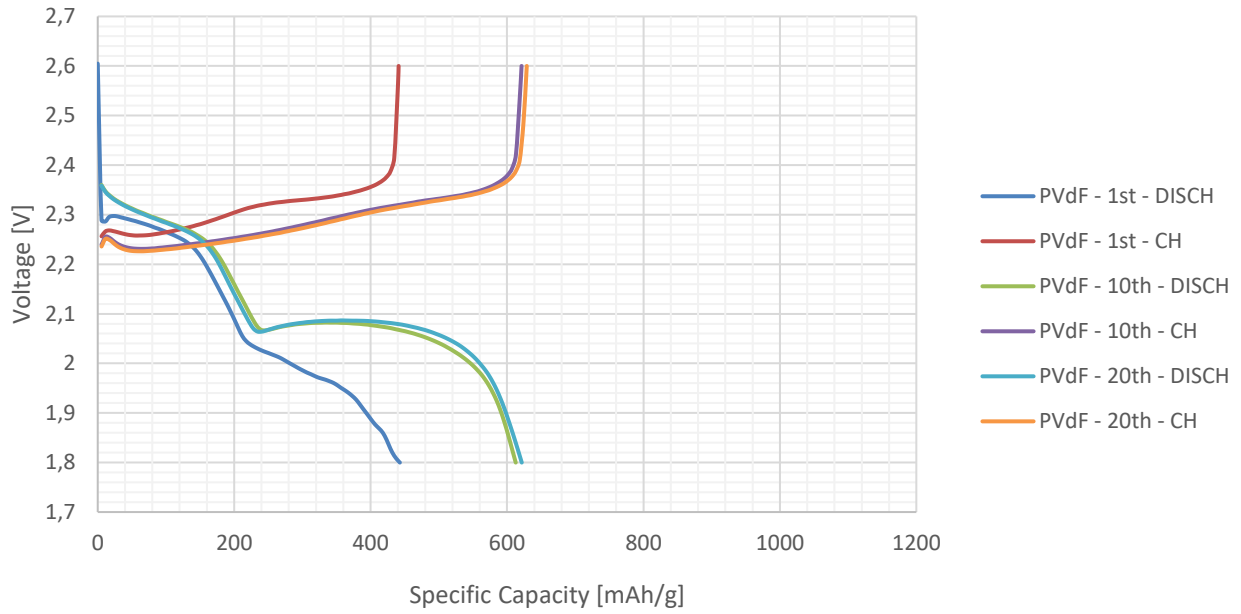
Graph.B3 - KJBC cathodes with 70% of Sulfur - Coulombic Efficiency Vs. N° of cycles



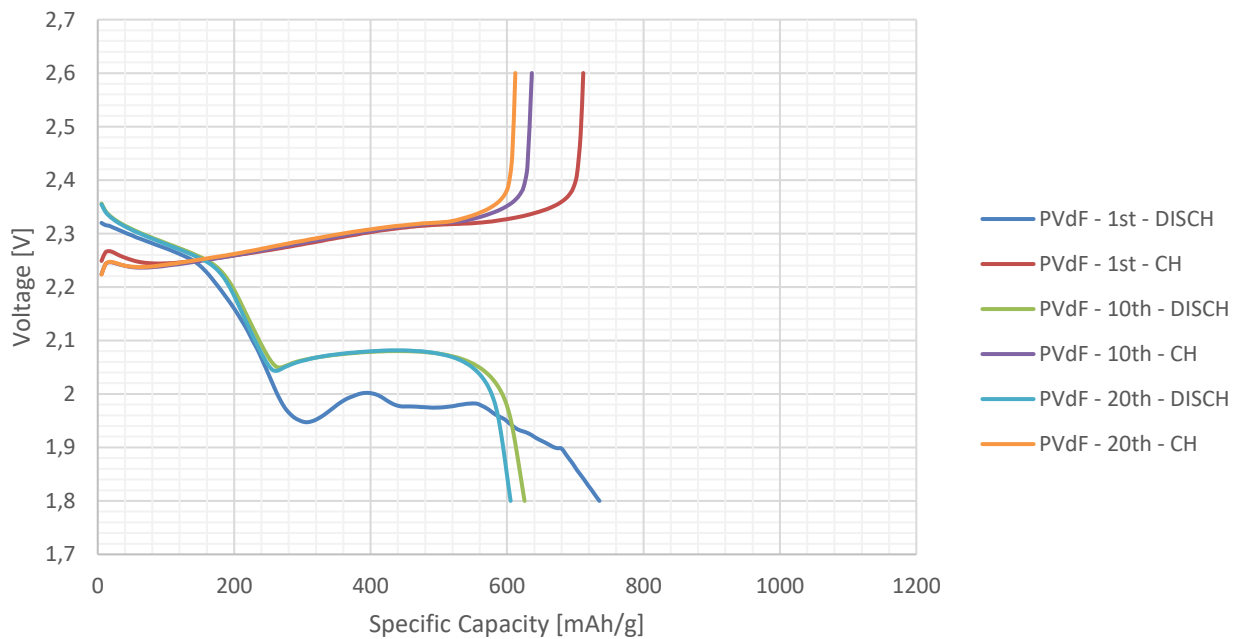
Graph.B4 - Activated Carbon with 70% of Sulfur - Coulombic Efficiency [%] Vs. N° of Cycles



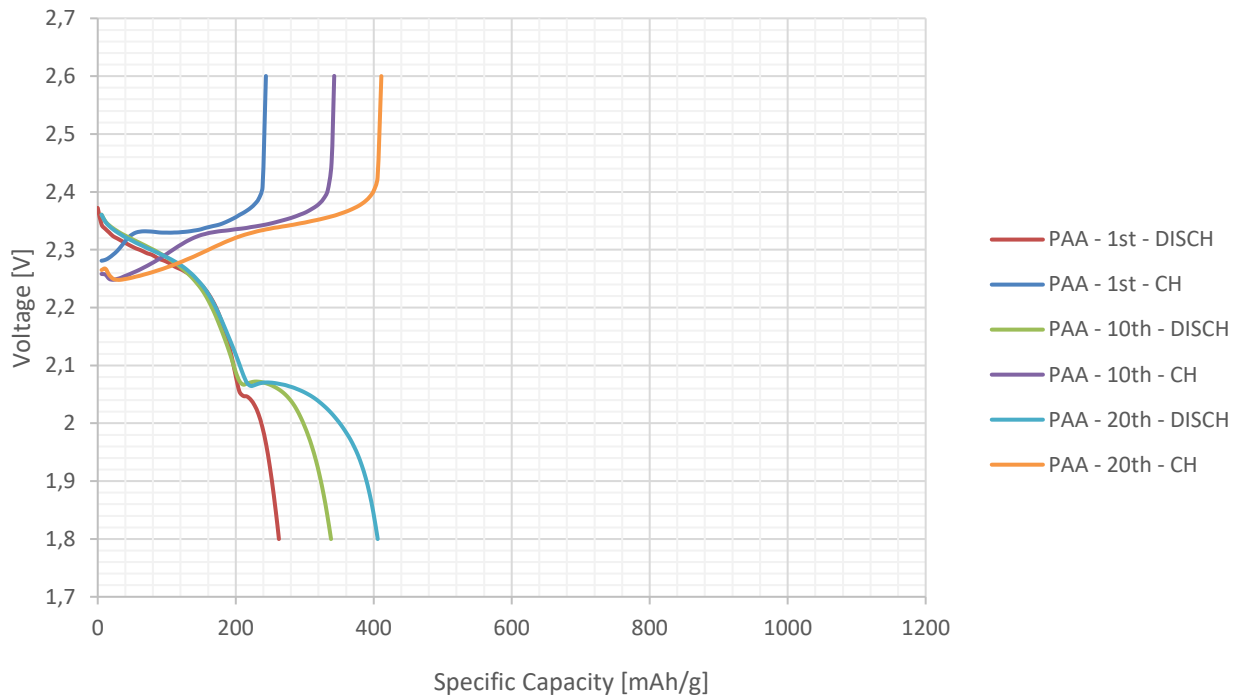
Graph.B5 - KJBC 70% Sulfur- **PVdF** binder - Voltage Vs. Capacity



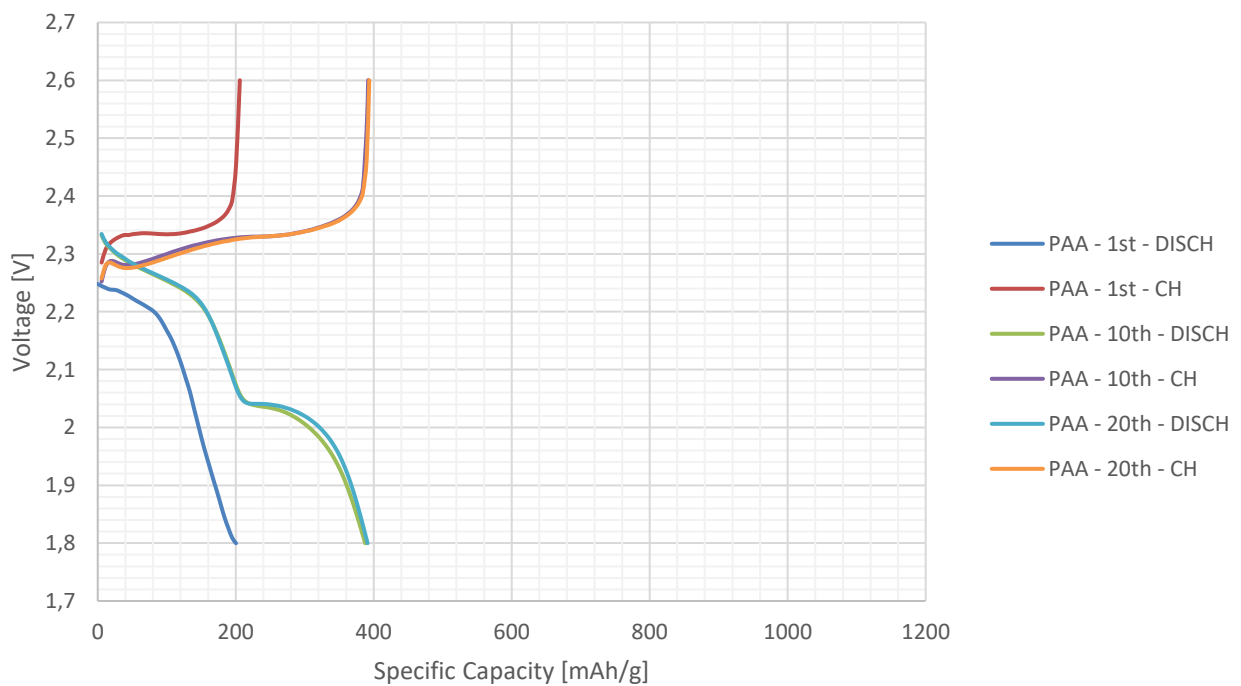
Graph B6 - Activated Carbon 70% Sulfur - **PVdF** binder - Voltage Vs. Capacity



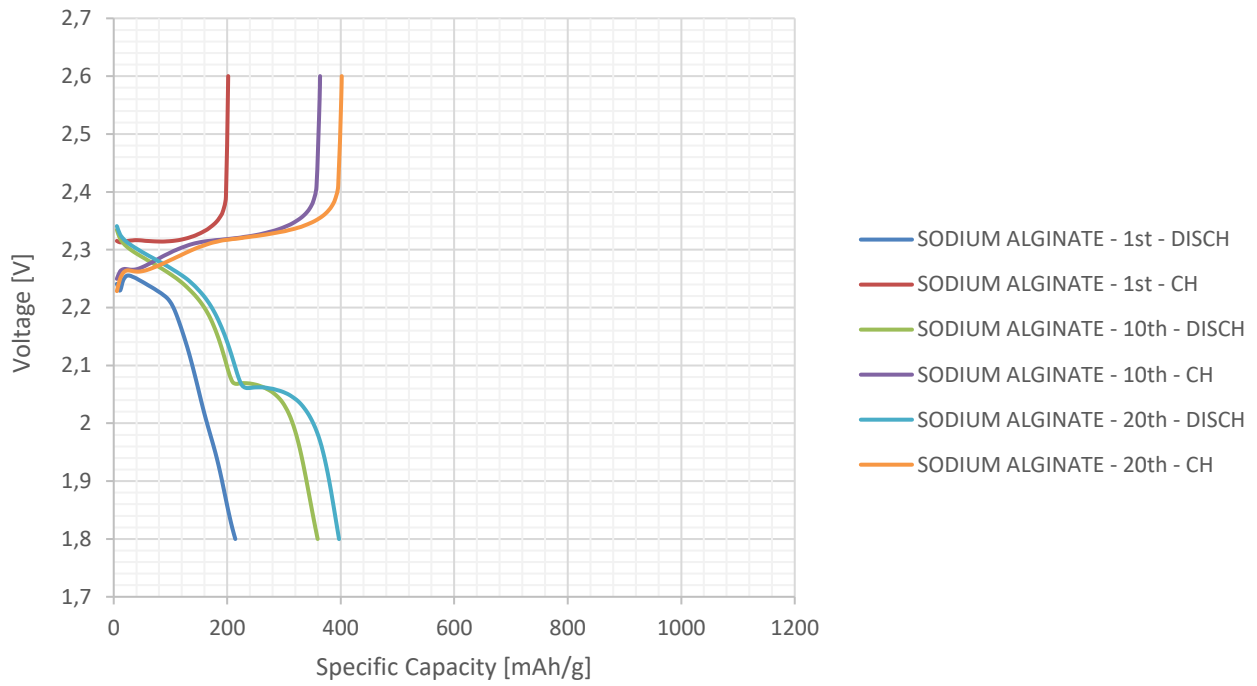
Graph.B7 - KJBC 70% Sulfur - PAA binder - Voltage Vs. Capacity



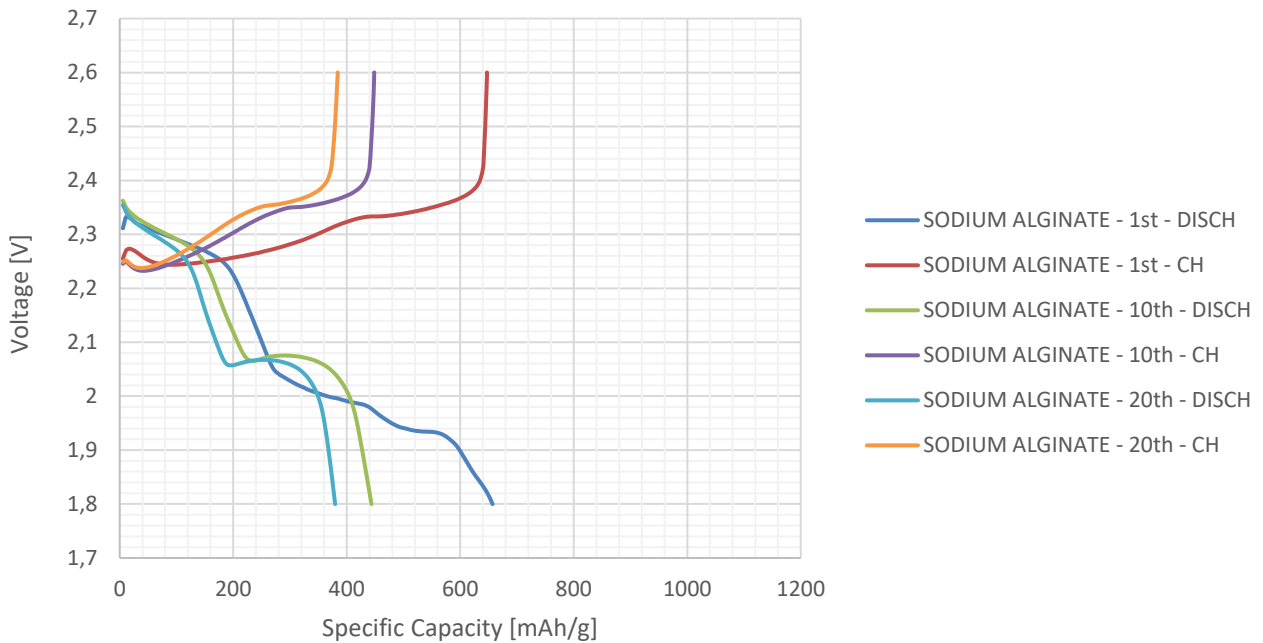
Graph.B8 - Activated Carbon - 70% Sulfur - PAA binder - Voltage Vs. Capacity



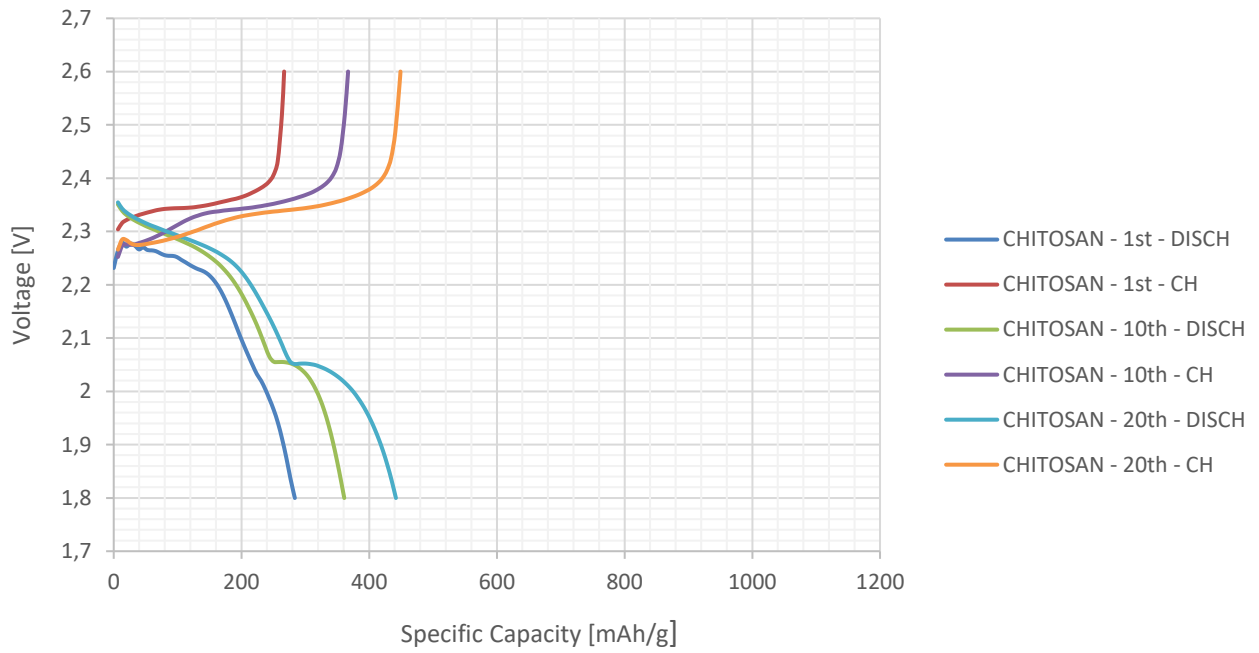
Graph.B9 - KJBC 70% Sulfur - **Sodium Alginate** binder - Voltage Vs. Capacity



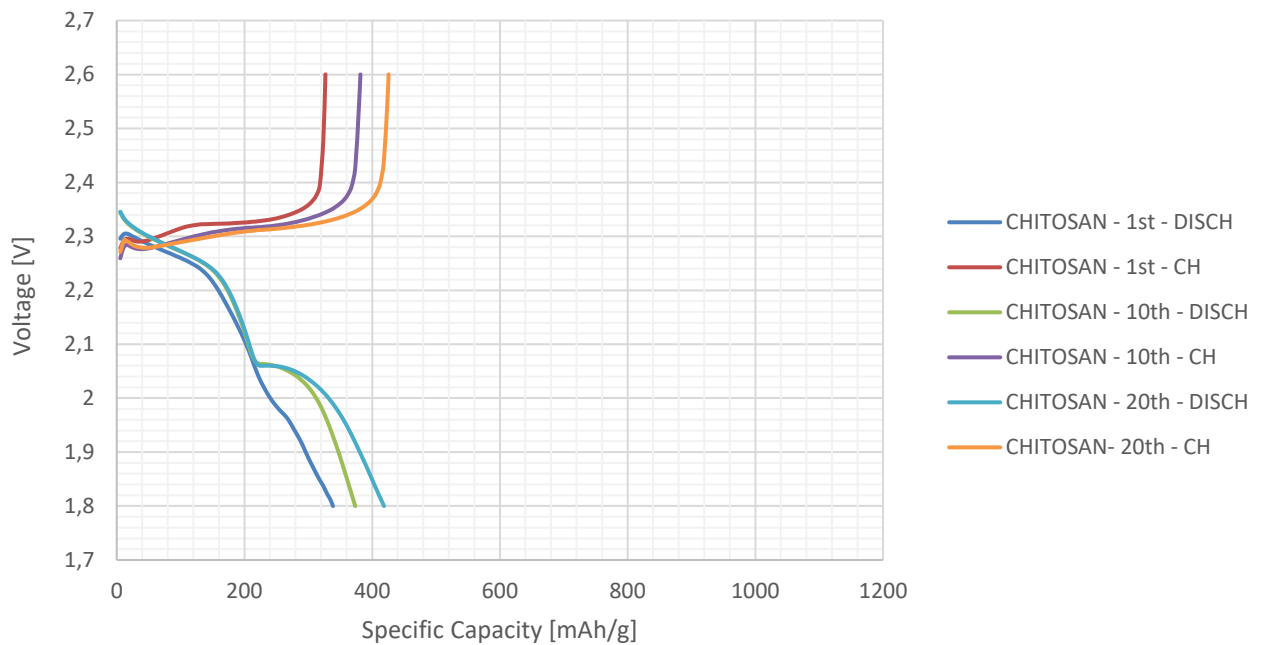
Graph.B10 - Activated Carbon 70% Sulfur -**Sodium Alginate** binder - Voltage Vs. Capacity



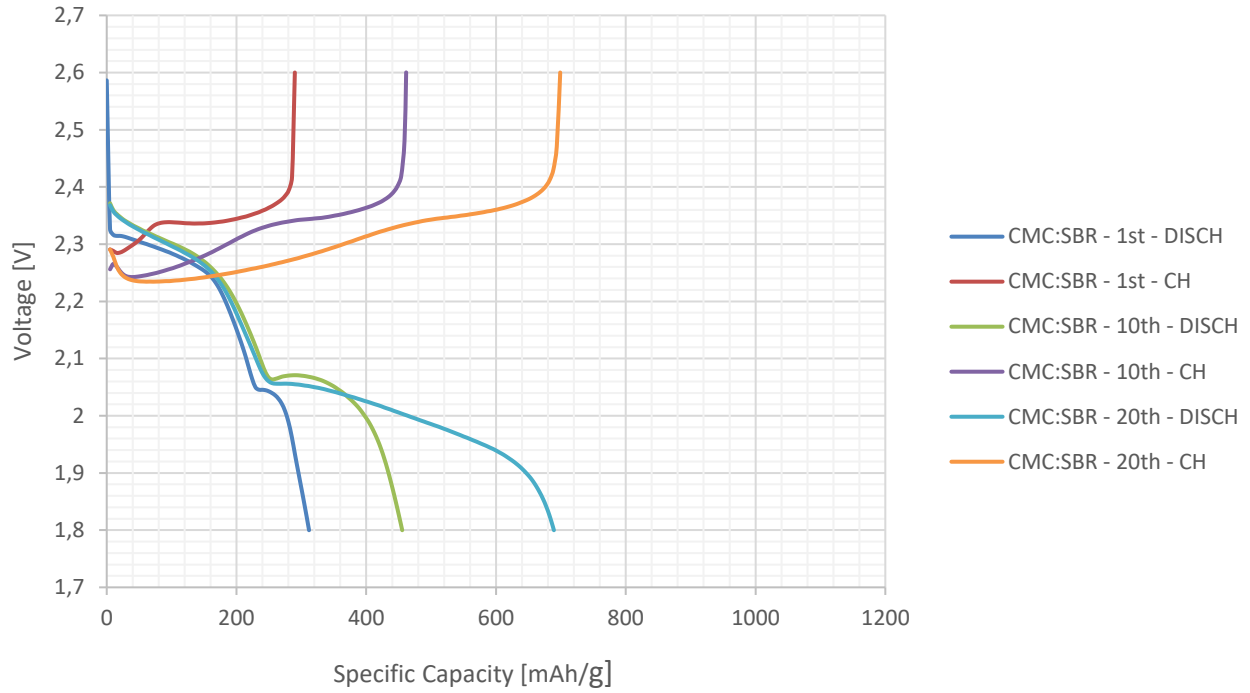
Graph.B11 - KJBC 70% Sulfur - **Chitosan** binder - Voltage Vs. Capacity



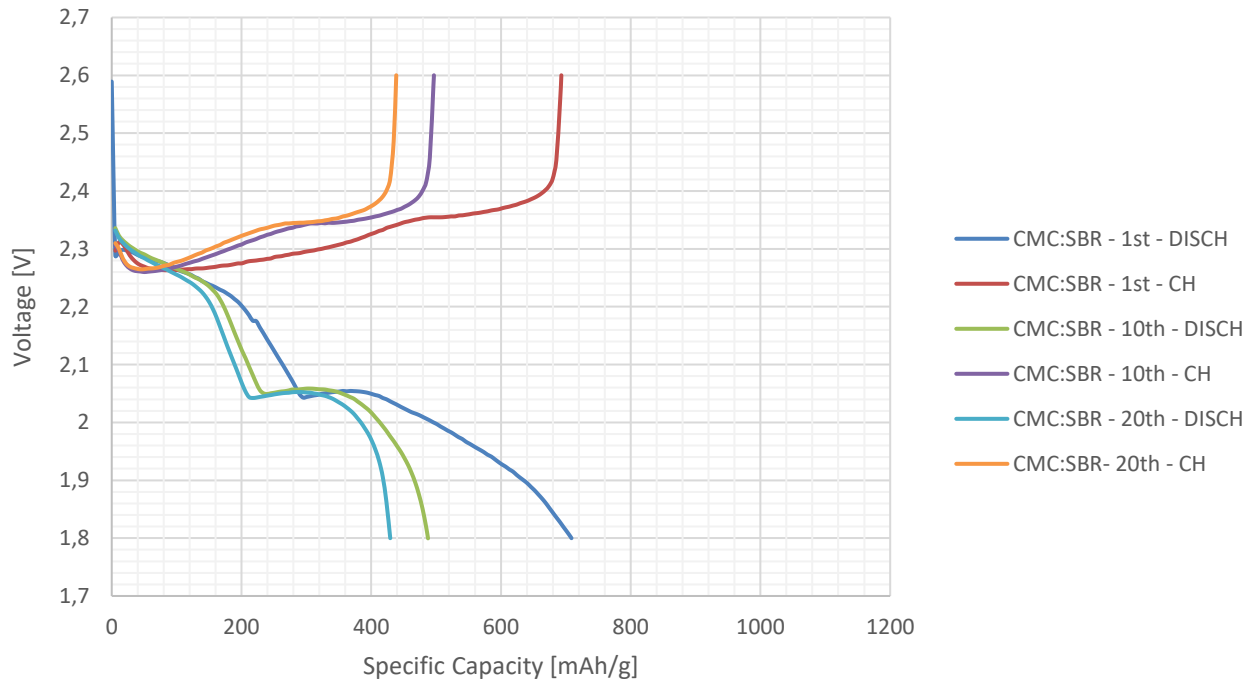
Graph.B12 - Activated Carbon 70% Sulfur - **Chitosan** binder - Voltage Vs. Capacity



Graph.B13 - KJBC 70% Sulfur - **CMC:SBR** binder - Voltage Vs. Capacity



Graph.B14 - AC 70% Sulfur - **CMC:SBR** binder - Voltage Vs. Capacity



3.2.2.1 – AC and KJBC cathodes with high content of sulfur - Critical Analysis of Results

- **Overall Observations on specific capacity and coulombic efficiency:** The phenomena of bad electrolyte soaking mentioned for PAA 50% with low sulfur content, is far more evident here especially for KJBC cathodes.

It is however rightful to underline that the value chosen of 10 μl of electrolyte is at limit. The reason of the gradual absorption of EL. is for sure related to the opening of new internal channels rich of sulfur cycle by cycle, that where for some reason blocked at the beginning, probably both because the non-homogeneity of the slurry (common in aqueous binders) or due to a too intense action of friction and normal forces during BM, whom have partially compressed the channels.

The cause of the opening could be resumed essentially in two hypothesis: the swelling of the polymers is harder when the sulfur content is higher, so that the slow expansion frees new space slowly. The continuous volume variation from S_8 to Li_2S during discharge, and vice versa during charge, could in some way move the internal structure C/binder, making new micro-tunnels available.

Referring to the graphic capacity Vs. N°of Cycles, surprisingly here the AC carbon worked in a better way, at least concerning initial capacities.

In the end, a curious fact is that at 20th cycle, for both the material, the various binders converges around a ~ 400 [mAh/g]. The only difference is that if the cycling were longer, looking at the positive slope of KJBC curves, the values would be probably become higher. [[Graph.B1](#)][[Graph.B2](#)]

If we look at coulombic efficiencies [[Graph.B3](#)][[Graph.B4](#)], going towards the end of the trial the % values of KJBC based electrodes tends to condense around 98-99% while for AC cathodes are more disperse. This last evidence match with the usual fading-like behavior of the standard Li-S cycling, especially where the capacity retention is low.

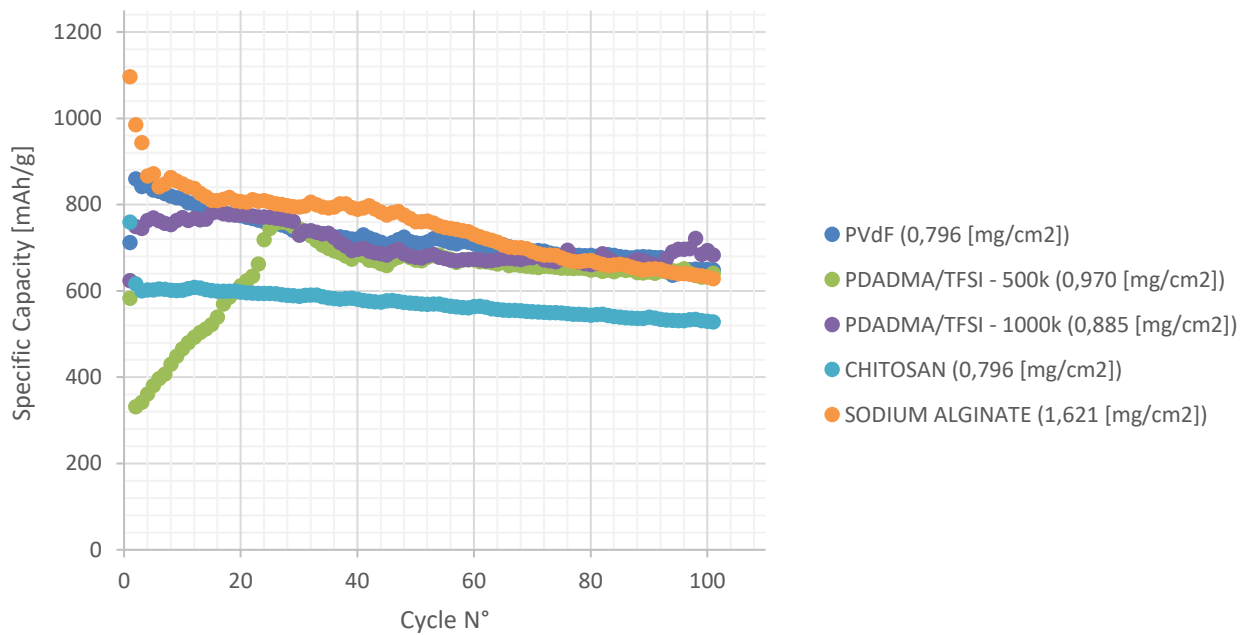
- **Sodium Alginate [[ch.2.2.2](#)]:** in both the materials the biodegradable Na- Alginate have a final capacity value of 400 [mAh/g]. The difference is that for KJBC cathode the material shows the up-mentioned problem. It'd go probably better if it were cycled for more time. The AC instead starts from more or less ~ 640 and rapidly decreases, a sing of a bad initial capacity retention, i.e. more ineffective action of functional groups with respect to PSs [[Graph.B1](#)][[Graph.B2](#)]
Concerning the coulombic efficiencies, in the end both converges to a value around 99% [[Graph.B3](#)][[Graph.B4](#)].
In regards of voltage/capacity curves, the KJBC-alginate presents almost an absence of the second plateau in the first 15 cycles, while AC, is a little bit more evident.
- **Chitosan [[ch.2.2.3](#)]:** in this case the capacities of the two carbons are really similar and end in a value of more or less 400 [mAh/g], and for both of them the charge discharge curves are steep and difficult to interpret [[Graph.B11](#)] [[Graph.B12](#)].

- **CMC:SBR** [[ch.2.2.5](#)]: the double component binder is the only one who shows an Incredible high discharge capacity for KJBC at the last cycle, with a very rapid increase during cycling from 300 to almost 700 [mAh/g]. On the contrary for AC carbon it starts from a value of 700 [mAh/g] and goes to a value of 440. Then it's really stable. A valuable theory is that SBR elasticity probably compensate, especially for KJBC, the hardness and compactness of the composite.

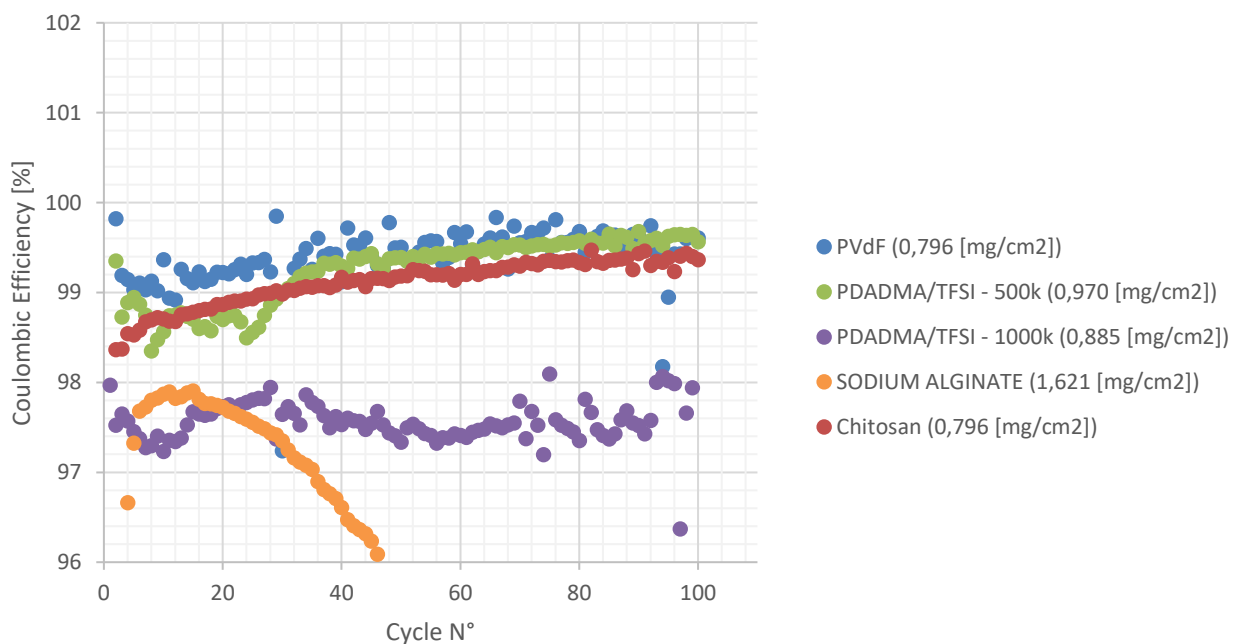
Concerning the shapes of the voltage-capacities curves, in case of CMC:SBR there is a more evident second plateau with respect to the other binders. Especially for KJBC cathode [[Graph.B13](#)].
- **PAA** [[ch.2.2.4](#)]: Also the PAA curves are really difficult to interpret. The KJBC positive electrode, in terms of voltage capacity curves express a very constant behavior in the first plateau, since the three reported cycles presents almost coincident curves,. The voltage gap is instead evident along cycles regarding the second plateau[[Graph.B7](#)][[Graph.B8](#)]. In terms of capacity, like in previous cases, the KJBC would probably continue well for cycles further than 20th, but the slope of the curve is lower and seems to go for a more stable tendency.
- **PVdF** [[ch.2.2.1](#)]: the standard PVdF cathode this time worked as well in a reverse way for KJBC carbon, showing an initial lower capacity with respect to the 20th cycle. Anyway, in this case AC and KJBC share the same constant like discharge behavior at ~600 [mAh/g] from the 10th cycle on[[Graph.B1](#)][[Graph.B2](#)]. The AC-PVdF positive electrode shows a voltage-capacity profile of discharge very strange at the first cycle, even if an high value of 670 [mAh/g][[Graph.B6](#)]. KJBC carbon PVdF electrodes instead assumes usual voltage profiles when discharging over the 10th cycle, with a clear soluble PSs formation section (2nd plateau) [[Graph.B5](#)].

3.3 - A Study of KJBC 70% S cathodes with higher mass content of biodegradable binders, innovative electroactive binders (PEBs), for long cycling: challenges, results, comparison with traditional PVdF.

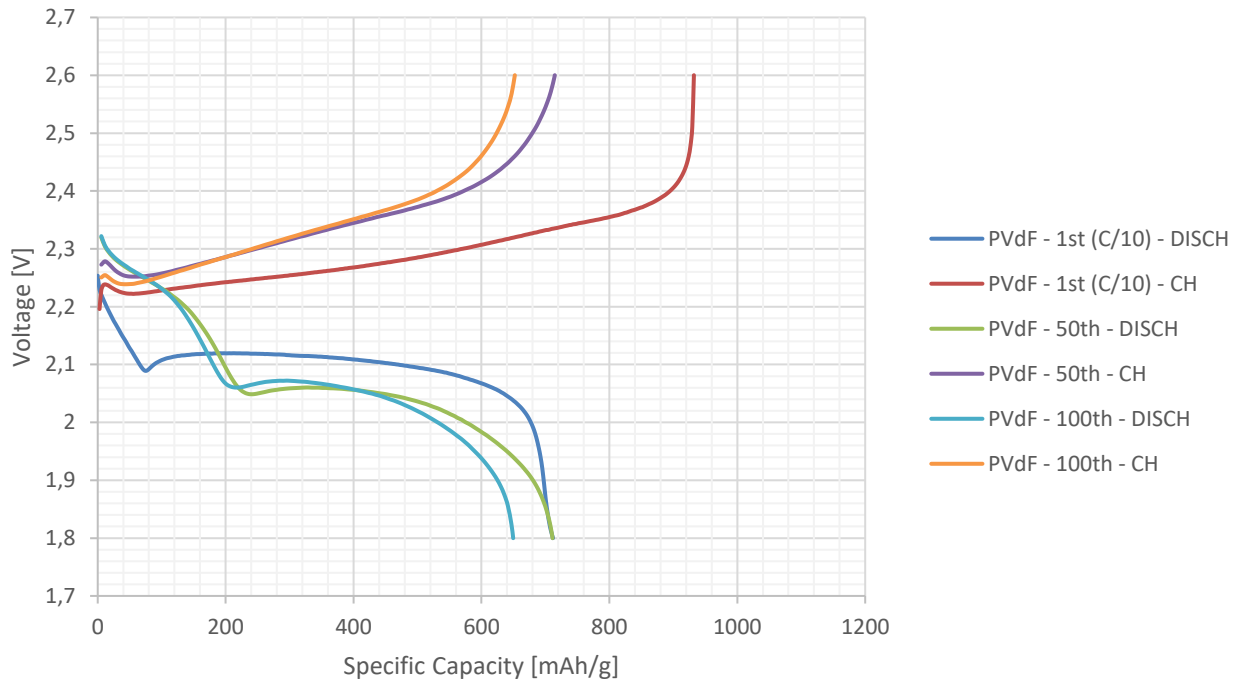
Graph.C1 - KJBC Cathode 70% of Sulfur with various Binders at 10% in mass - Specific Capacity Vs. N° Of Cycles



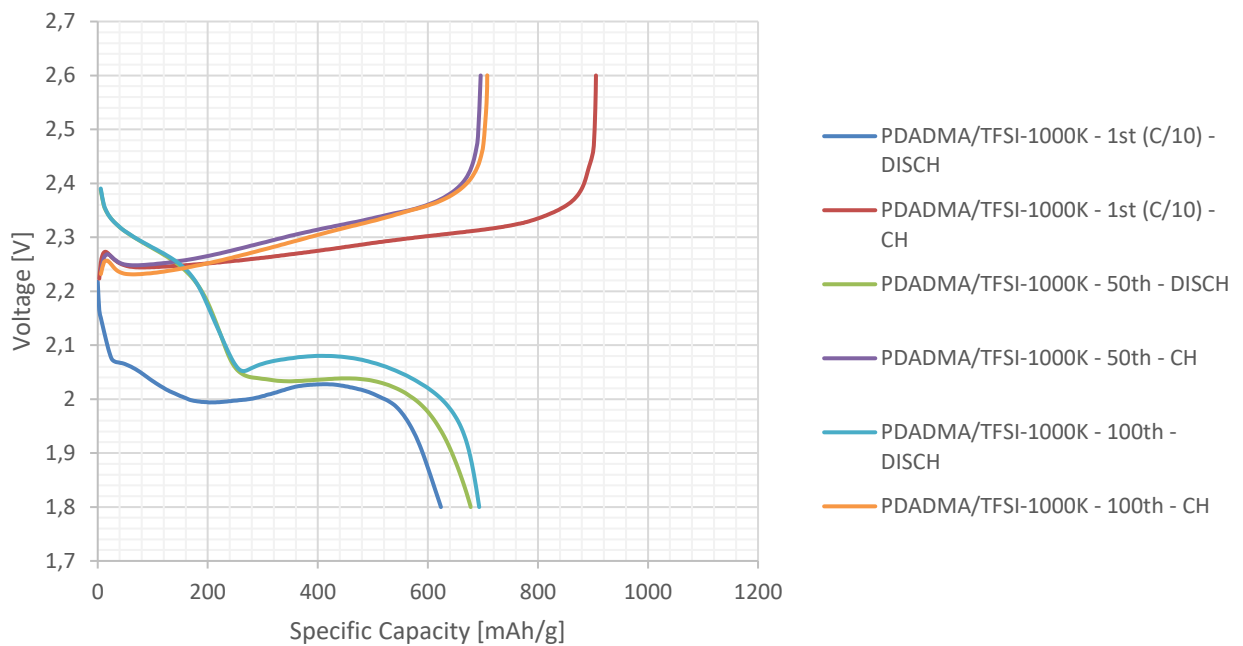
Graph.C2 - KJBC Cathode 70% of Sulfur with various Binders at 10% in mass - Coulombic Efficiency Vs. N° Of Cycles



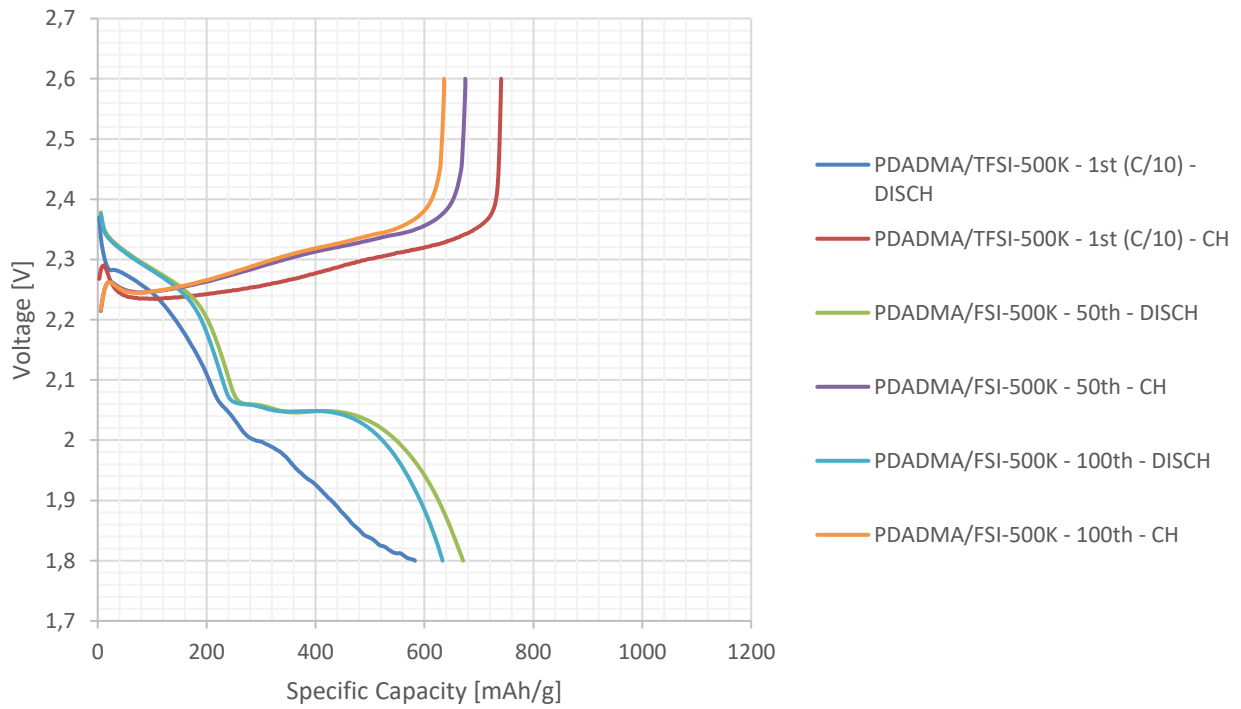
Graph.C3 - KJBC 70% Sulfur - **PVdF** Binder (10%w - LC) - Voltage Vs. Capacity



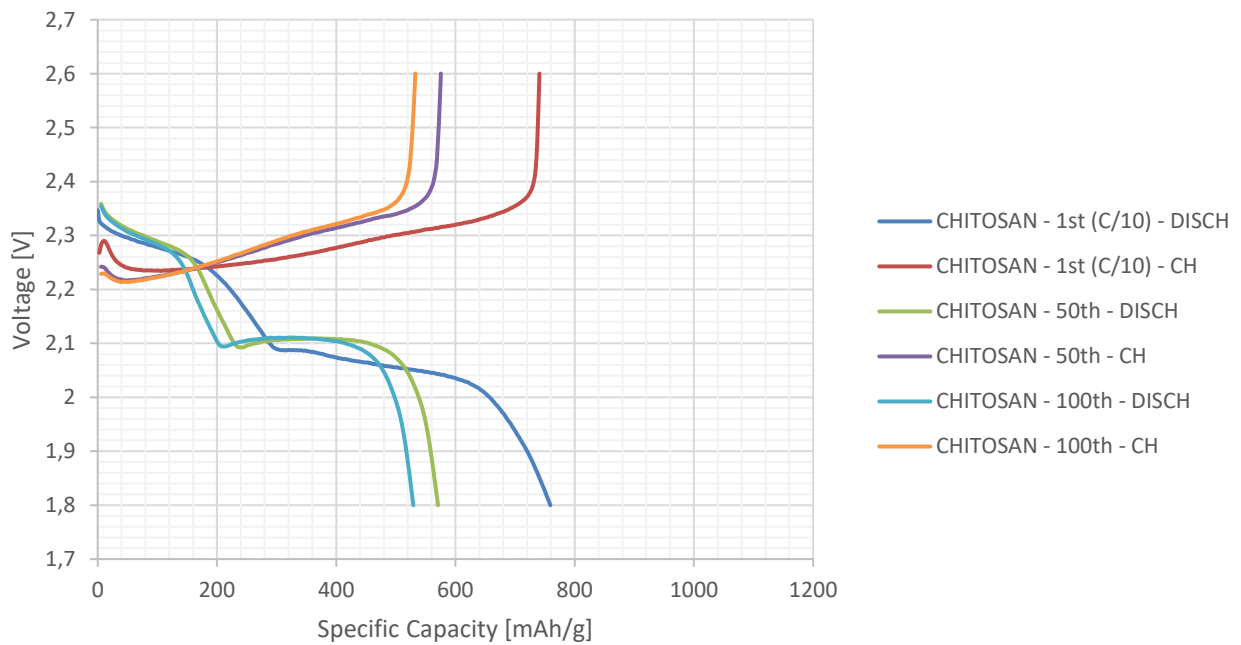
Graph.C4 - KJBC 70% Sulfur - **PDADMA/TFSI-1000k** Binder (10%w - LC) - Voltage Vs. Capacity



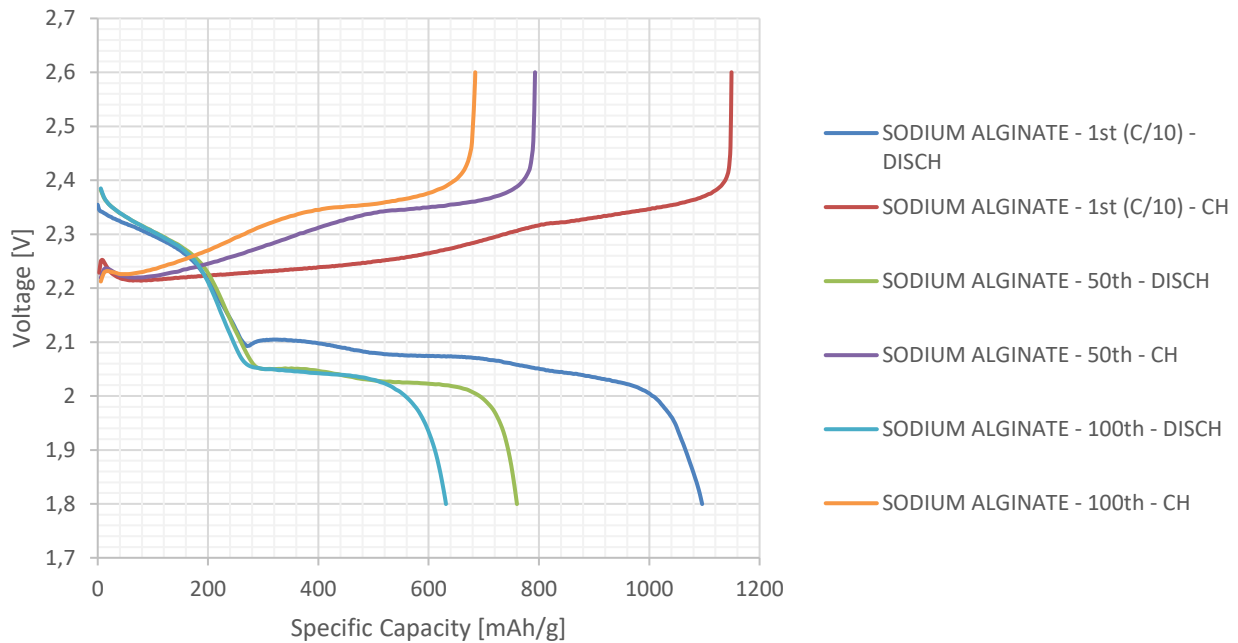
Graph.C5 - KJBC 70% Sulfur - **PDADMA/TFSI-500k** Binder (10%w - LC) - Voltage Vs. Capacity



Graph.C6 - KJBC 70% Sulfur - **Chitosan** Binder (10%w - LC) - Voltage Vs. Capacity



Graph.C7 - KJBC 70% Sulfur - **Sodium Alginate** Binder (10%w - LC) - Voltage
Vs. Capacity



3.3.1 – Critical analysis about Long Cycling trails: analysis of performances of Electroactive binders and Biodegradable Binders.

- Overall Observations:** in this standalone part of the work, several KJBC cathode with an high standard value of 10% in mass binders has been prepared. The choice of an higher binder content is justify by a better possibility to have a good comparison with other works in literature.

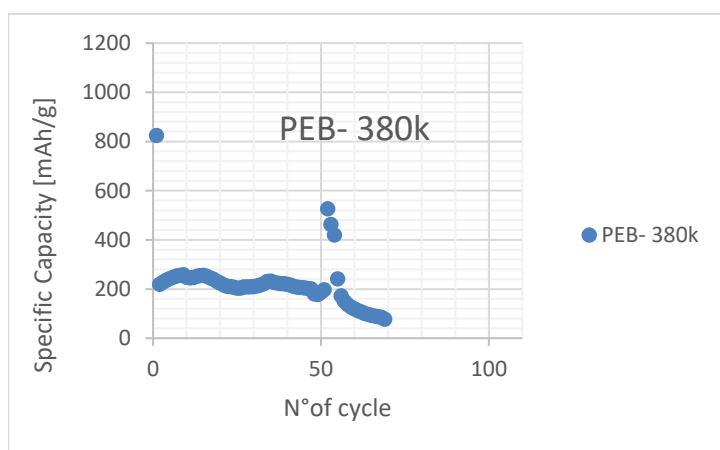
Further three binders have been introduced here, the so called PEBs -Polyelectrolyte Ionic Binders [Ch.2.2.6]. Thanks to TFSI and FSI groups, the PEBs surround the composite C/S particles with an electroactive barrier [Fig.31] able to avoid the loss of active material via polysulfides soluble species dissolution, that have origin during the second plateau of the Li-S voltage curve.

In addition to those innovative binders, the traditional PVdF as well as two biodegradable binders Na-Alginate and Chitosan has been prepared [Fig.48] and tested for 100 cycles.

In this case the graphs will be taken one by one and analyzed, since the only carbon selected is KJBC, considered the best one in literature [Ch.2.1.2]. Furthermore, due to the extension to 100 cycles, an approach for a better analysis on the long term life of the batteries can be attempt.

[Graph.C1] - Specific Capacity Vs. N° Of Cycles: starting from the 1st cycle (C/10), cathode with **Alginate**, who has also a very high load of Sulfur, shows an extreme high capacity of 1175 [mAh/g], but then terminates the trial with a low capacity. The High quantity of sulfur leads inevitably to a greter loss of active material inside the EL. The active role played by the
As a last remark, Na-alginate also maintain a good value of ~ 800 [mAh/g]. The ionic nature originating from the carboxylate groups in the Na alginate , which are able to disperse the hydrophobic particles through the electrostatic double-layer repulsion mechanism helps the dispersability, which is practically helpful to impart stability and uniformity to the cathode slurry during coating and drying process.

Chitosan is the most stable among all the cathodes despite it has the lowest capacity value from the start to the end (740 to 681 [mAh/g]). A similar stability it was present also in the case of AC-70%, but there was present in a lower mass ratio, index of a slow loss of active S after many cycles. A similar curve can be observed for **PVdF** (932 to 651 [mAh/g]), who favored a good capacity preservation of the cathode, probably due to the better dispersion in NMP of the mixture.



PDADMA-380K [Ch.2.2.6]: it has been tested but it did not work. After an initial acceptable specific capacity, the amount goes down until it reaches ~75 [mAh/g]. The molecular weight of the PEB probably was not sufficient enough to guarantee a good contact between the active material and the surrounding structure. Longer chain are required.

Also, short molecules probably make, under a mechanical point of view, the cathode not elastic enough to undergo a volumetric change during Li₂S formation, leading to progressive damage on the C/binder structure in charge to host S₈ molecules.

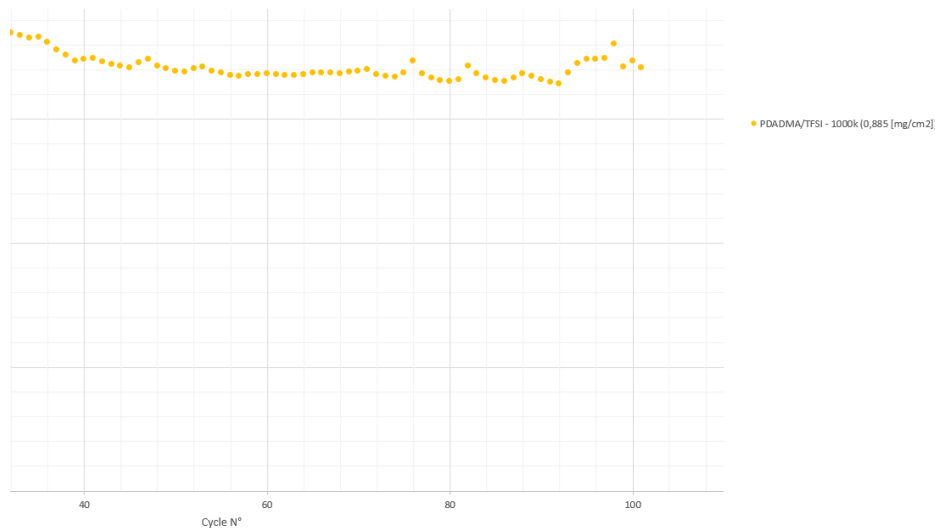
If we focus the attention to the first cycle at C/10, the integrity it's preserved because the initial value of discharge capacity is over 800 [mAh/g], but then it suddenly drop.

PDADMA-500k [Ch.2.2.6]: the first of the two innovative binders presents an initial low capacity. As a parallelism with the previous case of 70% of sulfur, the real activation of the binder starts after the 25th cycle, where the specific capacity starts decreasing after it reached a peak of ~760 [mAh/g].

After 25 cycles the available sulfur that is possible to exploit is reached, and the capacity starts fading until it reaches a good value of 644 [mAh/g].

PDADMA-1000k [Ch.2.2.6]: the second PEB tested resulted in an initial very good capacity of 905 at C/10. The most interesting part is from cycle 40th – 100th where the specific capacity fluctuates

among the range 750 – 650 [mAh/g] in a practical constant way [Fig.61]. Here it's clear how the property well underlined in the focus drawing of dedicated PEBs chapter [Fig.31]. The barrier formed by PEB-1000k chains is probably well distributed in the cathode and performs the polysulfide retention.



[Graph.C2] – **Coulombic Efficiency Vs. Number Of Cycles:** the first observation that comes in mind looking at the graph is the steep curve of **Alginate**, whom value of C_efficiency decreases really fast. The only reason is that this cathode contains practically the double content in mass of S per cm² with respect to the others. Looking at the PEBs, the situation is reversed with respect to capacity, i.e. 500k is the best one. **Chitosan**, **PVdF** and **500k-PEB** present all a constant capacity over 99% in the range 40th to 100th cycle.

[Graph.C3] - **Voltage Vs. Capacity – PVdF:** the Li-S' standard binder cathode shows a very constant second plateau at the first C/10 cycle. The difference in capacity is quite evident among charge at discharge both at the 1st cycle, meaning that the coulombic efficiency is very low. Furthermore the initial plateau of discharge at 1st cycle, where there is a breakage of S₈ is practically comparable to a negative straight line, with a negative value of slope, very high in absolute value. There is also a very steep Li₂S formation curve i.e. a sudden voltage drop (PVdF is itself poor in electronic conductivity, so it cannot compensate the lack of el-conductivity of Li₂S agglomerations).

Then, if we look at 50th and 100th the cycling tends to be stable with the classical two plateau of Li-S batteries. And a more smooth final voltage drop.

[Graph.C4][Graph.C5] - **Voltage Vs. Capacity -PEBs PDADMA/TFSI-1000k – 500k:** the most relevant evidences about the 500k is that the 1st-disch. curve is almost comparable to a straight line. Here the problem is mainly due to the inefficient wetting of the electrode, a phenomena described in previous paragraph. The internal resistance is so higher and the voltage drops in a sudden and unusual way. The 50th and 100th cycle are very comparable and presents the classical shapes.

[Graph.C6][Graph.C7] - Voltage Vs. Capacity - aqueous binders – Na- Alginate, Chitosan: both the renewable binders presents a very steep third step of Li_2S formation. This could be due again to a practical problem related to not a perfect dispersion of the aqueous binders, such that in certain zones of the cathode the lack of resistance cannot be compensate, as well as the Li_2S expansion. As a last remark, Chitosan presents two convex-like 2nd discharge plateau at 50th and 100th cycle. It seems so that for certain intermediate soluble species of polysulfide, chitosan interfere in a better way than others.

4 -Conclusions

The four types of trials put in evidence how difficult is to threat aqueous binders, especially sodium Alginate and Chitosan. Despite some difficulties in preparation and testing, in the last trial we were able to demonstrate, with a direct comparison, how the renewable binders can be competitive against PVdF.

In the end, they are also available in a cheap way in nature, and they don't presents any problem of disposal problem at the end of the battery life.

The use of toxic NMP, plus the problems that the recycling of the materials can originates at the and of the battery life, make the PVdF less interesting to further investigations. Furthermore, from an economical point of view much more expensive in terms of material and process cost (evaporation, treatment of NMP vapors and relative strict laws and regulations)

The PEBs also needed the same organic solvent, and also results to be very high cost. However, it worth to study them for the active role that play in the complex mechanism of Li_2S redox reactions.

In a scale up perspective, the Ball milling technique is a generally suitable for all the types of carbon/sulfur/binder composition, since it can be easily applied in a chain production, with relatively low cost. In terms of optimization of time and frequency as main parameters, the BM process worth a proper dedicated study, which has not been tackled deeply in the thesis.

BM is for sure far cheaper than other complex (but finer) methods presents in a small scale in various work in literature. So it is for sure the most feasible way of thinking a future mass production of lithium sulfur batteries in the future.

In the end, in our lab small scale experience, the results obtained make this method absolutely valuable, even in absence of a mathematical proper modelling of the grinding process.

5 - Acknowledgments/ Ringraziamenti

(IT) - Nel concludere il mio lavoro voglio ringraziare il Prof. Santarelli, la Prof.essa Carlotta Francia, che mi hanno fornito l'opportunità, gli strumenti e i consigli per la stesura della mia tesi di laurea. Ringrazio tutti i collaboratori del Dipartimento di Chimica ed in particolare il Usman Zubair, che mi ha costantemente seguito e mi ha trasmesso la sua conoscenza teorica e pratica dell'elettrochimica delle celle litio-zolfo.

Un particolare ringraziamento lo devo alla mia famiglia, ai miei genitori soprattutto che mi hanno sostenuto e dato l'opportunità di intraprendere e concludere questo percorso impegnativo.

Non posso non dedicare questo lavoro anche ai miei amici che sono stati fondamentali nel superare tutte le prove che mi sono presentate. Ringrazio anche chi, solo per una breve parte, ma non meno importante, ha condiviso con me i successi ed gli insuccessi che si sono presentati prima di raggiungere l'obiettivo.

Infine un grande ringraziamento è dovuto alla mia amata compagna di vita Chiara, senza la tua guida, senza il tuo costante indirizzami verso i giusti obiettivi e senza la tua fiducia nelle mie potenzialità non avrei mai potuto concludere questo percorso.

(EN) - In concluding my work I want to thank Prof. Santarelli, Prof. Carlotta Francia, who provided me with the opportunity, the tools and the advice for the writing of my degree thesis. I thank all the collaborators of the Department of Chemistry and in particular the Usman Zubair, who constantly followed me and gave me his theoretical and practical knowledge of the electrochemistry of lithium-sulfur cells.

I owe a special thanks to my family, to my parents above all who have supported me and given the opportunity to undertake and complete this challenging journey.

I cannot fail to dedicate this work to my friends who have been fundamental in passing all the tests presented to me. I also thank those who, just for a short part, but no less important, shared with me the successes and failures that occurred before reaching the goal.

Finally, a big thank you is due to my beloved life partner Chiara, without your guide, without your constant addressing me to the right goals and without your confidence in my potential I could never have concluded this journey.

Bibliography

- [1] - [Depletion of fossil fuels and anthropogenic climate change - A review \(2012\) - Mikael Höök, Xu Tang](#)
- [2] - [IEA - Key Word Energy Statistic 2017 pag. 59](#)
- [3] - [IEA Key World Energy Statistic 2017 pag.22-24](#)
- [4] - [Li-O₂ and Li-S batteries with high energy storage - Peter G. Bruce, Stefan A. Freunberger, Laurence J. Hardwick & Jean-Marie Tarascon \(2012\)](#)
- [5] - [Li-S Batteries - The Challenges, Chemistry, Materials and Future Perspectives – Ch.1.1 - Introduction and History of Lithium–Sulfur Batteries - Rezan Demir-Cakan \(2017\)](#)
- [6] - [A highly ordered nanostructured carbon–sulphur cathode for lithium/sulphur batteries - Xiulei Ji, Kyu Tae Lee and Linda F. Nazar \(2009\)](#)
- [7] - [Lithium/Sulfur Batteries: Electrochemistry, Materials, and Prospects - Ya-Xia Yin, Sen Xin, Yu-Guo Guo, Li-Jun Wan \(2012\)](#)
- [8] - [Electric dry cells and storage batteries \(Patent US3043896A\) - Herbert Danuta, Ulam Juliusz \(1962\)](#)
- [9] - [Electric cell containing amine electrolyte - Herbert Danuta \(1966\)](#)
- [10] - [Galvanic element with a negative electrode a positive electrode with sulfur as an active material and an electrolyte of an organic medium Geloes th ganic salt - Rao Mlarur Lakshmanar Blaskara \(1966\)](#)
- [11] - [Battery employing lithium - sulphur electrodes with non-aqueous electrolyte - Dominick A Nole, Vladimir Moss \(1970\)](#)
- [12] - [LiSM³ Conference 2017, opening slides \(2017\)](#)
- [13] - [Li-S Batteries - The Challenges, Chemistry, Materials and Future Perspectives – Ch.1.2 - Electrochemistry and Basic Reaction Mechanism of Li–S Batteries - Rezan Demir-Cakan \(2017\)](#)
- [14] - [Reversibility of electrochemical reactions of sulfur supported on inverse opal in glyme-Li saltmolten complex electrolytes - Naoki Tachikawa, Kento Yamauchi, Eriko Takashima, Jun-Woo Park, Kaoru Dokko and Masayoshi Watanabe \(2011\)](#)
- [15] - [New Approaches for High Energy Density Lithium-Sulfur Battery Cathodes – Scott Evers, Linda Nazar \(2012\)](#)
- [16] - [Synthesis of New, Nanoporous Carbon with Hexagonally Ordered Mesostructure - Shinae Jun, Sang Hoon Joo, Ryong Ryoo, Michal Kruk, Mietek Jaroniec, Zheng Liu, Tetsu Ohsuna and Osamu Terasaki \(2000\)](#)
- [17] - [Sulfur-Impregnated Activated Carbon Fiber Cloth as a Binder-Free Cathode for Rechargeable Li-S Batteries \(2011\)](#)
- [18] - [Smaller Sulfur Molecules Promise Better Lithium–Sulfur Batteries \(2012\)](#)
- [19] - [Li-S Batteries - The Challenges, Chemistry, Materials and Future Perspectives - Ch.5 - The Lithium Electrode Revisited through the Prism of Li–S Batteries \(2017\)](#)
- [20] - [Inhibiting Polysulfide Shuttling with a Graphene Composite Separator for Highly Robust Lithium-Sulfur Batteries \(2018\)](#)
- [21] - [Effect of chemical reactivity of polysulfide toward carbonate-based electrolyte on the electrochemical performance of Li-S batteries - Taeun Yim \(2013\)](#)
- [22] - [Electrochemical properties of ether-based electrolytes for lithium/sulfur rechargeable batteries – Céline Barchasz, Jean-Claude Le prêtre, Sébastien Patoux, Fannie Alloin \(2013\)](#)
- [23] - [Lithium/Sulfur batteries : development and understanding of the working mechanisms – SubCh. - 1.3.2. Electrolyte - Sylwia Walus \(2015\)](#)

- [24] - [A review of electrolytes for lithium/sulphur batteries - Johan Scheers, Sébastien Fantini, Patrik Johansson \(2014\)](#)
- [25] - [Effects of Liquid Electrolytes on the Charge/Discharge Performance of Rechargeable Lithium/Sulfur Batteries: Electrochemical and in-Situ X-ray Absorption Spectroscopic Studies - Jie Gao, Michael A. Lowe, Yasuyuki Kiya, Héctor D. Abruña \(2011\)](#)
- [26] - [Electrochemical Properties of Binary Electrolytes for Lithium-sulfur Batteries \(2011\)](#)
- [27] - [Carbon Materials for Lithium Sulfur Batteries - Ten Critical Questions - Dr. Lars Borchart, Dr. Martin Oschatz, Prof. Dr. Stefan Kaskel \(2016\)](#)
- [28] - [Li-S Batteries - The Challenges, Chemistry, Materials and Future Perspectives - Ch.4 Lithium–Sulfur Battery Electrolytes](#)
- [29] - [On the Surface Chemical Aspects of Very High Energy Density, Rechargeable Li–Sulfur Batteries - Doron Aurbach, Elad Pollak, Ran Elazari, Gregory Salitra, C. Scordilis Kelley, and John Affinito \(2009\)](#)
- [30] - [Role of \$\text{LiNO}_3\$ in rechargeable lithium/sulfur battery - Sheng S.Zhang \(2012\)](#)
- [31] - [Phosphorous Pentasulfide as a Novel Additive for High- Performance Lithium-Sulfur Batteries - Zhan Lin , Zengcai Liu , Wujun Fu , Nancy J. Dudney , and Chengdu Liang \(2012\)](#)
- [32] - [Recent Progress in All-Solid-State Lithium–Sulfur Batteries Using High Li-Ion Conductive Solid Electrolytes - Ediga Umeshbabu, Bizhu Zheng, Yong Yang \(2019\)](#)
- [33] - [A lithium–sulfur battery using a solid, glass-type \$\text{P2S5–Li2S}\$ electrolyte - Marco Agostini, Yuichi Aihara, Takanobu Yamada, Bruno Scrosati, Jusef Hassoun - \(2013\)](#)
- [34] - [Characterization of \$\text{Li}_2\text{S–P}_2\text{S}_5\$ glass-ceramics as a solid electrolyte for lithium secondary batteries - Akitoshi Hayashi, Shigenori Hama, Fuminori Mizuno, Kiyoharu Tadanaga, Tsutomu Minami, Masahiro Tatsumisago \(2004\)](#)
- [35] - [Chemistry of sulfur \(z=16\) - Chung \(Peter\) Chieh - \(2019\)](#)
- [36] - [Novel positive electrode architecture for rechargeable lithium/sulfur batteries - Céline Barchasz, Frédéric Mesguich, Jean Dijon, Jean-Claude Leprêtre , Sébastien Patoux, Fannie Alloin - \(2012\)](#)
- [37] - [High performance lithium–sulfur batteries: advances and challenges - Guiyin Xu, Bing Ding, Jin Pan, Ping Nie, Laifa Shen and Xiaoqiang Zhang - \(2014\)](#)
- [38] - [Porosity Blocking in Highly Porous Carbon Black by PVdF Binder and Its Implications for the Li–S System - Matthew J. Lacey, Fabian Jeschull, Kristina Edström, and Daniel Brandell – \(2014\)](#)
- [39] - [Recent progress of advanced binders for Li-S batteries - Jie Liu, Qian Zhang, Yang-Kook Sun \(2018\)](#)
- [40] - [Natural Polymeric Biomaterials Processing and Properties - Luis Alberto Loureiro Dos Santos – \(2017\)](#)
- [41] - [Enhanced cyclability of sulfur cathodes in lithium-sulfur batteries with Na-alginate as a binder - Weizhai Bao, Zhian Zhanga, Yongqing Gan, Xiwen Wang, Jie Lia - \(2013\)](#)
- [42] - [Chitosan as a Functional Additive for High-Performance Lithium- Sulfur Batteries - Yilei Chen, Naiqiang Liu, Hongyuan Shao, Weikun Wang, Mengyao Gao, Chengming Li, Hao Zhang, Anbang Wang and Yaqin Huang – \(2015\)](#)
- [43] - [Water-Soluble Polyacrylic Acid as a Binder for Sulfur Cathode in Lithium-Sulfur Battery - Zhian Zhang, Weizhai Bao, Hai Lu, Ming Jia, Keyu Xie, Yanqing Lai, and Jie Lia - \(2012\)](#)
- [44] - [Inhibiting the shuttle effect in lithium–sulfur batteries using a layer-by-layer assembled ion - permselective separator - Minsu Gu, Jukyong Lee, Yongil Kim, Joon Soo Kim, Bo Yun Jang, Kyu Tae Lee and Byeong-Su Kim - \(2014\)](#)
- [45] - [Enhanced Cyclability for Sulfur Cathode Achieved by a Water-Soluble Binder - Jin Pan, Guiyin Xu, Bing Ding, Jinpeng Han, Hui Dou and Xiaoqiang Zhang - \(2015\)](#)

- [46] - [*Pyrrolidinium FSI and TFSI-Based Polymerized Ionic Liquids as Electrolytes for High-Temperature Lithium-Ion Batteries* - Manfred Kerner, Patrik Johansson - \(2017\)](#)
- [47] - [Commercial PDADMA properties by Solvionic](#)
- [48] - [Molecular understanding of polyelectrolyte binders that actively regulate ion transport in sulfur cathodes - Longjun Li, Tod A. Pascal, Justin G. Connell, Frank Y.Fan, Stephen M.Meckler, Lin Ma, Yet-Ming Chiang, David Prendergast & Brett A. Helms - \(2017\)](#)
- [49] - [KERN ABT 220-4M balance technical specs. and overview](#)
- [50] - [Sulfur-graphene nanostructured cathodes via ball-milling for high-performance lithium-sulfur batteries - Jiantie Xu, Jianglan Shui, Jianli Wang, Min Wang, Hua-Kun Liu \(2014\)](#)
- [51] – [Retsch® Mixer Mill MM 400 general info](#)
- [52] – [Evaluation of Processes for Mechanical Manufacturing of Composite Materials for Li-Sulfur Batteries - Paul Titscher, Sabrina Zellmer, Christine F. Burmeister, Lars O. Schmidt, Sandra Breitung-Faes, Georg Garnweitner, and Arno Kwade \(2018\)](#)
- [53] - [Retsch® Mixer Mill MM 400 manual](#)
- [53.b) – [Chitosan solubility in formic acid](#)
- [54] - [BYK-Gardner® 2101 Automatic Film Applicator](#)
- [55] - [MTI® Micrometer Adjustable Film Applicator - 100 mm \(Film casting doctor blade\)](#)
- [56] - [BYK-Gardner® 2101 Automatic Film Applicator MANUAL](#)
- [57] - [Semiconductor Safety Handbook Safety and Health in the Semiconductor Industry 1998, Pages 204-268 Semiconductor Safety Handbook 4 - Industrial Hygiene - David G.Baldwin, Michael E.Williams](#)
- [58] - [Scope of the Risk Evaluation for N-Methylpyrrolidone \(2-Pyrrolidinone, 1-Methyl-\) – EPA – June 2017](#)
- [59] - [Microchemicals – NMP \(1-methyl-2-pyrrolidone\) properties](#)
- [60] - [Hohsen Corp. Electrode Punch](#)
- [61] - [Büchi® B-585 glass oven dryer data sheet](#)
- [62] - [Büchi® B-585 glass oven dryer Manual](#)
- [63] - [mBraun® Glovebox](#)
- [64] - [Cathode porosity is a missing key parameter to optimize lithium-sulfur battery energy density - Ning Kang, Yuxiao Lin, Li Yang, Dongping Lu, Jie Xiao, Yue Qi & Mei Cai \(2019\)](#)
- [65] - [Celgard® Dry-Process Lithium-Ion Battery Separators](#)
- [66] - [Stainless Steel Spacer for CR20XX Cell \(15.5 mm Dia x 0.2 mm\)](#)
- [67] - [Digital Pressure Controlled Electric Crimper for CR20XX Coin Cells \(Ar Glovebox Compatible\) - MSK-160E](#)
- [68] - [High-energy sustainable Lithium sulfur batteries for electrical vehicles and renewable energy applications - Development of innovative electrodes– Usman Zubair, PhD Thesis Ch.3.3.1 \(2019\)](#)
- [69] - [Arbin® Software MIT Pro \(version 4.32\)](#)
- [70] – [8 Channel Board for coin cells testing – MTI® Corporation](#)